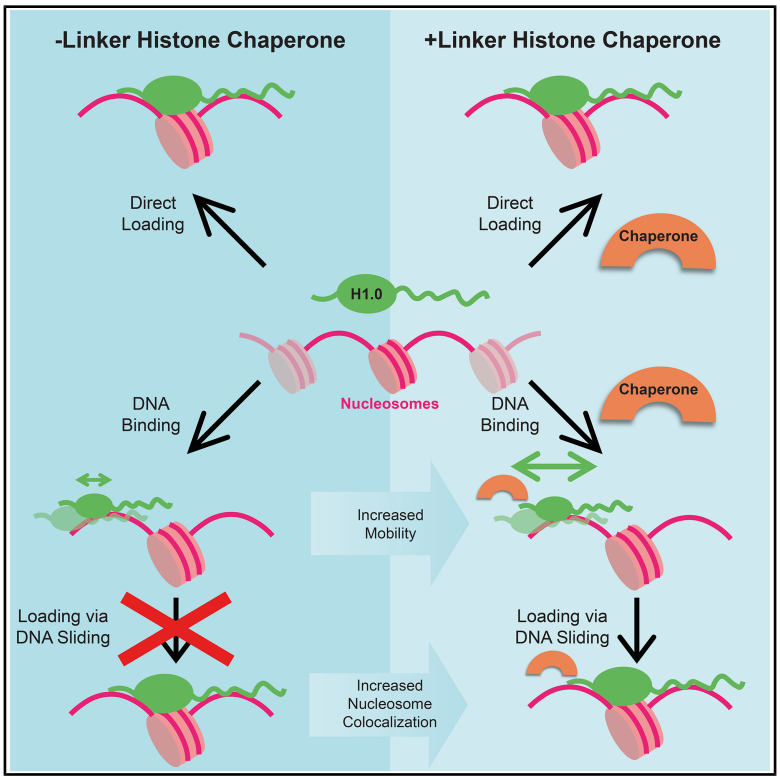
Molecular Cell

Article

Linker histone H1.0 loads onto nucleosomes through multiple pathways that are facilitated by histone chaperones

Graphical abstract



Highlights

- H1 directly binds nucleosomes and naked DNA with a preference toward nucleosomes
- DNA-bound H1 is largely mobile but does not load onto nucleosomes via DNA sliding
- Chaperones facilitate H1 loading onto nucleosomes by multiple mechanisms
- Nap1 is a more targeted H1 chaperone relative to other chaperones

Authors

Ehsan Akbari, Nathaniel L. Burge, Matti Valdimarsson, Aritra Chowdhury, Benjamin Schuler, Michael G. Poirier

Correspondence

poirier.18@osu.edu

In brief

Akbari et al. investigated the mechanisms of linker histone H1.0 loading onto nucleosomes. H1.0 directly binds nucleosomes and DNA, while DNA-bound H1.0 is mobile but does not load onto nucleosomes. Linker histone chaperones facilitate H1.0 loading through enhancing nucleosome binding, increasing H1.0 mobility, and enabling H1.0 loading through DNA sliding.

Akbari et al., 2026, Molecular Cell *86*, 3867–3881
October 1, 2026 © 2026 Elsevier Inc. All rights are reserved, including those for text and data mining, AI training, and similar technologies.
https://doi.org/10.1016/j.molcel.2026.09.001

CellPress

Molecular Cell

CellPress

Article

Linker histone H1.0 loads onto nucleosomes through multiple pathways that are facilitated by histone chaperones

Ehsan Akbari,[1] Nathaniel L. Burge,[2] Matti Valdimarsson,[3] Aritra Chowdhury,[3] Benjamin Schuler,[3,4] and Michael G. Poirier[1,2,5,6,*]

[1]Department of Physics, The Ohio State University, Columbus, OH 43210, USA
[2]Ohio State Biochemistry Graduate Program, The Ohio State University, Columbus, OH 43210, USA
[3]Department of Biochemistry, University of Zurich, 8057 Zurich, Switzerland
[4]Department of Physics, University of Zurich, 8057 Zurich, Switzerland
[5]Department of Chemistry & Biochemistry, The Ohio State University, Columbus, OH 43210, USA
[6]Lead contact
*Correspondence: poirier.18@osu.edu
https://doi.org/10.1016/j.molcel.2026.09.001

SUMMARY

Linker histone H1 is an essential chromatin architectural protein that compacts chromatin into transcriptionally silent regions by interacting with nucleosomal and linker DNA while rapidly exchanging *in vivo*. How H1 targets nucleosomes while being dynamic remains unanswered. Using a single-molecule strategy, we investigated human H1.0 interactions with DNA and nucleosomes. H1.0 directly binds nucleosomes and naked DNA with a preference toward nucleosomes. DNA-bound H1.0 exhibited a range of bound lifetimes with both mobile and immobile states, where H1.0 was largely mobile, diffused over kilobase distances in seconds, but surprisingly did not load onto nucleosomes. Linker histone chaperones significantly facilitated H1.0-nucleosome loading by enabling H1.0 loading through DNA sliding, reducing DNA resident times without impacting nucleosome resident times, increasing mobility along DNA, and targeting H1.0 loading onto the nucleosome dyad. These findings reveal the multiple distinct mechanisms linker histones and their chaperones use to interact with nucleosomes to regulate chromatin accessibility.

INTRODUCTION

Eukaryotic genomic DNA is organized into chromatin fibers by repeated wrapping into nucleosomes, 147 bp of DNA wrapped around a histone protein octamer that contains two copies of each core histone: H2A, H2B, H3, and H4.[1] The linker histone H1 dynamically regulates chromatin fiber compaction[2,3] to control genomic accessibility to transcription and DNA repair machinery.[4,5] H1 is an abundant chromatin architectural protein with about one H1 per nucleosome in metazoan cells,[6,7] while H1 expression level is critical for cell viability.[5] H1 binds within the nucleosome dyad region, stabilizing the DNA wrapped into nucleosomes[7] and maintaining chromatin condensation.[8,9] Interestingly, H1 dynamically exchanges between chromatin fibers,[10–12] while functioning with other chromatin-modifying complexes to maintain heterochromatic versus euchromatic states.[4,5] The molecular mechanism behind linker histone H1 regulation of chromatin states is not fully understood.

All human H1 isoforms[13,14] contain a tripartite structure: a globular winged helix domain (WHD) flanked by a short (20–35 residue) disordered N-terminal domain (NTD) and a long (~100 residue) disordered C-terminal domain (CTD).[7,15] Both the WHD and CTD interact with the nucleosome by binding specific nucleosomal DNA regions.[16–18] The H1 WHD interacts with the DNA at the nucleosome dyad and the first 10 bp of the linker DNA,[16–18] while the H1 CTD interacts with ~20 bp of linker DNA and becomes partially ordered.[19,20] However, recent single-molecule evidence,[21,22] along with NMR analysis[23] and computational modeling,[24,25] revealed that the structure of the DNA-bound H1 CTD remains highly dynamic. Collectively, these and other studies have established that H1-WHD and H1-CTD binding to DNA are the primary interactions for H1 loading into chromatin.

Despite interacting with chromatin through high-affinity DNA interactions,[26,27] H1 localizes onto the nucleosome dyad, instead of other nucleosomal DNA or linker DNA regions.[7] While structural analysis has provided atomic resolution of the H1 WHD within the chromatosome complex,[16,18,28] how H1 efficiently targets the nucleosome dyad while remaining dynamic is unresolved. Histone chaperones are important regulators of linker and core histone deposition onto chromatin both *in vivo* and *in vitro*.[29] Histone chaperones that regulate H1 interactions with chromatin *in vivo* include nucleosome assembly protein-1

All rights are reserved, including those for text and data mining, AI training, and similar technologies.

(Nap1),[30–32] prothymosin α (ProTα),[33,34] and somatic nuclear autoantigenic sperm protein (sNASP),[35,36] each of which directly interacts with H1 *in vitro*.[37–41] Interestingly, Nap1 and sNASP can also function as H2A-H2B[42–44] and H3-H4[45] chaperones, respectively. Understanding the role of histone chaperones in regulating H1-chromatin interactions is critical for determining H1 regulation of chromatin accessibility.

Here, we report combined single-molecule optical tweezers and fluorescence measurements of H1.0 interaction dynamics with DNA and nucleosomes. We find that most DNA-bound H1.0 is highly mobile, exploring micron distances in seconds by 1D diffusion, while ~16% is immobile. Both the mobile and immobile fractions of DNA-bound H1.0 remain bound for up to minutes, where both fractions have fast (sub-second to seconds) and slow (tens of seconds) resident times. Surprisingly, while we observe direct H1.0 loading onto nucleosomes, H1.0 alone does not load onto nucleosomes through DNA sliding. Histone chaperones facilitate H1.0 loading onto nucleosomes by biasing nucleosome resident times over DNA, enhancing H1.0 mobility along DNA, enabling H1.0-nucleosome loading through DNA sliding, and increasing H1.0 loading onto the nucleosome dyad. The linker histone chaperone, Nap1, is efficient at these functions, requiring substoichiometric concentrations relative to H1.0, while ProTα and sNASP need to be in large excess to H1.0, suggesting that Nap1 is a highly specific linker histone chaperone. Overall, these measurements reveal highly dynamic H1.0 interactions with DNA and nucleosomes and that linker histone chaperones regulate H1.0-nucleosome loading through synergistic mechanisms.

RESULTS

DNA-bound H1.0 exhibits long residence times with a complex combination of mobile and immobile states

Linker histone H1 interacts with nucleosomal and linker DNA to bind within the nucleosome dyad region.[16] H1 binding within this region reduces DNA accessibility through increasing chromatin compaction[46] and suppressing nucleosome unwrapping.[31,47] Given that H1 targets chromatin through DNA interactions, not surprisingly, H1 efficiently binds naked DNA,[26,27] which could be important for H1 loading onto chromatin.

To investigate the dynamics of H1-DNA interactions, we used a single-molecule approach where a 48.5 kb lambda DNA molecule is suspended between two polystyrene beads by a dual optical trap equipped with confocal fluorescence imaging.[48,49] This strategy allows for single-molecule fluorescence (SMF) detection of fluorophore-labeled H1.0 binding to, translocating along, and dissociating from a single DNA molecule. We focused on H1.0 because it is extensively studied[13] and highly relevant for human disease.[5] A microfluidic system was utilized to enable tethering of a single biotin-labeled lambda DNA between two optically trapped streptavidin-coated beads (Figure 1A, channels 1–3)[50] and confirmed using the worm-like chain (WLC) model of DNA force extension.[51]

To visualize dynamic binding interactions between DNA and H1.0, we used site-specific Cy3-labeled H1.0[47,52] at 3 nM (Figure 1A, channel 4). DNA-bound H1.0 was visualized with SMF confocal line scanning as kymographs of H1.0 interactions along the DNA tether (Figure 1B). The kymographs were recorded while the lambda DNA tether was held under a constant force (1, 3, or 10 pN). Kymographs revealed that H1.0 is bound to DNA for many seconds before dissociating (Figure 1B). Single-molecule H1.0 traces were quantified to extract the residence time and position as a function of time for each DNA-bound H1.0. DNA-bound H1.0 exhibited two types of dynamics: mobile (red box) and immobile (blue box), which were observed for 1, 3, and 10 pN (Figures 1B, 1C, S1A, and S1B).

To quantify whether H1.0 is mobile ($H1.0_{Mobile}$) or immobile ($H1.0_{Immobile}$), we prepared DNA tethers with a sparse number of Cy5-labeled nucleosomes as a reference for immobile DNA-bound protein (Figure S2) since nucleosomes are immobile for minutes.[53] Using nucleosome references (see STAR Methods), we determined at 1, 3, and 10 pN that 84% ± 1%, 91% ± 1%, and 91% ± 1% of tracked H1.0 were mobile, respectively (Figure 1D; Table S1). To quantify the mobility of $H1.0_{Mobile}$, we determined the mean squared displacement (MSD) versus time and fit it to $MSD = 2D\,t^{\alpha}$. D is the diffusion constant, while α of 1 indicates random-walk diffusion. We find that α is ~0.8 and independent of applied force (Figure 1F; Table S1). An $\alpha < 1$ suggests that H1.0 undergoes constrained diffusion. DNA-only tethers are not likely to present barriers to H1.0 1D diffusion. Instead, $H1.0_{Mobile}$ might have a distribution of pauses that results in α less than 1.[54,55] The distribution of diffusion constants, D, spanned over two orders of magnitude, while the increase in applied force from 1 to 10 pN resulted in a modest but statistically significant increase in the average D from 0.281 ± 0.002 to 0.368 ± 0.003 $\mu m^2/s$ (Figure 1E).

We then investigated that the time H1.0 remained bound to DNA with cumulative probability distributions (CPDs) of H1.0 dwell times (Figure 1G). These CPDs fit best to a double exponential for both $H1.0_{Mobile}$ and $H1.0_{Immobile}$ and for all three forces (Figures 1G, S1C, and S1D). These results imply four classes of DNA-bound H1.0: $H1.0_{Immobile\_\tau fast}$, $H1.0_{Immobile\_\tau slow}$, $H1.0_{Mobile\_\tau fast}$, and $H1.0_{Mobile\_\tau slow}$. The multi-second τ_{fast} for $H1.0_{Mobile}$ was significantly longer than the sub-second τ_{fast} for $H1.0_{Immobile}$, independent of force (Figure S1E; Table S2). At 1 and 3 pN, τ_{slow} was on the scale of 10 s or larger for both $H1.0_{Mobile}$ and $H1.0_{Immobile}$, while at 10 pN, the τ_{slow} was about 3-fold longer for $H1.0_{Mobile}$ (Figure S1E; Table S2). Finally, $H1.0_{Mobile}$ had a similar fraction of τ_{fast} and τ_{slow} transitions, while $H1.0_{Immobile}$ had more τ_{fast} than τ_{slow} transitions (Figure S1E; Table S2).

To investigate the conformational dynamics of DNA-bound $H1.0_{Mobile}$ and $H1.0_{Immobile}$, we determined the impact of Na^+ screening on the mobility and residence times of DNA-bound H1.0.[56] The fraction of mobile H1.0 was independent of Na^+ concentration (Figures S3A and S3F–S3H), suggesting that $H1.0_{Immobile}$ cannot be converted into $H1.0_{Mobile}$ through increased electrostatic screening. Increasing the Na^+ concentration from 20 to 200 mM reduced the τ_{fast} and τ_{slow} $H1.0_{Mobile}$ lifetimes on the DNA by 4-fold, while the fraction of τ_{fast} events remained constant (Figures S3D and S3E; Table S3). This 10-fold increase in Na^+ concentration also increased the diffusion constant by 5-fold (Figures S3B and S3C; Table S4). In contrast,

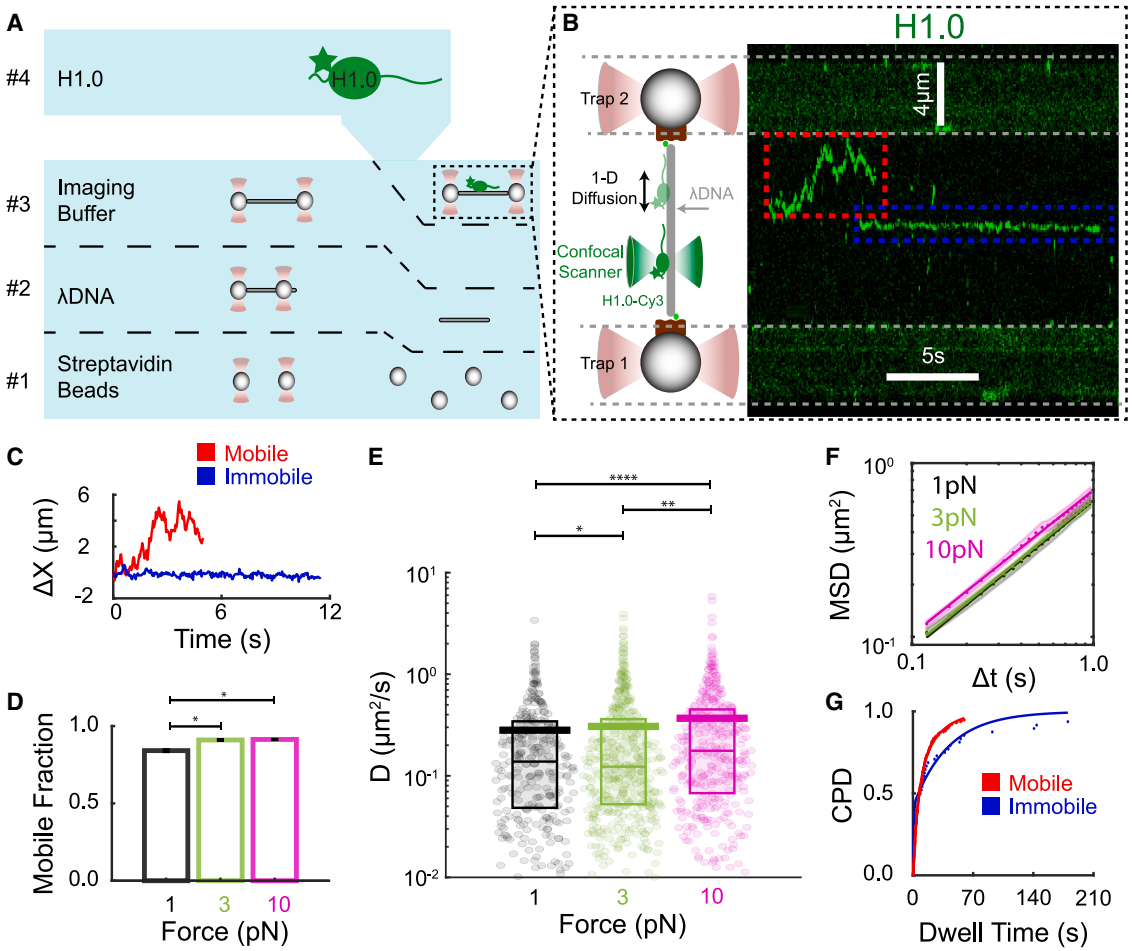


Figure 1. DNA-bound H1.0 is highly dynamic

(A) Schematic representation of the microfluidic apparatus utilized for the bottom-up assembly of single DNA tethers.

(B) A single-molecule assembly schematic of confocal fluorescent visualization of Cy3-labeled H1.0 bound to a λDNA tether and a representative kymograph that was cropped from the original kymograph. The red and blue boxes indicate $H1.0_{Mobile}$ and $H1.0_{Immobile}$, respectively.

(C) Displacement of $H1.0_{Mobile}$ (red) and $H1.0_{Immobile}$ (blue) from the kymograph in (B).

(D) Fraction of $H1.0_{Mobile}$ traces on the λDNA tether with a constant force of 1 pN (black), 3 pN (green), or 10 pN (magenta).

(E) Violin plots of the diffusion constants for each $H1.0_{mobile}$. Solid lines indicate the mean. The center, bottom, and top marks of each box indiate the median, the 25th percentile, and the 75th percentile, respectively.

(F) The average mean-squared displacement (MSD) versus time for $H1.0_{mobile}$ traces diffusing along λDNA held at a constant force of either 1 pN (black), 3 pN (green), or 10 pN (magenta).

(G) Cumulative probability distribution (CPD) of dwell times observed for $H1.0_{Mobile}$ and $H1.0_{Immobile}$ under 1 pN force. Both dwell time CPDs were best fit to a double-exponential model. * denotes $p < 0.05$. ** denotes $p < 0.01$. **** denotes $p < 0.0001$. Error bars denote standard error of the mean.

the $H1.0_{Immobile}$ lifetime with Na^+ below 130 mM had longer τ_{fast} and τ_{slow} with a similar fraction of τ_{fast} events to 130 mM Na^+, while 200 mM Na^+ eliminated the τ_{fast} events and τ_{slow} increased (Figure S3I). This indicates that 130 mM results in the shortest resident times for $H1.0_{Immobile}$. Applying the Lohman-Record polyelectrolyte framework,[57,58] the mobile population exhibits only modest counterion release ($\Delta n_{\tau fast} \approx 0.54$ and $\Delta n_{\tau slow} = 0.52$; Figures S3J and S3K). This suggests the observed electrostatic weakening is dominated by screening of dynamic CTD-DNA contacts rather than stoichiometric counterion release. In combination, these results reveal that DNA-bound $H1.0_{Mobile}$ is conformationally dynamic, while the $H1.0_{Immobile}$ is conformationally static, where Na^+ cannot screen its interactions with DNA.

To investigate the contribution of the H1.0 CTD to H1.0-DNA interactions, we prepared three H1.0 mutants with their CTD truncated to different lengths. H1.0ΔC44, H1.0ΔC66, and H1.0ΔC78 have 44, 66, and 78 amino acids (aa) removed from the C-terminal end of H1.0, respectively. We carried out kymograph measurements of each H1.0 truncation (Figures S4A and S4B). The removal of 78 aa eliminated detectable H1.0-DNA interactions, while H1.0ΔC44 and H1.0ΔC66 exhibited a significant increase in mobility (Figures S4C–S4E; Table S5). The DNA-bound H1.0 resident times were significantly reduced by

the removal of 44 and 68 aa where τ_{fast} was reduced 7- and 3-fold, respectively, and τ_{slow} was reduced 3- and 5-fold, respectively. Both truncations increased the fraction of τ_{fast} events (Figures S4F and S4G; Table S6). These results indicate that the CTD is important for DNA-H1.0 interactions, promoting stable DNA binding and restricting H1.0 mobility.

Finally, we considered the possibility that the fraction $H1.0_{Immobile}$ was due to oligomerization. We compared the fluorescence signal from DNA-bound $H1.0_{Immobile}$ with $H1.0_{Mobile}$. The average Cy3 fluorescence intensity of $H1.0_{Immobile}$ was ~5 times higher than $H1.0_{Mobile}$ (Figure S4H; Table S7), suggesting that DNA-bound $H1.0_{Immobile}$ is in a higher oligomeric state. We determined that the relative fluorescence signals between the immobile and mobile fractions of H1.0ΔC44 and H1.0ΔC66 are similar, indicating that the CTD promotes oligomerization of $H1.0_{Immobile}$ (Figure S4H; Table S7). Collectively, these findings reveal that H1.0 adopts a range of DNA binding modes that include mobile and immobile states with a wide range of times bound to the DNA.

H1.0 alone preferentially loads directly onto nucleosomes

After determining H1.0 binds to and is mobile on DNA, we investigated H1.0 loading onto nucleosomes. Properly loaded H1 binds nucleosomes near the dyad symmetry axis, where the H1 WHD interacts with DNA near the dyad and with linker DNA,[18,28] while the H1 CTD interacts with linker DNA.[16] Our findings that DNA-bound H1.0 is highly mobile and conformationally dynamic suggest that, in addition to H1.0 directly loading onto nucleosomes, H1.0 could load onto the nucleosome through DNA sliding.

To investigate the nucleosome loading pathways of H1.0, nucleosomes were reconstituted into lambda DNA, resulting in them being randomly positioned. The histone octamer was Cy5 labeled at H2A(K119C), allowing nucleosome positions to be quantified with Cy5 fluorescence. The nucleosome density along the DNA tether was less than 1 nucleosome per 5 kb of DNA so that confocal fluorescence scanning could resolve (1) nucleosome positions, (2) H1.0 sliding between nucleosomes, and (3) nucleosome-H1.0 colocalization events (Figures 2A and 2B).

We confirmed that properly formed nucleosomes reconstituted along lambda DNA by measuring the change in tether end-to-end distance and the number of Cy5 loci along the tether. On average, each Cy5 locus reduced the tether end-to-end distance by 44 ± 4 nm (Figures S5A–S4C). This value closely agrees with previously reported values for nucleosomes reconstituted on lambda DNA.[59] Also, when the tether was held with 15 pN of constant force, the expected 25 nm steps for individual nucleosomes were observed (Figures S5D–S5F) as previously reported.[59]

Kymographs were acquired with nucleosome-containing lambda DNA subjected to 1 pN of constant force (Figure 2A). 1 pN of force is below the force required to partially unwrap nucleosomes[60] while keeping the tether in the image plane for confocal line scanning. Dual fluorescence confocal line scanning visualized the positions of Cy5-labeled nucleosomes and DNA-bound Cy3-labeled H1.0 (Figures 2A and 2B). Upon the addition of 3 nM H1.0, we observed tether-bound H1.0, where the fraction of $H1.0_{Mobile}$ on nucleosome-containing tethers was similar to DNA-only tethers (Figure 2C; Table S8). The MSD power law dependence α for $H1.0_{Mobile}$ was not impacted by nucleosome-containing tethers (Figure 2D; Table S8). There was a modest (~1.2-fold) but statistically significant increase in the average diffusion constant of $H1.0_{Mobile}$ on nucleosome-containing tethers (Figure 2E; Table S8). This indicates that nucleosomes subtly influence the DNA sliding of $H1.0_{Mobile}$. Since truncations in H1.0 CTD enhance mobility along DNA (Figures S4D and S4E), this modest increase in H1.0 mobility could be due to conformational changes in H1.0 CTD that are induced during colocalization with nucleosomes that are retained after H1.0 diffuses away from the nucleosome.

We determined the dwell time CPD of mobile and immobile DNA-bound H1.0 on nucleosome-containing tethers. The fits required two exponentials, as was needed for DNA-only tethers (Figures 2F and 2G). The nucleosome-containing tethers did not significantly impact τ_{fast}, τ_{slow}, and A_{fast} for the mobile traces (Figure 2H; Table S9). In contrast, for $H1.0_{Immobile}$ on nucleosome-containing tethers, τ_{fast} and τ_{slow} increased from 1.4 ± 0.3 to 7 ± 1 s and from 44 ± 3 to 80 ± 20 s (Figure 2H; Table S9), while the fraction of τ_{fast} transitions (A_{fast}) did not change (Figure 2I; Table S9).

These findings suggest that while the presence of nucleosomes did not impact the resident time of $H1.0_{Mobile}$ on the tether, nucleosomes do impact the resident time of $H1.0_{Immobile}$. To further investigate this, we quantified the fraction of $H1.0_{Mobile}$ and $H1.0_{Immobile}$ that colocalized with nucleosomes when first binding nucleosome-containing tethers as compared to binding at 4 (the average number of nucleosomes per tether) random positions along DNA-only tethers (Figures 3A–3C and S6). We found that $H1.0_{Mobile}$ bound to nucleosomes and random DNA positions with the same frequency (Figure 3C). However, $H1.0_{Immobile}$ bound to nucleosomes about 4-fold more often than to random DNA positions (Figure 3C). These results indicate that $H1.0_{Immobile}$ is biased toward loading directly onto nucleosomes and are consistent with our observed increase in the τ_{fast} and τ_{slow} resident times of $H1.0_{Immobile}$ on nucleosome-containing tethers (Figures 2G–2I).

H1.0 alone does not load onto nucleosomes through DNA sliding and instead reflects away from nucleosomes

Visual inspection of the kymographs indicated that $H1.0_{Mobile}$ largely reflected away from nucleosomes. To quantify the interactions between mobile DNA-bound H1.0 and nucleosomes, we defined a colocalization event when H1.0 was within 200 nm of a nucleosome, our localization resolution. We found the nucleosome colocalization dwell time CPD to be essentially the same as the CPD for $H1.0_{Mobile}$ colocalized at random locations along a DNA-only tether (Figures 3D and 3E; Table S10). These results indicate that $H1.0_{Mobile}$ does not preferentially colocalize at nucleosomes during DNA sliding.

Each colocalization event has four outcomes: binding, reflecting, crossing, and dissociating (Figures 3F and 3G). The colocalization time CPD between H1.0 and random points along DNA-only tethers revealed an ~0.2 s colocalization time

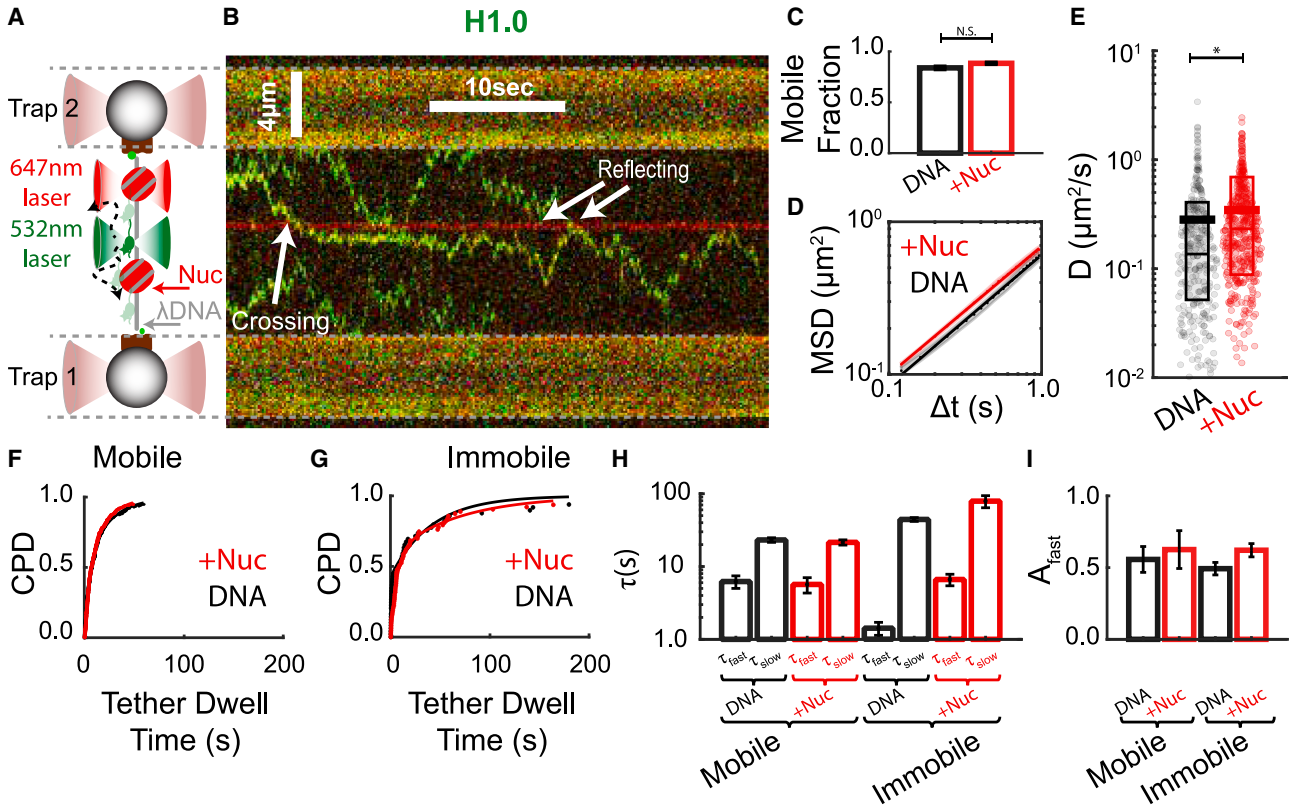


Figure 2. H1.0 dynamics on nucleosome-containing tethers

(A) Schematic of the single-molecule experimental setup with nucleosomes.

(B) A representative kymograph, which was cropped from the original kymograph, is of a single nucleosome-containing DNA tether. The red and green signals indicate the nucleosome-Cy5 and H1.0-Cy3 locations, respectively.

(C) Fraction of $H1.0_{Mobile}$ on DNA-only (black) and nucleosome-containing (red) tethers.

(D) Average MSD versus time for $H1.0_{Mobile}$ on DNA-only (black) and nucleosome-containing (red) tethers.

(E) Violin plots of diffusion coefficients for $H1.0_{Mobile}$ bound to DNA-only (black) and nucleosome-containing (red) tethers. Solid lines indicate the mean. The center, bottom, and top of each box indicate the median, the 25th percentile, and the 75th percentile, respectively.

(F and G) Dwell time CPD for $H1.0_{Mobile}$ and $H1.0_{Immobile}$, respectively, bound to nucleosome-containing (red) and DNA-only (black) tethers.

(H and I) Summary of the CPD fit parameters: τ_{fast}, τ_{slow}, and A_{fast} for $H1.0_{Mobile}$ and $H1.0_{Immobile}$ on DNA-only (DNA, black) and nucleosome-containing (+Nuc., red) tethers. All measurements were done with a constant force of 1 pN. Error bars denote standard error of the mean.

($\tau_{colocalization}$, Figure 3E). We therefore considered a colocalization event as a binding event if the H1.0 and nucleosome were colocalized for more than 0.4 s (twice $\tau_{colocalization}$ on DNA). If a colocalization event was not a binding event, it was considered a crossing, reflecting, or dissociating event based on whether the $H1.0_{Mobile}$ maintained direction, reversed direction, or dissociated, respectively. To control for the mobility of H1.0 on DNA-only tethers, colocalization events for H1.0 at randomly selected points along the tether were determined (Figure 1, 1 pN of force). The binding probability of H1.0 to nucleosomes was not statistically different from that at random points along DNA-only tethers (Figure 3H; Table S11). Instead, H1.0 exhibited a higher likelihood of reflecting from a nucleosome (Figure 3H; Table S11), suggesting that nucleosomes constrain DNA-bound $H1.0_{Mobile}$, limiting that the distance H1.0 can travel by 1D diffusion. These results suggest that H1.0 alone does not efficiently load onto a nucleosome if bound first to linker DNA.

Linker histone chaperones regulate the lifetime and mobility of DNA-bound H1.0

Since DNA-bound H1.0 is conformationally dynamic and does not efficiently load onto nucleosomes through DNA sliding, we considered the possibility that linker histone chaperones regulate H1.0 interactions with chromatin. To investigate the influence of histone chaperones on H1.0-DNA dynamics, we first acquired kymographs of DNA-bound H1.0 with 1 pN of constant force and increasing concentrations of Nap1 histone chaperone (Figures 4A, 4B, and S7). At concentrations of Nap1 (<3 nM) below H1.0, H1.0 continued to bind DNA, while above 3 nM Nap1, H1.0-DNA binding was largely abolished (Figure S7). We therefore focused on Nap1 concentrations below 3 nM. Interestingly, at these Nap1 concentrations, we did not observe an immobile fraction of DNA-bound H1.0. Therefore, the mobile fraction of DNA-bound H1.0 without Nap1 was used as a control for the mobility and lifetime measurements with Nap1.

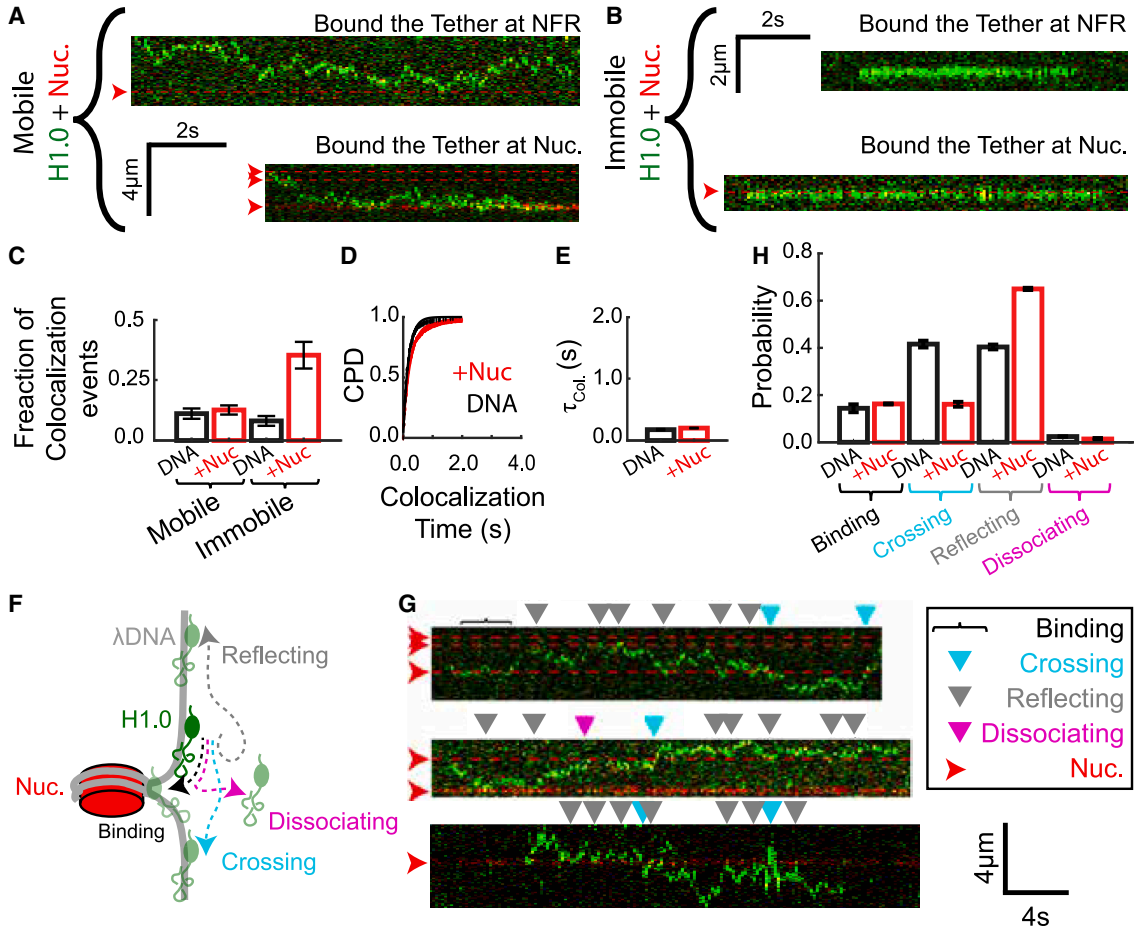


Figure 3. H1.0 directly loads onto nucleosomes but not through DNA sliding

(A and B) Representative kymographs of (A) H1.0$_{Mobile}$ and (B) H1.0$_{Immobile}$ that first bound to a nucleosome-free region (NFR) and a nucleosome.

(C) The probability of an initial H1.0 binding event on a nucleosome-containing tether is colocalized at a nucleosome (+Nuc, red). This is compared with the probability that an initial H1.0 binding event on a DNA-only tether is colocalized at a randomly selected DNA position (DNA, black).

(D) CPD of H1.0$_{Mobile}$ colocalization events with nucleosomes (red) and with randomly selected positions along DNA-only tethers (black). Both CPDs were best fit to a single exponential model.

(E) The colocalization dwell times, $\tau_{colocalization}$, from the exponential fits of the CPD in (D).

(F) Illustration of the four possible outcomes following an H1.0$_{Mobile}$-nucleosome colocalization event: binding, crossing, reflecting, and dissociating.

(G) Representative kymographs of H1.0$_{Mobile}$ (green) bound to nucleosome-containing tethers. Dotted red lines indicate nucleosome locations.

(H) Probability of binding, crossing, reflecting, and dissociating events for H1.0$_{Mobile}$ colocalization events with nucleosomes (red) and random points along DNA-only tethers (black). All measurements were done with 1 pN constant force. The representative kymographs in (A), (B), and (G) are cropped from original kymographs. Error bars denote standard error of the mean.

To investigate the impact of Nap1 on the mobility of DNA-bound H1.0, we determined the MSD versus time and found that it fits a power law of $\alpha \sim 1$ as the Nap1 concentration was increased (Figure 4E; Table S12). This suggests that Nap1 suppresses H1.0 pauses that might lead to an $\alpha < 1$. In addition, the average diffusion constant of H1.0$_{Mobile}$ without Nap1 (D = 0.281 ± 0.002 μm^2/s) increased to 0.40 ± 0.02, 0.60 ± 0.06, and 1.0 ± 0.3 μm^2/s, with 1, 2, and 3 nM of Nap1, respectively (Figure 4F; Table S12). These results reveal that Nap1 enhances random-walk diffusion of DNA-bound H1.0.

Next, we quantified the dwell time of each DNA-H1.0 binding event and fitted their CPDs to exponential functions (Figure 4C). We found that the range of DNA-bound H1.0 dwell times decreased with increasing Nap1 (Figure 4C). In the presence of 1 nM Nap1, 2 exponential functions were required to fit the H1.0 dwell time CPD, where the τ_{fast} did not change, while τ_{slow} decreased from 23 ± 2 to 14 ± 3 s (Figure 4D; Table S13). Furthermore, the fraction of fast transitions, A_{fast}, increased from 55% ± 9% to 70% ± 20%. In contrast, the dwell time CPD of DNA-bound H1.0 with 2 and 3 nM of Nap1 required a single exponential with dwell times of 10.7 ± 0.8 and 3.8 ± 0.6 s, respectively (Figure 4D; Table S13). These results indicate that substoichiometric concentrations of Nap1 not only prevent DNA-bound H1.0$_{Immobile}$ but also suppress the long-lived bound states of H1.0$_{Mobile}$. Collectively, these studies reveal that Nap1 influences the occupancy and mobility of DNA-bound H1.0,

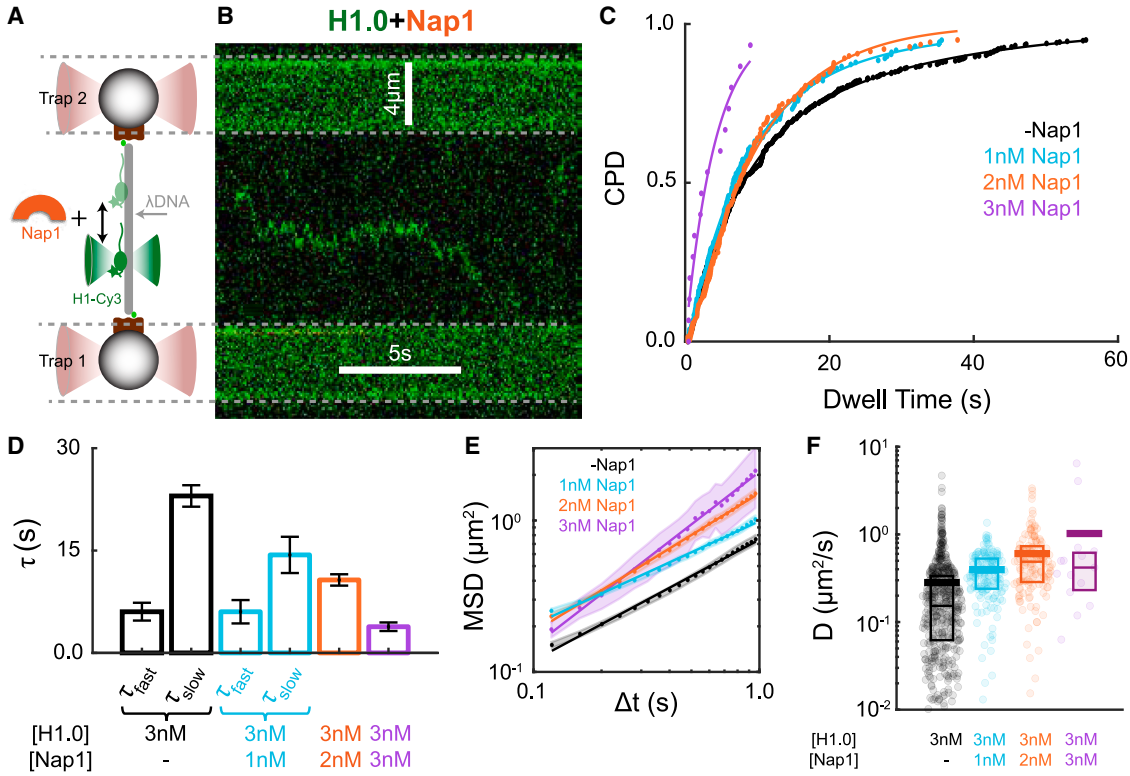


Figure 4. Nap1 reduces H1.0 binding to DNA while enhancing H1.0 mobility

(A) Illustration of the single-molecule experiment.

(B) Representative kymograph of H1.0 (green) diffusing along a DNA-only tether with 2 nM Nap1. This kymograph trace is cropped from the original kymograph.

(C) Dwell time CPD of DNA-bound H1.0 with increasing concentrations of Nap1. The CPDs were best fit with two exponentials for 0 and 1 nM Nap1 and a single exponential for 2 and 3 nM Nap1.

(D) Characteristic dwell times (τ) from the CPDs in (C). τ_{fast} and τ_{slow} are provided for double-exponential fits, while a single τ is provided for single exponential fits.

(E) Average MSD versus time for increasing concentrations of Nap1.

(F) Violin plots of $H1.0_{Mobile}$ diffusion coefficients for increasing concentrations of Nap1 (1–3 nM). Solid lines indicate the mean. The center, bottom, and top of each box indicate the median, the 25th percentile, and the 75th percentile, respectively. Measurements were done with 1 pN constant force. Error bars denote standard error of the mean.

suggesting that Nap1 can regulate H1.0 binding to chromatin by controlling H1.0 interactions with linker DNA.

To determine if other linker histone chaperones influence the dynamics of H1.0 interactions with DNA, we carried out similar studies with ProTα and sNASP. In addition, as a control for a general anionic molecule, we studied a 30 bp DNA molecule (DNA_{30bp}), which has a similar total negative charge to Nap1. We acquired kymographs of DNA-bound H1.0 with 1 pN of constant force and increasing concentrations of ProTα (Figures S8A–S8F), sNASP (Figures S8G–S8L), or DNA_{30bp} (Figures S8M–S8R). Unlike Nap1, H1.0 continued to bind to DNA-only tethers at concentrations of ProTα (10 μM), sNASP (100 nM), and DNA_{30bp} (100 nM) in significant excess of the H1.0 concentration (3 nM; Figure S7B). However, these higher concentrations of ProTα, sNASP, and DNA_{30bp} resulted in an impact similar to 2 nM Nap1 on the dynamics of H1.0-DNA interactions. This includes a decrease in the lifetime of DNA-bound H1.0 (Figures 4C, 4D, S8C, S8D, S8I, S8J, S8O, and S8P; Table S13), an increase in the mobility of $H1.0_{Mobile}$ (Figures 4E, 4F, S8E, S8F, S8K, S8L, S8Q, and S8R; Table S12), and a significant reduction of $H1.0_{Immobile}$ (Table S12). The finding that Nap1 requires substoichiometric concentrations relative to H1.0, while ProTα and sNASP required large excess concentrations, indicates that Nap1 is a more specific and targeted linker histone chaperone.

Linker histone chaperones enhance H1.0 loading onto nucleosomes by eliminating immobile DNA-bound H1.0 while maintaining direct loading of H1.0 onto nucleosomes

Given that chaperones are reported to regulate H1.0-nucleosome interactions *in vitro* and *in vivo*,[30,33–36,38–41] we investigated the influence of linker histone chaperones on H1.0 loading onto nucleosomes. We first focused on Nap1, given its efficient regulation of H1.0-DNA interactions. 2 nM of Nap1 was included in kymograph measurements of H1.0 interactions with nucleosome-containing tethers held at 1 pN of constant force (Figures 5A and 5B). The kymograph measurements were then quantified to determine the impact of Nap1 on the fraction of $H1.0_{Mobile}$ and the CPD of H1.0-bound dwell times. We observed that 84% ± 1% of all

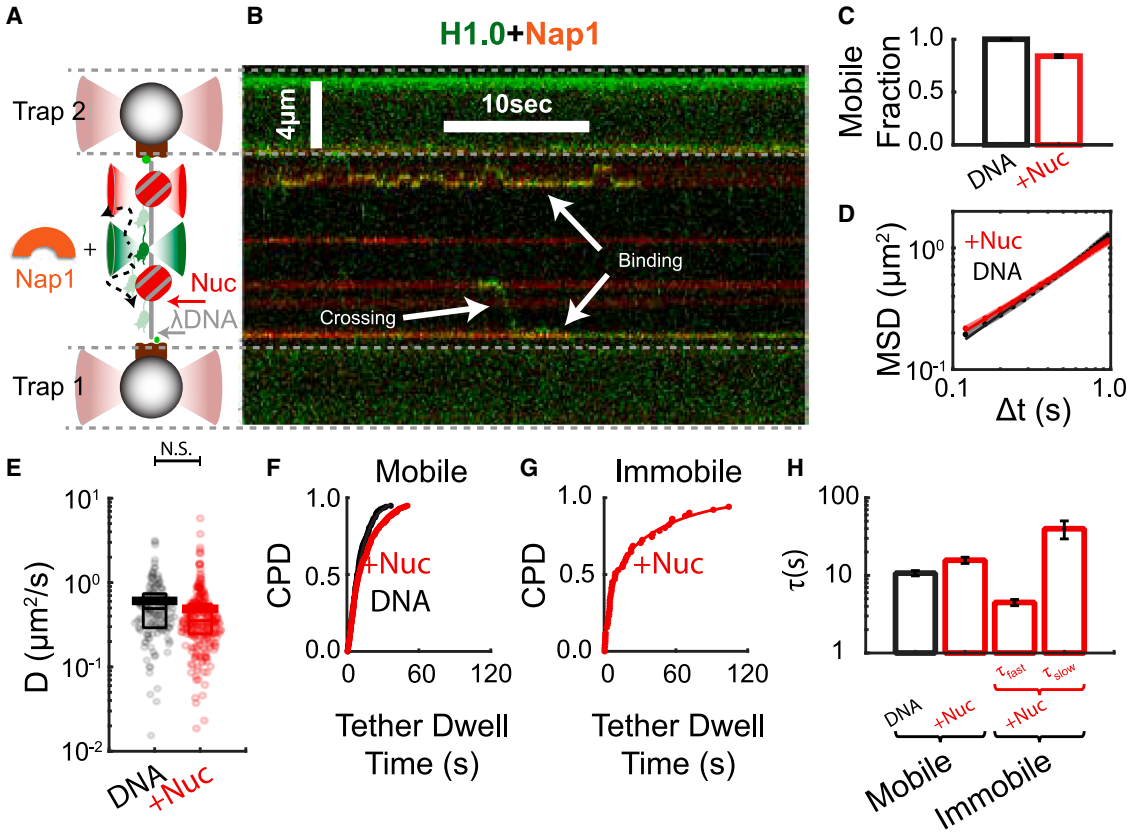


Figure 5. H1.0 dynamics on nucleosome-containing tethers in the presence of Nap1

(A) Illustration of the single-molecule experiment.

(B) Representative kymograph of H1.0 (green) bound to a nucleosome-containing tether in the presence of Nap1. Red indicates the locations of the nucleosomes. This kymograph is cropped from the original kymograph.

(C) Fraction of $H1.0_{Mobile}$ with Nap1 when bound to DNA-only (black) and nucleosome-containing (red) tethers.

(D) Average MSD versus time of $H1.0_{Mobile}$ on DNA-only (black) and nucleosome-containing (red) tethers.

(E) Diffusion coefficient violin plots for $H1.0_{Mobile}$ on DNA-only (black) and nucleosome-containing (red) tethers in the presence of Nap1. Solid lines indicate the mean. The center, bottom, and top marks of each box indicate the median, the 25th percentile, and the 75th percentile, respectively.

(F and G) Dwell time CPD for $H1.0_{Mobile}$ and $H1.0_{Immobile}$, respectively, bound to DNA-only (black) and nucleosome-containing (red, +Nuc) tethers in the presence of Nap1. Nap1 eliminated $H1.0_{immobile}$ on DNA-only tethers, so it is not included. The CPD of $H1.0_{Mobile}$ on DNA-only and +Nuc tethers fit best to single exponentials. The CPD of $H1.0_{Immobile}$ on +Nuc tethers fit best to a double exponential with $A_{fast} = 0.4 \pm 0.1$.

(H) Dwell times for $H1.0_{Mobile}$ and $H1.0_{Immobile}$ on DNA-only (black) and +Nuc (red) tethers with Nap1. All measurements were done at a constant force of 1 pN and 2 nM Nap1. Error bars denote standard error of the mean.

bound H1.0 was mobile (Figure 5C; Table S12). This is in stark contrast to the impact of 2 nM of Nap1 on H1.0 bound to DNA-only tethers, where all $H1.0_{Immobile}$ was eliminated, resulting in 100% $H1.0_{Mobile}$. We carried out similar studies of H1.0 on nucleosome-containing tethers with 10 μM ProTα, 100 nM sNASP, and 100 nM DNA_{30bp} (Figure S9), the maximum concentrations used in the measurements with DNA-only tethers. We find that a significant fraction of $H1.0_{Immobile}$ is observed on nucleosome-containing tethers in the presence of these additional chaperones (Figures S9C, S9P, and S9S; Table S8), while the $H1.0_{Immobile}$ fraction is largely suppressed on DNA-only tethers (Table S12). These observations that nucleosomes and linker histone chaperones in combination increase the fraction of immobile H1.0 suggest that linker histone chaperones promote H1.0-nucleosome interactions.

We further investigated the impact of these histone chaperones on H1.0 interactions with nucleosome-containing DNA tethers by determining the H1.0 dwell time CPD with each chaperone, which were compared to the dwell time CPDs of H1.0 bound to DNA-only tethers with each chaperone (Figures 5F and 5G) and the dwell time CPDs of H1.0 on nucleosome-containing tethers without a chaperone (Figures 2F and 2G). With 2 nM Nap1, the CPD for $H1.0_{Mobile}$ bound to nucleosome-containing tethers fit best with a single exponential with a $\tau = 16 \pm 1$s (Figures 5F–5H; Table S9), which is similar to the τ for $H1.0_{Mobile}$ on DNA-only tethers in the presence of Nap1 (Figures 4C and 4D; Table S13). The CPD of $H1.0_{Mobile}$ on nucleosome-containing tethers without Nap1 required two exponentials (Figure 2F), where τ_{slow} is similar to the τ on nucleosome-containing tethers with Nap1 (Table S9). We also determined the impact of other

histone chaperones on the dwell time CPD of $H1.0_{Mobile}$ on nucleosome-containing tethers (Figures S9F, S9H, S9N, S9P, S9V, and S9X; Table S9). CPD with 100 nM sNASP fits with a single exponential, while the CPDs with 10 μM ProTα and 100 nM DNA_{30bp} fit best with two exponentials. However, the dwell time τ with sNASP and the slow dwell times, τ_{slow}, with ProTα and DNA_{30bp} were within a factor of 2 of the $H1.0_{Mobile}$ dwell time without a histone chaperone. These results suggest that the dwell time distribution of $H1.0_{Mobile}$ on nucleosome-containing tethers is not drastically impacted by these histone chaperones.

We separately determined the dwell time CPD for $H1.0_{Immobile}$ on nucleosome-containing tethers in the presence of 2 nM Nap1, which fit best with 2 exponentials (τ_{fast}, τ_{fast}, and A_{fast} of 4 ± 1 s, 56 ± 4 s, and 48% ± 7%, respectively, Figures 5G and 5H). This is in stark contrast to our observation that Nap1 eliminates $H1.0_{Immobile}$ on DNA-only tethers (Figure 5C). Interestingly, these dwell times were similar to $H1.0_{Immobile}$ on nucleosome-containing tethers without Nap1 (Figures 2G–2I). We also determined the influence of 10 μM ProTα, 100 nM sNASP, and 100 nM DNA_{30bp} on the $H1.0_{Immobile}$ dwell time CPD. While the quantitative impact of these chaperones on dwell time distributions varies (Figures S9G, S9H, S9O, S9P, S9W, and S9X; Table S9), each chaperone introduces a fraction of $H1.0_{Immobile}$ dwell-time events (Table S8) that is significantly larger than the fraction of $H1.0_{Immobile}$ on DNA-only tethers (Table S12). Combined, these results reveal that, while the presence of nucleosomes did not dramatically impact the influence of chaperones on $H1.0_{Mobile}$, nucleosomes were required for a fraction of $H1.0_{Immobile}$ to form in the presence of linker histone chaperones.

Finally, based on our observation that $H1.0_{Immobile}$ preferentially binds nucleosomes directly (Figure 3C), we investigated the impact of linker histone chaperones on direct H1.0 binding to nucleosomes. In the presence of 2 nM Nap1, we compared the direct H1.0 binding to nucleosomes relative to binding at random positions within a DNA-only tether where the number of random positions is the same as the number of nucleosomes per tether (Figures 6A–6C). As we observed without Nap1, the fraction of $H1.0_{Mobile}$ colocalized with nucleosomes when first loaded onto the tether was similar to binding to random DNA positions (Figure 6C), suggesting that Nap1 does not facilitate the direct loading of $H1.0_{Mobile}$ onto nucleosomes. For direct colocalization of $H1.0_{Immobile}$ with nucleosomes, we find that 31% ± 4% of $H1.0_{Immobile}$ load directly onto nucleosomes, 35% ± 4% of $H1.0_{Immobile}$ load onto DNA and then colocalize with a nucleosome soon after loading, which is why they were categorized as immobile, and 33% ± 4% of $H1.0_{Immobile}$ are not co-localized with a nucleosome (Figures 6C and S10; Table S14). We observe similar fractions of $H1.0_{Immobile}$ with 10 μM ProTα, 100 nM sNASP, and 100 nM DNA_{30bp} (Figures S11A–S11C, S12A–S12C, and S13A–S13C; Table S14). These fractions of $H1.0_{Immobile}$ direct loading onto nucleosomes are within a factor of 2 of $H1.0_{Immobile}$ without a linker histone chaperone (Table S14). Since each histone chaperone largely eliminates $H1.0_{Immobile}$ on DNA-only tethers (Table S12), the $H1.0_{Immobile}$ that do not show colocalization with a Cy5-labeled nucleosome in the presence of a linker histone chaperone are likely to have colocalized with an unlabeled or photobleached nucleosome. Overall, these results indicate that linker histone chaperones enhance H1.0 targeting to nucleosomes by suppressing H1.0-DNA binding while maintaining direct H1.0 loading onto nucleosomes.

Linker histone chaperones enable the loading of mobile DNA-bound H1.0 onto nucleosomes through DNA sliding

Visual inspection of the kymographs of H1.0 bound to nucleosome-containing tethers revealed that, in the presence of each linker histone chaperone, H1.0 co-localizes to nucleosomes for many seconds and then co-localizes at an adjacent nucleosome through DNA sliding (Figures 5B, S9B, S9J, S9R, and S14A). To quantify this, we determined the CPD for H1.0-nucleosome co-localization times when 2 nM Nap1 is included (Figure 6D). With Nap1, the dwell-time CPD for H1.0 co-localization at nucleosomes was significantly extended compared to co-localization at random positions along DNA-only tethers (Figures 6D and S14B). The nucleosome co-localization dwell-time CPD fit best to a double exponential with τ_{fast} = 0.30 ± 0.01 s and τ_{slow} = 1.10 ± 0.04 s, while the dwell-time CPD at random DNA positions fit to a single exponential with a τ = 0.20 ± 0.01 s (Figure 6E). We also determined the CPD for H1.0-nucleosome co-localization time with either 10 μM ProTα, 100 nM sNASP, or 100 nM DNA_{30bp}. Again, we find that the presence of these linker histone chaperones significantly increased the H1.0-nucleosome co-localization times (Figures S11D, S11E, S12D, S12E, S13D, and S13E). These results indicate that these linker histone chaperones facilitate nucleosome loading of $H1.0_{Mobile}$ through DNA sliding.

We then determined for each colocalization event if H1.0 bound to, crossed over, reflected away, or dissociated from the nucleosome (Figures 6F and 6G). Using the criteria that H1.0-nucleosome co-localization events longer than 0.4 s were considered binding events, 2 nM Nap1 increased H1.0-nucleosome binding probability by ~3-fold as compared to random positions along DNA-only tethers (Figure 6H; Table S11). Since the localization of H1.0 and a nucleosome is diffraction limited, H1.0 could localize within the diffraction-limited distance of a nucleosome but not bind. In addition, 2 nM Nap1 increased the mobility of H1.0, resulting in a reduced number of dwell times at random points along DNA-only tethers that exceed the 0.4 s threshold (14% for H1.0 alone compared to 9% for H1.0 + Nap1). Therefore, the influence of Nap1 on H1.0 loading onto nucleosomes through DNA sliding was determined by comparing the binding probability between nucleosome-containing tethers and DNA-only tethers. With 2 nM Nap1, H1.0 binding to nucleosomes significantly increased (Figure 6H), while H1.0 continued to be more likely to reflect away from nucleosomes than cross over nucleosomes (compare Figure 6H with Figure 3H; Table S11). In addition, the DNA-only control indicated that Nap1 causes H1.0 to be biased toward continuing in the same direction instead of being equally likely to continue in the same direction or reverse directions (compare Figure 6H with Figure 3H; Table S11). We also determined the influence of the other linker histone chaperones, 10 μM ProTα, 100 nM sNASP, or 100 nM DNA_{30bp}. As with 2 nM Nap1, the fraction of H1.0-nucleosome binding was significantly increased by each chaperone, while H1.0 continued to reflect away from nucleosomes more frequently than crossing over nucleosomes (Figures S11H, S12H, and S13H; Table S11). In combination, these results revealed that linker histone chaperones facilitate the loading of

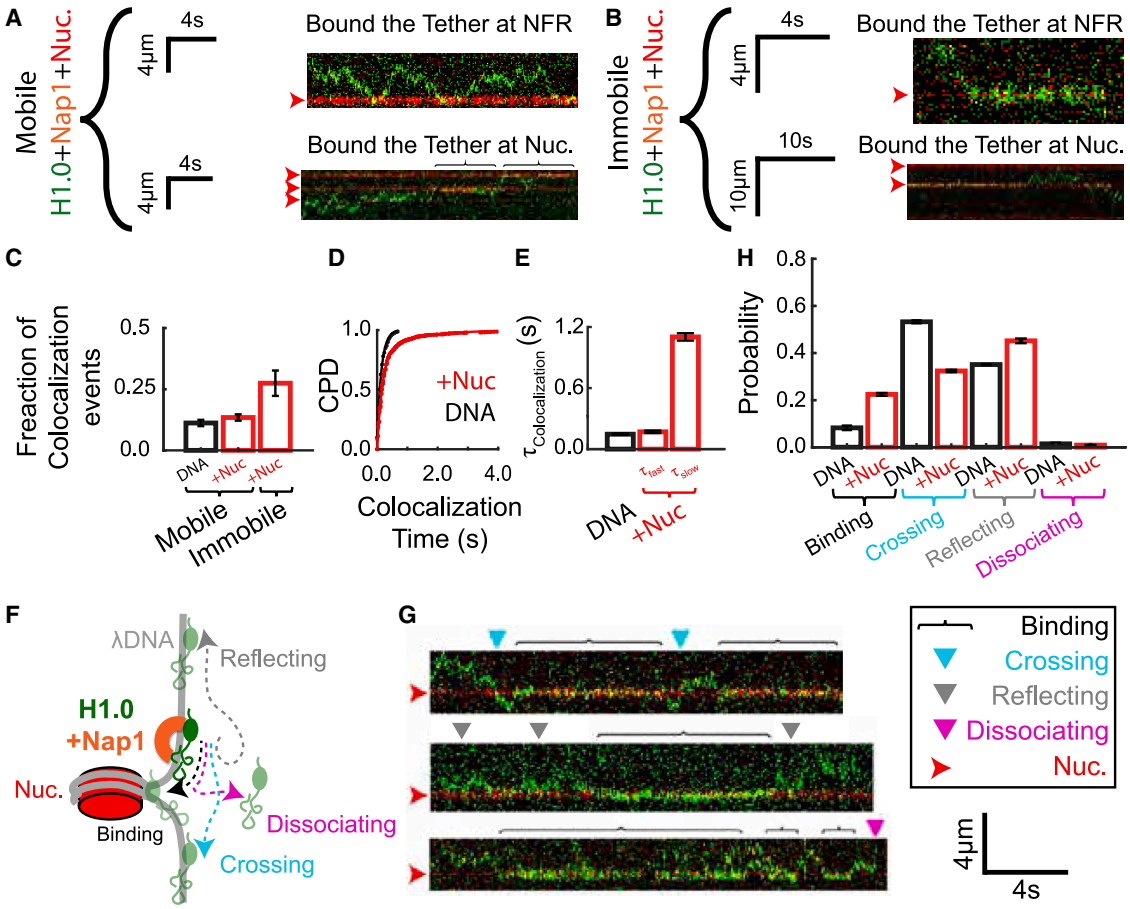


Figure 6. Nap1 facilitates the efficient loading of H1.0 onto nucleosomes

(A and B) Representative kymographs of (A) $H1.0_{Immobile}$ and (B) $H1.0_{Mobile}$ binding to a nucleosome-containing tether at an NFR and at a nucleosome with Nap1.

(C) With Nap1, the probability of an initial H1.0 binding event being colocalized with a nucleosome (+Nuc, red). This is compared to the probability of an initial H1.0 binding event being colocalized at random points along DNA-only tethers (DNA, black) with Nap1.

(D) With Nap1, the CPDs of $H1.0_{Mobile}$-nucleosome colocalization events (red) and of $H1.0_{mobile}$ colocalization events at random points along DNA-only tethers (black). The CPD at random positions on DNA-only tethers fit best to a single exponential, while the CPD at nucleosomes fit best to a double exponential.

(E) The colocalization dwell times, $\tau_{colocalization}$, from the exponential fits of the CPDs in (D).

(F) Illustration of the four possible outcomes following an $H1.0_{Mobile}$-nucleosome colocalization event: binding, crossing, reflecting, and dissociating.

(G) Representative kymographs of $H1.0_{Mobile}$ (green) on nucleosome-containing tethers. Dotted red lines indicate nucleosome locations.

(H) The probability of binding, crossing, reflecting, and dissociating for $H1.0_{Mobile}$-nucleosome colocalization events (red) and $H1.0_{Mobile}$ colocalization events at random points along DNA-only tethers (black). All measurements were done with 1pN constant force and 2 nM Nap1. The kymographs in (A), (B), and (G) are cropped from original kymographs. Error bars denote standard error of the mean.

$H1.0_{Mobile}$ onto nucleosomes by increasing the mobility of DNA-bound H1.0 and enabling H1.0 loading onto nucleosomes through DNA sliding.

Linker histone chaperones facilitate H1.0 loading into the dyad region of nucleosomes

While these co-localization measurements show linker histone chaperones facilitate H1.0 loading onto nucleosomes, they do not determine if H1.0 is bound in the nucleosome dyad region as resolved in structural studies.[16,28] To investigate if H1.0 is localized near the nucleosome dyad when bound, we utilized Förster resonance energy transfer (FRET) efficiency measurements between Cy3-labeled H1.0(S22C) and Cy5-labeled histone octamer at H2A(K119C) (Figure S15A). In a previous study, H1.0 binding to the nucleosome dyad region resulted in a significant increase in FRET efficiency.[47] The H1.0 kymographs were analyzed to quantify the Cy5 (acceptor) fluorescence and Cy3 (donor) fluorescence during H1.0-nucleosome binding events. To estimate the FRET efficiency, the acceptor fluorescence divided by the donor + acceptor fluorescence was used. We determined the average FRET efficiency for over 100 binding events separately with 2 nM Nap1, 10 μM ProTα, 100 nM sNASP, 100 nM DNA_{30bp}, and no chaperone (Figure S15B; Table S15). Nucleosome-bound H1.0 exhibited both low and high FRET states, suggesting that not all binding events involved H1.0 integrating near the nucleosome dyad, while the presence of linker histone chaperones did not impact the measured Cy5 fluorescence directly

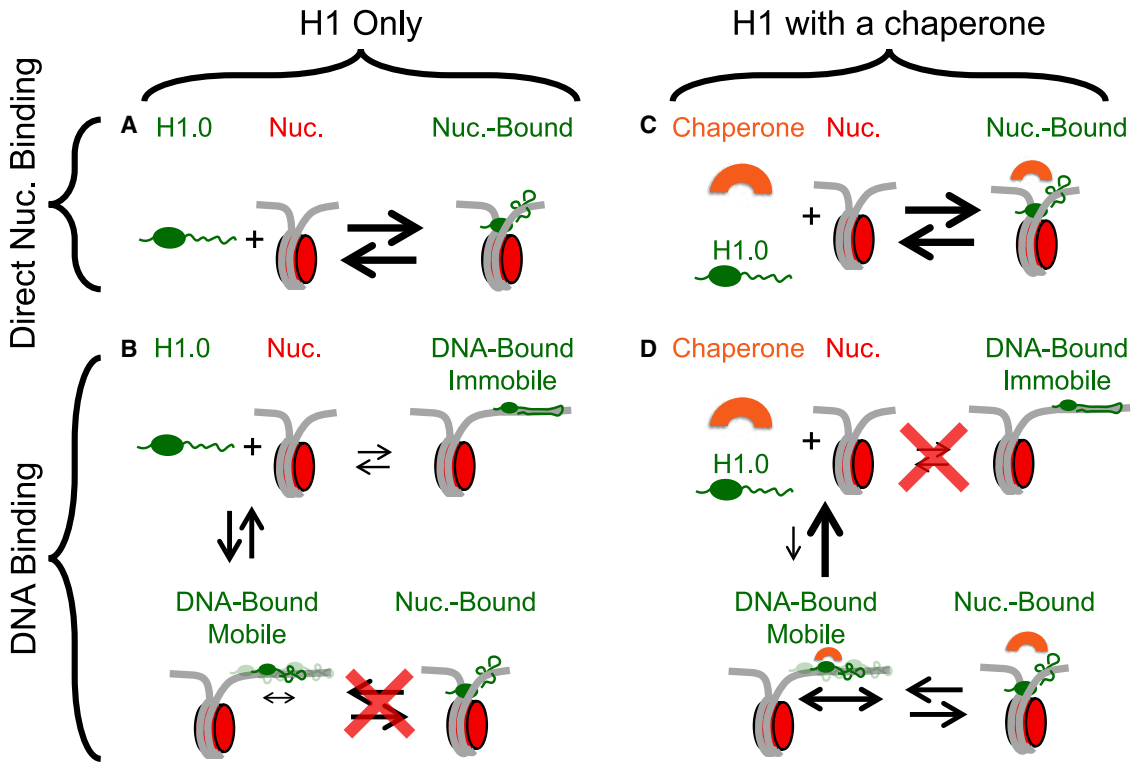


Figure 7. Model of H1.0 loading onto nucleosomes and how linker histone chaperones facilitate the loading pathways of H1.0

(A) In the absence of an H1 chaperone, H1.0 can directly load onto nucleosomes.

(B) In the absence of Nap1, H1.0 directly binds DNA, where the majority fraction is mobile on the DNA, while the minor fraction is immobile, but both are unable to load onto nucleosomes through DNA sliding.

(C) H1.0 direct loading onto nucleosomes is unaffected by Nap1.

(D) H1.0 loading onto DNA in the immobile state is eliminated by Nap1. H1.0 still loads onto DNA in a mobile state, but Nap1 lowers the binding rate and increases the dissociation rate. However, Nap1 increases the 1D mobility of H1.0 and facilitates H1.0 loading onto nucleosomes through DNA sliding.

(Figure S15G). However, each chaperone induced a significant increase in the average FRET efficiency between H1.0 and nucleosomes. In addition, representative time series of Cy3 and Cy5 fluorescence revealed anti-correlated changes in Cy3 and Cy5 fluorescence before and after H1.0-nucleosome colocalization events with high FRET efficiency (Figures S16–S20). These observations confirm that linker histone chaperones increase H1.0-nucleosome binding with high FRET efficiency. In combination, these results suggest that these chaperones facilitate near-dyad positioning of H1.0.

We considered the possibility that linker histone chaperones differentially impact H1.0 loading into the nucleosome dyad for loading directly or through DNA sliding. We separated binding events into direct nucleosome loading and binding through DNA sliding (Figures S15C–S15F). The average FRET efficiencies of H1.0 that loaded directly (Figures S15C and S15D) and through DNA sliding (Figures S15E and S15F) were significantly higher with each linker histone chaperone as compared to no chaperone (Table S16). Overall, these results reveal that in addition to linker histone chaperones enhancing H1.0 targeting to nucleosomes, they enhance H1.0 near-dyad loading, irrespective of the nucleosome loading pathway.

DISCUSSION

Using a single-molecule strategy that combines dual optical trapping with confocal fluorescence microscopy, we visualized and quantified the dynamics of H1.0 interactions with DNA and nucleosomes. We find that H1.0 alone preferentially targets nucleosomes over naked DNA by about 4-fold (Figure 7A) but does not efficiently load near the nucleosome dyad. Furthermore, while H1.0 does bind DNA strongly, where ~84% rapidly diffuses along DNA and encounters nucleosomes, H1.0 alone is unable to load onto nucleosomes through DNA sliding (Figure 7B). Instead, it preferentially reflects away from nucleosomes. These results suggest that H1.0 alone does not efficiently load onto nucleosomes. However, linker histone chaperones appear to help H1.0 load onto nucleosomes by four separate mechanisms. (1) They suppress H1.0 binding to DNA without impacting H1.0 direct binding to nucleosomes (Figures 7C and 7D). (2) They enhance H1.0 mobility along DNA, allowing H1.0 to repeatedly encounter nucleosomes (Figure 7D). (3) They facilitate H1.0 loading onto nucleosomes through DNA sliding, providing an additional pathway for nucleosome loading (Figure 7D). (4) They increase H1.0 near-dyad binding so that it is properly loaded onto nucleosomes (Figures S15–S20). Most

likely, chaperones carry out these functions by directly interacting with linker histones. This hypothesis is supported by our observation that linker histone chaperones appear to suppress H1.0 oligomerization, which converts immobile to mobile H1.0. Given that linker histone chaperones and C-terminal tail truncations of H1.0 reduce oligomerization and increase H1.0 mobility, we suspect that histone chaperones interact with the C-terminal tail of H1.0. These mechanisms of H1.0 loading onto nucleosomes are likely important for how H1.0 suppresses DNA accessibility through reducing nucleosome partial unwrapping and enhancing chromatin compaction. Future studies will be important to investigate the precise basis of chaperone-linker histone interactions.

These findings reveal that H1.0, in combination with a histone chaperone, uses multiple pathways for H1.0 targeting and loading onto nucleosomes. While there has been significant progress in understanding the interactions H1 makes with dyad and linker DNA,[61] less is known about the pathway(s) for H1 loading onto nucleosomes. Previous work proposed that H1 interactions with linker DNA are important for linker histone loading.[12,62] Our studies reveal that linker histones can load onto nucleosomes directly and through first interacting with linker DNA followed by sliding onto the nucleosome (Figure 7). However, the second pathway is enhanced by linker histone chaperones.

Importantly, our finding that Nap1 carries out the above linker histone chaperone functions at substoichiometric concentrations relative to H1.0, while ProTα and sNASP require orders of magnitude higher concentrations as does the DNA_{30bp} control, reveals that Nap1 regulation of H1.0 is more specific than ProTα and sNASP. A comparison of dwell-time distributions (Figures 2F–2I, S3D, S3E, S8C, S8D, S8I, and S8J; Tables S3 and S13) indicates that increasing NaCl from 20 to 200 mM results in a similar ~3-fold change in H1.0-DNA dwell times to the addition of 2 nM Nap1, 10 μM ProTα, and 100 nM sNASP. Consequently, these chaperone concentrations achieve a similar screening effect as increasing NaCl by ~180 mM. Treating the chaperones as competitive ligands that displace the same number of counter ions, the 5,000- and 50-fold concentration difference corresponds to a specificity free-energy advantage of $\Delta\Delta G = \sim 5$ and 2.3 kcal/mol for Nap1 over ProTα and sNASP, respectively. This substantial energetic preference suggests that Nap1 functions through targeted molecular recognition, while ProTα and sNASP function through generic polyelectrolyte screening.

Previous single-molecule studies have provided important insight into H1.0 interactions with DNA and nucleosomes. A single-molecule total internal reflection fluorescence study showed H1.0 remained bound to DNA and nucleosomes for minutes.[37] A single-molecule optical trapping study that focused on the interactions of the DNA methyltransferase MeCP2 with DNA and nucleosomes included data showing that the linker histone H1.4 diffuses along DNA.[63] In addition, Nap1 facilitated dissociation of H1.0 from DNA and super-stoichiometric bound H1.0 from nucleosomes.[37] These studies are consistent with our findings. A separate single-molecule force-fluorescence study investigated the dynamic coalescence of H1.4 along single-stranded DNA that was induced by force. They find that H1.4 localizes at the junction between duplex and single-stranded DNA,[64] which could be important for linker histone-facilitated genome condensate formation. Comparison of this complementary study with ours suggests there are likely multiple mechanisms by which linker histones interact with chromatin to regulate genome accessibility.

In vivo, nucleosomes are spaced with linker DNA lengths of 30–60 bp.[65] However, our study investigated H1.0 interactions with nucleosomes that are spaced by kilobases, allowing the dynamics of individual linker histones and nucleosomes to be visualized and quantified. The physiological density of nucleosomes will likely increase the probability of direct loading onto nucleosomes, while decreasing the distance along the DNA that H1.0 must diffuse to encounter a nucleosome. We anticipate that H1.0 loading within chromatin *in vivo* will be more efficient through both nucleosome loading pathways.

The findings here provide a foundation for further investigating the role of linker histones in regulating genome accessibility. For example, determining the dynamics of the 11 human linker histone isoforms[13] with DNA and chromatin, and the pathways used for loading onto nucleosomes, will be important for understanding how different linker histone isoforms are targeted to chromatin and differentially regulate genome accessibility. In addition, understanding how linker histone chaperones with very different H1.0 specificities function distinctly or synergistically will be important for understanding how they regulate the pathways for H1.0 loading onto chromatin. Finally, both linker and core histones are significantly post-translationally modified (PTM), which is important for genome function and disease. Building off these findings to determine the influence of histone PTMs on linker histone dynamics and loading pathways is an important future research direction.

Limitations of the study

This study did not directly visualize the linker histone chaperone Nap1. Therefore, the mechanisms by which this linker histone chaperone influences H1.0 interactions with DNA and nucleosomes, and facilitates H1.0 loading onto nucleosomes, were not determined. Future quantitative studies will be important to determine the mechanisms behind how linker histone chaperones regulate the proper loading of linker H1 onto nucleosomes.

RESOURCE AVAILABILITY

Lead contact

Further information and request for resources and reagents should be directed to, and will be fulfilled by, the lead contact, Michael G. Poirier (poirier.18@osu.edu).

Materials availability

Unique and stable reagents generated in this study are available upon request.

Data and code availability

- Original single-molecule data files are deposited online and made publicly available (doi: 10.5281/zenodo.21924344 and 10.5281/zenodo.22211598).
- Customized MATLAB scripts used for single-molecule data analysis are deposited online and made publicly available (doi: 10.5281/zenodo.22149059).
- Additional information required for reanalysis of single-molecule traces reported in this paper is available from the lead contact upon request.

ACKNOWLEDGMENTS

The authors acknowledge the feedback and insights provided by the Poirier Lab members and the members of the LUMICKS team. We are grateful to Stefan Dimitrov for the mouse Nap1 expression vector. We are grateful to Mark Parthun for the sNASP expression vector. We would like to acknowledge the staff at the Nanosystems Laboratory at the Ohio State University Department of Physics. Partial funding for shared facilities used in this research was provided by the Center for Emergent Materials: an NSF MRSEC, under award number DMR-2011876. Support for the LUMICKS C-Trap was provided by The National Institutes of Health (S10OD028705 to M.G.P.). This work was funded by the National Institutes of Health (R35 GM139564 to M.G.P.); National Science Foundation (MCB 2411725 to M.G.P.); funding for open access charge was provided by National Institutes of Health R35 GM139564.

AUTHOR CONTRIBUTIONS

E.A. and M.G.P. conceived the experiments. E.A. wrote the original draft with input from M.G.P. M.G.P. and B.S. edited the manuscript. E.A. performed single-molecule and ensemble experiments. E.A. carried out the data analysis with feedback and guidance from M.G.P. and B.S. E.A., N.L.B., M.V., and A.C. prepared all the samples. M.G.P. supervised and obtained funding for the experiments.

DECLARATION OF INTERESTS

The authors declare no competing interests.

STAR★METHODS

Detailed methods are provided in the online version of this paper and include the following:

- KEY RESOURCES TABLE
- EXPERIMENTAL MODEL AND STUDY PARTICIPANT DETAILS
  - Bacteria strains
- METHOD DETAILS
  - H1 Expression and Purification
  - H1.0 Labeling
  - H1.0 Concentration Determination
  - Histone Octamer Preparation and Labeling
  - Nap1 Expression and Purification
  - sNASP Expression and Purification
  - Prothymosin-α Expression and Purification
  - DNA Preparation and Purification
  - Lambda Tether Preparation
  - Nucleosome Preparation and Validation
  - Dual optical tweezers and fluorescence confocal imaging experimental system
- QUANTIFICATION AND STATISTICAL ANALYSIS
  - H1.0 single-molecule tracking and data analysis
  - Statistical analysis

SUPPLEMENTAL INFORMATION

Supplemental information can be found online at https://doi.org/10.1016/j.molcel.2026.09.001.

Received: March 10, 2025
Revised: July 10, 2026
Accepted: September 1, 2026
Published: September 22, 2026

REFERENCES

1. Luger, K., Mäder, A.W., Richmond, R.K., Sargent, D.F., and Richmond, T.J. (1997). Crystal structure of the nucleosome core particle at 2.8 Å resolution. Nature *389*, 251–260. https://doi.org/10.1038/38444.
2. Kornberg, R.D. (1974). Chromatin Structure: A Repeating Unit of Histones and DNA. Science *184*, 868–871. https://doi.org/10.1126/science.184.4139.868.
3. Kornberg, R.D. (1977). Structure of chromatin. Annu. Rev. Biochem. *46*, 931–954. https://doi.org/10.1146/annurev.bi.46.070177.004435.
4. Saha, A., and Dalal, Y. (2021). A glitch in the snitch: the role of linker histone H1 in shaping the epigenome in normal and diseased cells. Open Biol. *11*, 210124. https://doi.org/10.1098/rsob.210124.
5. Soshnev, A.A., Allis, C.D., Cesarman, E., and Melnick, A.M. (2021). Histone H1 Mutations in Lymphoma: A Link(er) between Chromatin Organization, Developmental Reprogramming, and Cancer. Cancer Res. *81*, 6061–6070. https://doi.org/10.1158/0008-5472.CAN-21-2619.
6. Bates, D.L., and Thomas, J.O. (1981). Histories H1 and H5: one or two molecules per nucleosome? Nucleic Acids Res. *9*, 5883–5894. https://doi.org/10.1093/nar/9.22.5883.
7. Cutter, A.R., and Hayes, J.J. (2015). A brief review of nucleosome structure. FEBS Lett. *589*, 2914–2922. https://doi.org/10.1016/j.febslet.2015.05.016.
8. Hansen, J.C. (2002). Conformational dynamics of the chromatin fiber in solution: determinants, mechanisms, and functions. Annu. Rev. Biophys. Biomol. Struct. *31*, 361–392. https://doi.org/10.1146/annurev.biophys.31.101101.140858.
9. Allan, J., Mitchell, T., Harborne, N., Bohm, L., and Crane-Robinson, C. (1986). Roles of H1 domains in determining higher order chromatin structure and H1 location. J. Mol. Biol. *187*, 591–601. https://doi.org/10.1016/0022-2836(86)90337-2.
10. Lever, M.A., Th'ng, J.P., Sun, X., and Hendzel, M.J. (2000). Rapid exchange of histone H1.1 on chromatin in living human cells. Nature *408*, 873–876. https://doi.org/10.1038/35048603.
11. Misteli, T., Gunjan, A., Hock, R., Bustin, M., and Brown, D.T. (2000). Dynamic binding of histone H1 to chromatin in living cells. Nature *408*, 877–881. https://doi.org/10.1038/35048610.
12. Catez, F., Ueda, T., and Bustin, M. (2006). Determinants of histone H1 mobility and chromatin binding in living cells. Nat. Struct. Mol. Biol. *13*, 305–310. https://doi.org/10.1038/nsmb1077.
13. Happel, N., and Doenecke, D. (2009). Histone H1 and its isoforms: contribution to chromatin structure and function. Gene *431*, 1–12. https://doi.org/10.1016/j.gene.2008.11.003.
14. Hergeth, S.P., and Schneider, R. (2015). The H1 linker histones: multifunctional proteins beyond the nucleosomal core particle. EMBO Rep. *16*, 1439–1453. https://doi.org/10.15252/embr.201540749.
15. Allan, J., Hartman, P.G., Crane-Robinson, C., and Aviles, F.X. (1980). The structure of histone H1 and its location in chromatin. Nature *288*, 675–679. https://doi.org/10.1038/288675a0.
16. Bednar, J., Garcia-Saez, I., Boopathi, R., Cutter, A.R., Papai, G., Reymer, A., Syed, S.H., Lone, I.N., Tonchev, O., Crucifix, C., et al. (2017). Structure and dynamics of a 197 bp nucleosome in complex with linker histone H1. Mol. Cell *66*, 384–397.e8. https://doi.org/10.1016/j.molcel.2017.04.012.
17. Syed, S.H., Goutte-Gattat, D., Becker, N., Meyer, S., Shukla, M.S., Hayes, J.J., Everaers, R., Angelov, D., Bednar, J., and Dimitrov, S. (2010). Single-base resolution mapping of H1-nucleosome interactions and 3D organization of the nucleosome. Proc. Natl. Acad. Sci. USA *107*, 9620–9625. https://doi.org/10.1073/pnas.1000309107.
18. Zhou, B.R., Jiang, J., Feng, H., Ghirlando, R., Xiao, T.S., and Bai, Y. (2015). Structural Mechanisms of Nucleosome Recognition by Linker Histones. Mol. Cell *59*, 628–638. https://doi.org/10.1016/j.molcel.2015.06.025.

19. Fang, H., Clark, D.J., and Hayes, J.J. (2012). DNA and nucleosomes direct distinct folding of a linker histone H1 C-terminal domain. Nucleic Acids Res. *40*, 1475–1484. https://doi.org/10.1093/nar/gkr866.

20. Fang, H., Wei, S., Lee, T.H., and Hayes, J.J. (2016). Chromatin structure-dependent conformations of the H1 CTD. Nucleic Acids Res. *44*, 9131–9141. https://doi.org/10.1093/nar/gkw586.

21. Das, S.K., Kumar, A., Hao, F., Cutter DiPiazza, A.R., Fang, H., Lee, T.H., and Hayes, J.J. (2023). Histone H3 Tail Modifications Alter Structure and Dynamics of the H1 C-Terminal Domain Within Nucleosomes. J. Mol. Biol. *435*, 168242. https://doi.org/10.1016/j.jmb.2023.168242.

22. Heidarsson, P.O., Mercadante, D., Sottini, A., Nettels, D., Borgia, M.B., Borgia, A., Kilic, S., Fierz, B., Best, R.B., and Schuler, B. (2022). Release of linker histone from the nucleosome driven by polyelectrolyte competition with a disordered protein. Nat. Chem. *14*, 224–231. https://doi.org/10.1038/s41557-021-00839-3.

23. Turner, A.L., Watson, M., Wilkins, O.G., Cato, L., Travers, A., Thomas, J.O., and Stott, K. (2018). Highly disordered histone H1-DNA model complexes and their condensates. Proc. Natl. Acad. Sci. USA *115*, 11964–11969. https://doi.org/10.1073/pnas.1805943115.

24. Sridhar, A., Farr, S.E., Portella, G., Schlick, T., Orozco, M., and Collepardo-Guevara, R. (2020). Emergence of chromatin hierarchical loops from protein disorder and nucleosome asymmetry. Proc. Natl. Acad. Sci. USA *117*, 7216–7224. https://doi.org/10.1073/pnas.1910044117.

25. Wu, H., Dalal, Y., and Papoian, G.A. (2021). Binding Dynamics of Disordered Linker Histone H1 with a Nucleosomal Particle. J. Mol. Biol. *433*, 166881. https://doi.org/10.1016/j.jmb.2021.166881.

26. Clark, D.J., and Thomas, J.O. (1988). Differences in the binding of H1 variants to DNA. Cooperativity and linker-length related distribution. Eur. J. Biochem. *178*, 225–233. https://doi.org/10.1111/j.1432-1033.1988.tb14447.x.

27. Clark, D.J., and Thomas, J.O. (1986). Salt-dependent co-operative interaction of histone H1 with linear DNA. J. Mol. Biol. *187*, 569–580. https://doi.org/10.1016/0022-2836(86)90335-9.

28. Zhou, B.R., Feng, H., Kale, S., Fox, T., Khant, H., de Val, N., Ghirlando, R., Panchenko, A.R., and Bai, Y. (2021). Distinct Structures and Dynamics of Chromatosomes with Different Human Linker Histone Isoforms. Mol. Cell *81*, 166–182.e6. https://doi.org/10.1016/j.molcel.2020.10.038.

29. Gurard-Levin, Z.A., Quivy, J.P., and Almouzni, G. (2014). Histone chaperones: assisting histone traffic and nucleosome dynamics. Annu. Rev. Biochem. *83*, 487–517. https://doi.org/10.1146/annurev-biochem-060713-035536.

30. Miller, K.E., and Heald, R. (2015). Glutamylation of Nap1 modulates histone H1 dynamics and chromosome condensation in Xenopus. J. Cell Biol. *209*, 211–220. https://doi.org/10.1083/jcb.201412097.

31. Bernier, M., Luo, Y., Nwokelo, K.C., Goodwin, M., Dreher, S.J., Zhang, P., Parthun, M.R., Fondufe-Mittendorf, Y., Ottesen, J.J., and Poirier, M.G. (2015). Linker histone H1 and H3K56 acetylation are antagonistic regulators of nucleosome dynamics. Nat. Commun. *6*, 10152. https://doi.org/10.1038/ncomms10152.

32. Shintomi, K., Iwabuchi, M., Saeki, H., Ura, K., Kishimoto, T., and Ohsumi, K. (2005). Nucleosome assembly protein-1 is a linker histone chaperone in Xenopus eggs. Proc. Natl. Acad. Sci. USA *102*, 8210–8215. https://doi.org/10.1073/pnas.0500822102.

33. Karetsou, Z., Sandaltzopoulos, R., Frangou-Lazaridis, M., Lai, C.Y., Tsolas, O., Becker, P.B., and Papamarcaki, T. (1998). Prothymosin alpha modulates the interaction of histone H1 with chromatin. Nucleic Acids Res. *26*, 3111–3118. https://doi.org/10.1093/nar/26.13.3111.

34. Gomez-Marquez, J., and Rodríguez, P. (1998). Prothymosin alpha is a chromatin-remodelling protein in mammalian cells. Biochem. J. *333*, 1–3. https://doi.org/10.1042/bj3330001.

35. Richardson, R.T., Alekseev, O.M., Grossman, G., Widgren, E.E., Thresher, R., Wagner, E.J., Sullivan, K.D., Marzluff, W.F., and O'Rand, M.G. (2006). Nuclear autoantigenic sperm protein (NASP), a linker histone chaperone that is required for cell proliferation. J. Biol. Chem. *281*, 21526–21534. https://doi.org/10.1074/jbc.M603816200.

36. Finn, R.M., Browne, K., Hodgson, K.C., and Ausió, J. (2008). sNASP, a histone H1-specific eukaryotic chaperone dimer that facilitates chromatin assembly. Biophys. J. *95*, 1314–1325. https://doi.org/10.1529/biophysj.108.130021.

37. Yue, H., Fang, H., Wei, S., Hayes, J.J., and Lee, T.H. (2016). Single-Molecule Studies of the Linker Histone H1 Binding to DNA and the Nucleosome. Biochemistry *55*, 2069–2077. https://doi.org/10.1021/acs.biochem.5b01247.

38. Kepert, J.F., Mazurkiewicz, J., Heuvelman, G.L., Tóth, K.F., and Rippe, K. (2005). NAP1 modulates binding of linker histone H1 to chromatin and induces an extended chromatin fiber conformation. J. Biol. Chem. *280*, 34063–34072. https://doi.org/10.1074/jbc.M507322200.

39. Papamarcaki, T., and Tsolas, O. (1994). Prothymosin alpha binds to histone H1 in vitro. FEBS Lett. *345*, 71–75. https://doi.org/10.1016/0014-5793(94)00439-0.

40. Richardson, R.T., Batova, I.N., Widgren, E.E., Zheng, L.X., Whitfield, M., Marzluff, W.F., and O'Rand, M.G. (2000). Characterization of the histone H1-binding protein, NASP, as a cell cycle-regulated somatic protein. J. Biol. Chem. *275*, 30378–30386. https://doi.org/10.1074/jbc.M003781200.

41. Wang, H., Ge, Z., Walsh, S.T.R., and Parthun, M.R. (2012). The human histone chaperone sNASP interacts with linker and core histones through distinct mechanisms. Nucleic Acids Res. *40*, 660–669. https://doi.org/10.1093/nar/gkr781.

42. Laskey, R.A., Honda, B.M., Mills, A.D., and Finch, J.T. (1978). Nucleosomes are assembled by an acidic protein which binds histones and transfers them to DNA. Nature *275*, 416–420. https://doi.org/10.1038/275416a0.

43. Ito, T., Ikehara, T., Nakagawa, T., Kraus, W.L., and Muramatsu, M. (2000). p300-mediated acetylation facilitates the transfer of histone H2A-H2B dimers from nucleosomes to a histone chaperone. Genes Dev. *14*, 1899–1907. https://doi.org/10.1101/gad.14.15.1899.

44. Chen, X., D'Arcy, S., Radebaugh, C.A., Krzizike, D.D., Giebler, H.A., Huang, L., Nyborg, J.K., Luger, K., and Stargell, L.A. (2016). Histone Chaperone Nap1 Is a Major Regulator of Histone H2A-H2B Dynamics at the Inducible GAL Locus. Mol. Cell. Biol. *36*, 1287–1296. https://doi.org/10.1128/MCB.00835-15.

45. Cook, A.J.L., Gurard-Levin, Z.A., Vassias, I., and Almouzni, G. (2011). A specific function for the histone chaperone NASP to fine-tune a reservoir of soluble H3-H4 in the histone supply chain. Mol. Cell *44*, 918–927. https://doi.org/10.1016/j.molcel.2011.11.021.

46. Mishra, L.N., and Hayes, J.J. (2018). A nucleosome-free region locally abrogates histone H1-dependent restriction of linker DNA accessibility in chromatin. J. Biol. Chem. *293*, 19191–19200. https://doi.org/10.1074/jbc.RA118.005721.

47. Burge, N.L., Thuma, J.L., Hong, Z.Z., Jamison, K.B., Ottesen, J.J., and Poirier, M.G. (2022). H1.0 C Terminal Domain Is Integral for Altering Transcription Factor Binding within Nucleosomes. Biochemistry *61*, 625–638. https://doi.org/10.1021/acs.biochem.2c00001.

48. Heller, I., Sitters, G., Broekmans, O.D., Biebricher, A.S., Wuite, G.J.L., and Peterman, E.J.G. (2014). Mobility analysis of super-resolved proteins on optically stretched DNA: comparing imaging techniques and parameters. ChemPhysChem *15*, 727–733. https://doi.org/10.1002/cphc.201300813.

49. Heller, I., Hoekstra, T.P., King, G.A., Peterman, E.J.G., and Wuite, G.J.L. (2014). Optical tweezers analysis of DNA-protein complexes. Chem. Rev. *114*, 3087–3119. https://doi.org/10.1021/cr4003006.

50. Newton, M.D., Taylor, B.J., Driessen, R.P.C., Roos, L., Cvetesic, N., Allyjaun, S., Lenhard, B., Cuomo, M.E., and Rueda, D.S. (2019). DNA stretching induces Cas9 off-target activity. Nat. Struct. Mol. Biol. *26*, 185–192. https://doi.org/10.1038/s41594-019-0188-z.

51. Marko, J.F., and Siggia, E.D. (1995). Stretching DNA. Macromolecules *28*, 8759–8770. https://doi.org/10.1021/ma00130a008.

52. Luo, Y., North, J.A., and Poirier, M.G. (2014). Single molecule fluorescence methodologies for investigating transcription factor binding kinetics to nucleosomes and DNA. Methods *70*, 108–118. https://doi.org/10.1016/j.ymeth.2014.09.011.

53. Rudnizky, S., Khamis, H., Malik, O., Melamed, P., and Kaplan, A. (2019). The base pair-scale diffusion of nucleosomes modulates binding of transcription factors. Proc. Natl. Acad. Sci. USA *116*, 12161–12166. https://doi.org/10.1073/pnas.1815424116.

54. Saxton, M.J. (2020). Diffusion of DNA-Binding Species in the Nucleus: A Transient Anomalous Subdiffusion Model. Biophys. J. *118*, 2151–2167. https://doi.org/10.1016/j.bpj.2020.03.015.

55. Metzler, R., and Klafter, J. (2000). The random walk's guide to anomalous diffusion: a fractional dynamics approach. Phys. Rep. *339*, 1–77. https://doi.org/10.1016/S0370-1573(00)00070-3.

56. Carcamo, C.C., Poyton, M.F., Ranjan, A., Park, G., Louder, R.K., Feng, X.A., Kim, J.M., Dzu, T., Wu, C., and Ha, T. (2022). ATP binding facilitates target search of SWR1 chromatin remodeler by promoting one-dimensional diffusion on DNA. eLife *11*, e77352. https://doi.org/10.7554/eLife.77352.

57. Holmstrom, E.D., Liu, Z., Nettels, D., Best, R.B., and Schuler, B. (2019). Disordered RNA chaperones can enhance nucleic acid folding via local charge screening. Nat. Commun. *10*, 2453. https://doi.org/10.1038/s41467-019-10356-0.

58. Record, M.T., Jr., Anderson, C.F., and Lohman, T.M. (1978). Thermodynamic analysis of ion effects on the binding and conformational equilibria of proteins and nucleic acids: the roles of ion association or release, screening, and ion effects on water activity. Q. Rev. Biophys. *11*, 103–178. https://doi.org/10.1017/s003358350000202x.

59. Kim, J.M., Carcamo, C.C., Jazani, S., Xie, Z.P., Feng, X.A., Yamadi, M., Poyton, M., Holland, K.L., Grimm, J.B., Lavis, L.D., et al. (2024). Dynamic 1D search and processive nucleosome translocations by RSC and ISW2 chromatin remodelers. eLife *12*, RP91433. https://doi.org/10.7554/eLife.91433.

60. Mihardja, S., Spakowitz, A.J., Zhang, Y., and Bustamante, C. (2006). Effect of force on mononucleosomal dynamics. Proc. Natl. Acad. Sci. USA *103*, 15871–15876. https://doi.org/10.1073/pnas.0607526103.

61. Chen, P., Li, W., and Li, G. (2021). Structures and Functions of Chromatin Fibers. Annu. Rev. Biophys. *50*, 95–116. https://doi.org/10.1146/annurev-biophys-062920-063639.

62. Brown, D.T., Izard, T., and Misteli, T. (2006). Mapping the interaction surface of linker histone H1(0) with the nucleosome of native chromatin in vivo. Nat. Struct. Mol. Biol. *13*, 250–255. https://doi.org/10.1038/nsmb1050.

63. Chua, G.N.L., Watters, J.W., Olinares, P.D.B., Begum, M., Vostal, L.E., Luo, J.A., Chait, B.T., and Liu, S. (2024). Differential dynamics specify MeCP2 function at nucleosomes and methylated DNA. Nat. Struct. Mol. Biol. *31*, 1789–1797. https://doi.org/10.1038/s41594-024-01373-9.

64. Leicher, R., Osunsade, A., Chua, G.N.L., Faulkner, S.C., Latham, A.P., Watters, J.W., Nguyen, T., Beckwitt, E.C., Christodoulou-Rubalcava, S., Young, P.G., et al. (2022). Single-stranded nucleic acid binding and coacervation by linker histone H1. Nat. Struct. Mol. Biol. *29*, 463–471. https://doi.org/10.1038/s41594-022-00760-4.

65. Valouev, A., Johnson, S.M., Boyd, S.D., Smith, C.L., Fire, A.Z., and Sidow, A. (2011). Determinants of nucleosome organization in primary human cells. Nature *474*, 516–520. https://doi.org/10.1038/nature10002.

66. Wang, H., Walsh, S.T.R., and Parthun, M.R. (2008). Expanded binding specificity of the human histone chaperone NASP. Nucleic Acids Res. *36*, 5763–5772. https://doi.org/10.1093/nar/gkn574.

67. Gast, K., Damaschun, H., Eckert, K., Schulze-Forster, K., Maurer, H.R., Müller-Frohne, M., Zirwer, D., Czarnecki, J., and Damaschun, G. (1995). Prothymosin alpha: a biologically active protein with random coil conformation. Biochemistry *34*, 13211–13218. https://doi.org/10.1021/bi00040a037.

68. Chowdhury, A., Borgia, A., Ghosh, S., Sottini, A., Mitra, S., Eapen, R.S., Borgia, M.B., Yang, T., Galvanetto, N., Ivanović, M.T., et al. (2023). Driving forces of the complex formation between highly charged disordered proteins. Proc. Natl. Acad. Sci. USA *120*, e2304036120. https://doi.org/10.1073/pnas.2304036120.

69. Lowary, P.T., and Widom, J. (1998). New DNA sequence rules for high affinity binding to histone octamer and sequence-directed nucleosome positioning. J. Mol. Biol. *276*, 19–42. https://doi.org/10.1006/jmbi.1997.1494.

70. Luger, K., Rechsteiner, T.J., and Richmond, T.J. (1999). Preparation of nucleosome core particle from recombinant histones. In Methods in Enzymology, *304* (Elsevier), pp. 3–19. https://doi.org/10.1016/S0076-6879(99)04003-3.

71. Vestergaard, C.L., Blainey, P.C., and Flyvbjerg, H. (2014). Optimal estimation of diffusion coefficients from single-particle trajectories. Phys. Rev. E Stat. Nonlin. Soft Matter Phys. *89*, 022726. https://doi.org/10.1103/PhysRevE.89.022726.

STAR★METHODS

KEY RESOURCES TABLE

REAGENT or RESOURCE	SOURCE	IDENTIFIER
Bacterial and virus strains		
BL21(DE3) pLysS Chemically Competent E. Coli	Invitrogen	Cat#C606010
Rosetta 2(DE3) Singles Competent Cells	Novagen	Cat#71400-3
BL21(DE3) Chemically Competent E. Coli	Invitrogen	Cat#C600003
Chemicals, peptides, and recombinant proteins		
Human H2A K119C Histone	The Histone Source	SKU HH2A_K119C
Human H2B Histone	The Histone Source	SKU HH2B
Xenopus H3 C110A Histone	The Histone Source	SKU XH3_C110A
Xenopus H4 Histone	The Histone Source	SKU XH4
Human H1.0 and H1.0 with truncated C-Terminus Domains	In House	N/A
Mouse Nap1	In House	N/A
Human sNASP	In House	N/A
Human ProTα	In House	N/A
Critical commercial assays		
Gen-Pak FAX anion-exchange Column	Waters	Cat#WAT015490
Superdex 200 Increase 10/300 GL	Cytiva	Cat#28990944
Amicon 30K filters	Millipore	Cat#UFC201024
Amicon 3K filters	Millipore	Cat#UFC500324
C10/10 Column	Cytiva	Cat#19500101
Biorex70 50-100 Resin	Bio-Rad	Cat#1435832
Biorex70 100-200 Resin	Bio-Rad	Cat#1425842
Pierce Modified Lowry Assay	ThermoFisher Scientific	Cat#23240
HisTrap™ HP His tag protein purification columns	Cytiva	Cat#17524801
HiRes ion exchange chromatography Column	Cytiva	Cat#29275877
Ni Sepharose™ Excel Beads	Cytiva	Cat#17371202
HiTrap™ Q HP anion exchange chromatography column	Cytiva	Cat#17115401
Streptavidin-Coated Beads	Spherotech	Cat#SVP-40-5
Deposited data		
Single Molecule Kymographs part 1	This study	Doi: 10.5281/zenodo.21924344
Single Molecule Kymographs part 2	This study	Doi: 10.5281/zenodo.22211598
Customized MATLAB Scripts	This study	Doi: 10.5281/zenodo.22149059
Oligonucleotides		
Primer Carrier DNA Forward: 5′-GCATAATTCTCTTACTGTCATGCCATCCG-3′	IDT	N/A
Primer Carrier DNA Reverse: 5′-CTGCTATGTGGCGCGGTATTATCC-3′	IDT	N/A
Primer 601 Carrier DNA Forward: 5′-CTGTGCCACCACGGAACAGGATGTATATATCTGACACGTGCCTGG-3′	IDT	N/A
Primer 601 Carrier DNA Reverse: 5′-GAAGAGGTGGCGCGTAACTGGAGAATCCCGGTGCCG-3′	IDT	N/A
DNA_{30bp} Forward: 5’-TCATAAGGAGGACACTGGGACATGCATCGG-3’	IDT	N/A
DNA_{30bp} Reverse Complement: 5’-CCGATGCATGTCCCAGTGTCCTCCTTATGA-3’	IDT	N/A
Recombinant DNA		
Escherichia coli expression vector pDEST-17 with human sNASP	Wang et al.[66]	N/A

(*Continued on next page*)

Continued

REAGENT or RESOURCE	SOURCE	IDENTIFIER
pET-32a expression vector with ProTα-Intein-12His for ProTα expression and purification	This study	N/A
His-tagged Nap1 expression vector	Syed et al.[17]	N/A
Human H1.0 Expression vector	Burge et al.[47]	N/A
Software and algorithms		
MATLAB	Mathworks	www.mathworks.com
Lakeview	Lumicks	www.lumicks.com/documentation/lakeview#
Pylake	Lumicks	https://lumicks-pylake.readthedocs.io/en/stable/

EXPERIMENTAL MODEL AND STUDY PARTICIPANT DETAILS

Bacteria strains

BL21(DE3) pLysS competent *E. coli* (Invitrogen) was used for expression of human H1.0 and human sNASP. Rosetta2 (DE3) competent *E. coli* (Novagen) was used for expression of mouse Nap1. BL21(DE3) competent *E. coli* (Invitrogen) was used for expression of human ProTα. DH5α (Fisher Scientific) was used for plasmid propagation.

METHOD DETAILS

H1 Expression and Purification

H1.0 was recombinantly expressed as previously described (Figures S21A–S1D).[47] Briefly, for labeling, a Serine in the N-terminal domain was mutated to a Cystine (S22C) using site-directed mutagenesis. BL21(DE3) pLysS competent *E. coli* were transformed with the H1.0 expression vector that includes the S22C mutation. Single colonies of transformed E-Coli were selected on an agar plate inoculated with ampicillin. Individual transformed colonies were grown in LB growth media to an OD_{600} of 0.4-0.6 at 37C. Expression was induced by adding 0.4mM IPTG and incubation for three hours at 37C. Successful expression was confirmed using 16% acrylamide sodium dodecyl sulfate (SDS) gel electrophoresis. Following expression, the cells were pelleted at 4000g for 10 minutes, the pellet was flash frozen in liquid nitrogen, and stored in -80C for less than a week prior to purification.

To purify the expressed H1, the cell pellets were thawed on ice and resuspended in H1 lysis buffer (50mM Tris-HCl pH 8, 500mM NaCl, 10% Glycerol, 1mM EDTA, 5mM 2-Mercaptoethanol, 0.5mM PMSF). Before lysis, a complete protease inhibitor cocktail tablet (Roche) was added to 50mL of lysis buffer. The cells were lysed by sonication with a micro-needle, and the cell lysate was pelleted at 23000g for 20min at 4C. The supernatant containing soluble H1 was purified using Bio-Rex 70, 50-100 mesh, cation exchange resin packed into an FPLC-grade column. After stabilizing the resin with lysis buffer, the supernatant was added to bind H1.0 (S22C) to the column, which was then eluted off the column with a NaCl gradient using elution buffer (50mM Tris-HCl pH 8, 1M NaCl, 10% Glycerol, 1mM EDTA, 5mM 2-Mercaptoethanol, 0.5mM PMSF).

The eluted fractions were analyzed on a 16% acrylamide SDS gel, and the pooled fractions were diluted with dilution buffer (50mM Tris-HCl pH 8, 0mM NaCl, 10% Glycerol, 1mM EDTA, 5mM 2-Mercaptoethanol, and 0.5mM PMSF) so that the NaCl concentration would be reduced to ~500mM for a second round of chromatography purification using Bio-Rex 70, 100-200 mesh (Bio-Rad), cation exchange resin. The second round of purification was performed using the same protocol used in the first round. The eluted fractions were analyzed on a 16% acrylamide SDS gel, and the pooled fractions were combined and dialyzed into MilliQ water with 2mM 2-Mercaptoethanol and 0.5mM PMSF in 4°C overnight and lyophilized. The lyophilized H1 mutants were resuspended in the storage buffer (20mM Sodium Phosphate pH7, 300mM NaCl, and 1mM EDTA), and individual aliquots were flash frozen with 10% glycerol for storage in -80°C.

H1.0 Labeling

Each H1 mutant was labeled with Cy3 maleimide as previously described.[47] Briefly, purified H1.0(S22C) was incubated with 10mM TCEP to ensure the mutated Cystine was reduced before the labeling reaction. Next, H1.0(S22C) was dialyzed overnight into labeling buffer (5mM PIPES pH6.1 and 2M NaCl), and mixed with 1.5M HEPES pH7.1 buffer following purging with Argon for 20min to remove the oxygen from the reaction solution. The HEPES buffer was added to the unlabeled H1.0(S22C) at a final concentration of 100mM immediately before adding 20mM Cy3-maleimide dissolved in DMF at a 7-excess molar concentration. The labeling reaction was incubated at room temperature for 1h, before incubation overnight at 4°C. The following day, the reaction solution was diluted with the binding buffer (50mM Tris-HCl pH 8, 250mM NaCl, 10% Glycerol, 1mM EDTA, 5mM 2-Mercaptoethanol, and 0.5mM PMSF) and mixed with the Bio-Rex 70, 50-100 mesh (Bio-Rad), cation exchange resin to enable binding of the labeled

H1.0(S22C). The excess dye was washed with the binding buffer buffer, following by eluting the labeled H1 with elusion buffer (50mM Tris-HCl pH 8, 1M NaCl, 10% Glycerol, 1mM EDTA, 5mM 2-Mercaptoethanol, and 0.5mM PMSF). Fractions were analyzed on a 16% acrylamide SDS gel, and the pooled fractions were dialyzed into MilliQ water containing 2mM 2-Mercaptoethanol and 0.5mM PMSF, and lyophilized. Lyophilized Cy3-labeled H1.0 was resuspended in the storage buffer and individual aliquots were flash frozen with 10% glycerol for storage in -80°C (Figures S21A–S1D).

H1.0 Concentration Determination

H1.0 concentration was determined using the modified Lowry assay based on H1.0 samples with known concentrations between 100ng/uL to 1000ng/uL. The estimated concentrations were verified by examining equal amounts of purified H1.0 and the reference H1.0 on a 16% acrylamide SDS gel.

Histone Octamer Preparation and Labeling

Human H2A(K119C), H2B, H3(C110A), and H4 were purchased from the Histone Source at Colorado State University. The lyophilized histones were resuspended in unfolding buffer (20mM Tris-HCl pH7.4, 7M Guanidinium, 1mM DTT) at 5mg/mL, and the unfolded histones were mixed at 1:1.2 mass ratio between H3:H4 tetramer and H2A(K119C):H2B heterodimer. Successful refolding of octamers was achieved by an overnight double dialysis into octamer refolding buffer (20 mM Tris-HCl pH 7.4, 1 mM EDTA, 2 M NaCl, and 5 mM 2-Mercaptoethanol). The refolded octamer was recovered and, H2A(K119C) was labeled with Cy5 maleimide using the same protocol described above for H1.0(S22C) labeling with Cy3. Prior to purifying the labeled octamer from the heterodimer and free histones, and labeling reaction was quenched with 10mM DTT. The quenched reaction was purified using gel-filtration FPLC chromatography with a Superdex™ 200 Increase 10/300 GL gel-filtration column (GE Healthcare), and the fractions were analyzed on a 16% acrylamide SDS gel. The pooled fractions were buffer exchanged and concentrated in octamer storage buffer 0.5X TE (10mM Tris-HCl pH 8.0, 1mM EDTA), and stored in -20°C with 40% glycerol (Figure S21E).

Nap1 Expression and Purification

Rosetta2 (DE3) competent *E. coli* were transformed with a mouse Nap1 expression vector (a gift from Stefan Dimitrov). Single colonies were selected on an agar plate inoculated with ampicillin and chloramphenicol. Individual transformed colonies were grown in LB growth media to an OD_{600} of 0.4-0.6 at 37°C. Expression was induced by adding 0.25mM IPTG and incubation for three hours at 37°C. Successful expression was confirmed using 12% acrylamide sodium dodecyl sulfate (SDS) gel electrophoresis. Following expression, the cells were pelleted at 4000g for 10 minutes, the pellet was flash frozen in liquid nitrogen, and stored at -80°C for less than a week before purification.

To purify the expressed Nap1, the cell pellets were thawed on ice and resuspended in Nap1 buffer A (20mM Tris-HCl pH 7.4, 20mM imidazole, 100mM NaCl, 10% Glycerol, 1mM BME, 0.5mM PMSF). Before lysis, two complete Roche EDTA-free protease inhibitor cocktail tablets were added to 30mL of Nap1 buffer A. The cells were lysed by sonication with a micro-needle, and the cell lysate was pelleted at 23000g for 15min at 4°C. The supernatant containing soluble Nap1 was purified using a Nickel column (Cytiva). After stabilizing the column with Nap1 buffer A, the supernatant was added to bind to the column, which was then eluted off the column with Nap1 buffer B (20mM Tris-HCl pH 7.4, 500mM imidazole, 100mM NaCl, 10% Glycerol, 1mM BME, 0.5mM PMSF).

The eluted fractions were analyzed on a 12% acrylamide SDS gel. The pooled fractions were further purified using ion exchange chromatography with a MonoQ column (Cytiva). The pooled Nap1 fractions were bound to the column in Nap1 buffer C (20mM Tris-HCl pH 7.4, 100mM NaCl, 10% Glycerol, 1mM BME, 0.5mM PMSF) and eluted with Nap1 buffer D (20mM Tris-HCl pH 7.4, 1M NaCl, 10% Glycerol, 1mM BME, 0.5mM PMSF). The eluted fractions were analyzed on a 12% acrylamide SDS gel, and the pooled fractions were combined and concentrated in Nap1 buffer C. Individual aliquots were flash frozen with 10% glycerol for storage in -80°C (Figure S21F).

sNASP Expression and Purification

N-terminally His-tagged human sNASP in the pDEST-17 expression vector (a gift from Mark Parthun) was used for expression.[66] sNASP was expressed in E. coli BL21 (DE3) pLysS cells (Invitrogen) in LB media for 4 hours at 37 °C after induction with 0.4 mM IPTG at an $O.D._{600}$ of 0.45. After expression, cells were spun at 4,000 g for 15 minutes, supernatant was removed, and the cell pellet was frozen with liquid nitrogen and stored at -80 °C. Cells were resuspended with 30 mL of NASP Ni buffer A (20 mM NaH_2PO_4 pH 7.4, 50 mM imidazole, 500 mM NaCl, 0.5 mM PMSF) with 1 complete protease inhibitor cocktail tablet (Roche) added. Resuspended cells were sonicated for a total of 3 minutes on time using an amplitude of 45 with cycles of 15 seconds on time and 45 seconds off time then spun at 23,000 g for 15 minutes at 4 °C. The supernatant was applied to a Ni column then E. coli proteins were washed away with NASP Ni buffer A. sNASP was eluted with NASP Ni buffer containing 500 mM imidazole. Fractions were run on a 12% acrylamide SDS gel then pooled and dialyzed into DN200 buffer (25 mM Tris pH 7, 200 mM NaCl, 0.1 mM EDTA, 0.5 mM PMSF). Further purification was performed with a MonoQ (Cytiva) anion exchange column. E. coli proteins were washed away with DN200 buffer then sNASP was eluted with a gradient from 200 - 600 mM NaCl. Fractions were run on a 12% acrylamide SDS gel and those containing sNASP were pooled. sNASP was concentrated and the buffer was exchanged with a centrifugal filter into DN200 buffer + 10% glycerol. Final protein was examined on SDS gel (Figure S21G) frozen with liquid nitrogen and stored at -80 °C.

Prothymosin-α Expression and Purification

ProTα was cloned as an N-terminal fusion to an Intein(Mxe GyrA)-12 His tag in a pET-32a vector. For expression, *E. coli* BL21 DE3 were transformed with the construct. A single transformant colony was cultured overnight in LB medium with 100 μg/mL carbenicillin at 37°C with shaking. On the day of expression, 1L TB medium with 100 ug/mL carbenicillin was inoculated at a 1:50 dilution with the overnight culture, incubated at 37°C and shaken at >160 RPM in a 5L baffled flask. The culture was induced at an OD600 of ~1 with 2 mM IPTG and grown for 8 hours or until OD600 stabilized for 1 hour. The culture was harvested by centrifugation at 10 000 g for 15 minutes at 4°C and frozen at -20°C. The harvested cell pellet was resuspended in lysis buffer (100 mM sodium phosphate, 500 mM NaCl, 1 mM PMSF, 10 mM imidazole, 0.1% Triton X-100, 5 mM EDTA, pH 8.0). Cells were disrupted using a high-pressure homogenizer, pre-cooled to 4°C.

The cell lysate was centrifuged (Sorvall RC5C plus centrifuge with SS-34rotor) at 16,000 rpm for one hour at 4°C. The clarified lysate was incubated on Ni-Sepharose excel beads (Cytiva, 17371202) for two hours at 4°C; 1 ml of washed beads, pre-equilibrated in equilibration buffer (20 mM sodium phosphate, 500 mM NaCl, 10 mM imidazole, pH 8.0), was used per 1 L of expression. The bead-lysate suspension was poured into a polypropylene column, and the beads were washed with 10 column volumes (CV) of wash buffer (20 mM sodium phosphate, 1000 mM NaCl, 10 mM imidazole, pH 8.0). The protein was eluted with 5 CV of elution buffer (20 mM sodium phosphate, 500 mM NaCl, 400 mM imidazole, pH 8.0) and incubated overnight with 20 mM DTT at room temperature to induce cleavage of the intein-12 His tag. The sample was subsequently dialyzed at 4°C against reverse IMAC buffer (20 mM Tris, 200 mM KCl, pH 8.0) overnight (with 3.5 kDa MWCO membrane). The dialyzed sample was incubated on Ni-Sepharose excel beads (1 ml per 1 L of expression, pre-equilibrated in dialysis buffer before the addition of the sample) for four hours at 4°C. This suspension was poured into a polypropylene column and the flow-through was collected. The collected flow-through was dialyzed against ion exchange buffer A (20 mM Bis-Tris, 50 mM NaCl, pH 6.0) overnight. The dialyzed sample was loaded onto 2x5 mL HiTrap Q HP (Cytiva, 17115401) columns connected in series on an Äkta Pure 25, pre-equilibrated in the same buffer. The protein was eluted using a gradient of 5-50% of ion exchange buffer B (20 mM Bis-Tris, 2000 mM NaCl, pH 6.0) over 20 CV. The primary fractions without 280 nm absorption were collected, concentrated using centrifugal filters (3 kDa MWCO) and buffer-exchanged to storage buffer (10 mM Tris, 200 mM KCl, 0.1 mM EDTA, pH 7.5). The concentrated samples were then dialyzed against storage buffer overnight and quantified via measuring absorbances of several serial dilutions both at 215 nm and 225 nm (extinction coefficients from Gast et al.[67]) on a NanoDrop spectrophotometer, and examined on SDS-PAGE gel (Figure S21H) prior to snap freezing in liquid nitrogen and storage at -80°C. A conservative estimate of the error on concentration is ~20%.[68] The integrity of the samples was confirmed by mass spectroscopy. All buffers were filtered through a 0.22 μm filter and degassed.

DNA Preparation and Purification

All short DNA constructs were synthesized using polymeric chain reaction with Pfu polymerase. To prepare the 147 bp carrier DNA for lambda DNA chromatinization, unmodified forward (5′-GCATAATTCTCTTACTGTCATGCCATCCG-3′) and reverse (5′-CTGC TATGTGGCGCGGTATTATCC-3′) primers (IDT) were used to amplify from pUC19 plasmid as the template. A second carrier DNA (179bp in length) was amplified for lambda DNA chromatinization using unmodified forward (5′-CTGTGCCACCACGGAACAGGATG-TATATATCTGACACGTGCCTGG-3′) and reverse (5′-GAAGAGGTGGCGCGTAACTGGAGAATCCCGGTGCCG-3′) primers (IDT) and a pUC19 plasmic containing Widom 601 DNA[69] as the template. For experiments pertaining DNA_{30bp} as a generic anionic linker histone chaperone, two complementary oligos (5'-TCATAAGGAGGACACTGGGACATGCATCGG-3' and 5'-CCGATGCATGTCCCAG TGTCCTCCTTATGA-3', IDT) were annealed and purified. All PCR reactions along with DNA_{30bp} were purified using anion exchange chromatography with a Gen-Pak™ Fax 4.6 × 100mm column (Waters) and buffer exchanged into the 0.5X TE storage buffer using a 30kDa Amicon filter (Millipore).

Lambda Tether Preparation

To synthesize lambda tether with multi-biotin modification on each end, the 12-base 5′ single-stranded overhangs on each end of the bacteriophage λ DNA were filled with the DNA polymerase I Klenow fragment that lacks 5′→3′ endonuclease activity. The reaction solution contained 6nM Lambda DNA, 100μM dATP, 100μM dTTP, 100μM dGTP, 80μM biotin-14-dCTP and 0.075 U/μL Klenow fragment in 1X NEB2 buffer to enable incorporation of biotinylated nucleotides during the polymerase reaction. The reaction solution was incubated at 37°C for 30min followed by heat inactivation at 75°C for 20min. Following the filling of the single-stranded lambda DNA ends, the enzyme was removed using phenol extraction followed by exchanging into 0.5X TE at 4°C. The concentrated tether was aliquoted and stored at -20°C.

Nucleosome Preparation and Validation

NaCl gradient dialysis was used to reconstitute nucleosomes along the prepared lambda tethers with multi-biotin ends as previously implemented.[70] The chromatinization density was regulated by changing the concentrations of the 147bp low-affinity carrier DNA, the 187bp 601 carrier DNA, and the Cy5-Octamer in the reconstitution mixture. To include sparse numbers of nucleosomes along the Lambda tether, the 187bp 601 carrier DNA was included in the reconstitution mixture to control the number nucleosome reconstituted into the lambda DNA. Lambda tether, carrier DNA and Cy5-octamer mixture in refolding buffer (10mM Tris-HCl pH 8.0, 1mM EDTA, 2M NaCl, and 1mM Benzamidine-HCl) were reconstituted into the buffer condition without NaCl (10mM Tris-HCl pH 8.0, 1mM EDTA, and 1mM Benzamidine-HCl) at 4°C for 4-6 hours using double dialysis. The dialysis bag was moved to a fresh buffer condition

without NaCl to continue the NaCl gradient dialysis overnight at 4°C. The reconstituted nucleosomes were analyzed by agarose gel electrophoresis to confirm the formation of Cy5-labeled nucleosomes along the lambda DNA tether (Figure S21I).

To further confirm nucleosomes formed along Lambda DNA, the reduction of tether end-to-end distance due to each nucleosome was measured and compared to the number of Cy5 loci detected along the tether. Force-extension measurements were performed on tethers with nucleosomes by increasing the force from 1pN to 50pN. Next, the tether was moved to a 2M NaCl-containing buffer (50mM HEPES pH 7.4, 2M NaCl) to remove the remaining histones and then returned to the imaging buffer with 130mM NaCl for a second force-extension measurement of the DNA-only tether. The change in end-to-end distance at 5pN was then determined and compared to the number of Cy5 loci. In addition, we measured the change in tether length of nucleosome unwrapping events while 15pN of force is applied to the tether.

Dual optical tweezers and fluorescence confocal imaging experimental system

Single-molecule experiments were performed using a dual optical trap C-Trap instrument (LUMICKS). A microfluidic flow cell was implemented to separately introduce each reagent needed for a single molecule test. Low Reynolds Number laminar flow enabled minimal mixing between different reagents within the flow cell, while a computer-controlled stage enabled rapid movement of the two optical traps within the flow cell. Streptavidin-coated polystyrene beads (4.34μm in size, Spherotech), biotinylated lambda tethers, and imaging buffer (50mM HEPES pH 7.4, 130mM NaCl, 0.005% Tween-20, 2mM Trolox, 450 ug/mL glucose oxidase, 22ug/mL catalase, 0.0115% v/v COT (Cyclooctatetraen), 0.012% v/v NBA (3-Nitrobenzyl alcohol), 1.6% w/v glucose) were introduced in parallel in channels 1 through 3, respectively. An additional, orthogonal channel 4 was used to introduce 3nM Cy3- H1.0 diluted in the imaging buffer. Laminar flow was introduced while the traps were held in channel 1 to enable trapping of a single streptavidin-coated bead in each optical trap. To calibrate the trap stiffness, the beads were moved to channel 3 while the flow was stopped. A spectral analysis was performed to achieve trap stiffness of ~0.2-0.4pN/nm for each trap. The stage was moved to bring the trapped beads to channel 2 to enable the successful capture of a single lambda tether between the two streptavidin-coated beads. Binding interactions between the biotinylated dCTPs on the tether ends and streptavidin on the surface of the beads enabled stable capturing of the lambda tether between the two beads. The presence of a captured lambda tether was detected by probing the tether force-extension curve as the two beads were subjected to repeated approach-retraction movement with respect to each other. The flow was stopped, and the captured tether was brought into channel 3 to verify the presence of a single tethered molecule using a lambda DNA worm-like chain reference model. For experiments with nucleosome-containing tethers, confocal line scanning along the tether was implemented using the 640nm laser to visualize the location of the reconstituted nucleosomes. The mechanical force corresponding to each test was set using the Bluelake software (LUMICKs). Before transferring the tether to the H1.0-Cy3 channel, the 640nm excitation laser was turned off, so only the 532nm excitation laser (green) remained on. This allowed for the H1.0-Cy3 molecules to be visualized following the transfer of the tether into the H1.0-Cy3 channel. The stage was then moved to bring the assembled construct into the orthogonal channel 4 containing Cy3-H1 to monitor H1 binding and one-dimensional diffusion.

QUANTIFICATION AND STATISTICAL ANALYSIS

H1.0 single-molecule tracking and data analysis

HDF5 format files were processed using the commercial Lakeview software (LUMICKs) along with the commercial Pylake Python package (LUMICKs) to detect individual traces. For each individual H1.0-Cy3 tracked trace, the extracted position and time data were further processed to quantify the dwell time and diffusion coefficient using a custom-built MATLAB code.

The mean-square displacement (MSD) for each tracked particle was calculated using:

$$\mathrm{MSD}\,(n, N) = \sum_{i=1}^{N-n} \frac{(X_{i+n}-X_i)^2}{N-n} \qquad \text{(Equation 1)}$$

where N is the total number of time points for each trace, n is the MSD time-lag size (n=1→N-1), i is the window of displacement measurement, and X_i is the estimated position of each tracked H1.0-Cy3 in the frame i. Assuming H1.0 exhibits Brownian diffusion, the diffusion coefficient (D) for each tracked H1.0 was estimated using an ordinary least square estimator by solving for D in the following equation, MSD=2Dt, based on MSD measured within the first 1s window as previously described.[56]

Position measurements of immobile DNA-bound proteins

Cy5 labeled histone octamer was reconstituted onto lambda DNA to provide a reference for immobile DNA-bound protein (Figure S2A). Position of Cy5-labeled nucleosomes was quantified when the tether was under 1pN, 3pN and 10pN of force to represent immobile tether-bound molecules. Time traces (n = 354) of Cy5-labeled nucleosomes were quantified (146 under 1pN, 151 under 3pN, and 57 under 10pN). The estimated mean-squared displacement of a single molecule over time t (MSD(t)) can be described as:

$$\mathrm{MSD}(t) = 2Dt^{\alpha}$$

where D is the diffusion coefficient and α is the temporal scaling exponent.[71] The MSD was determined with a time step of 40ms over a time window of 1s. For a molecule exhibiting unconstrained Brownian motion, α = 1, while for a completely immobile molecule, α = zero. We fit the averaged MSD vs. time to the above equation to determine α for each nucleosome. The values of α and the MSD at

t = 1s ($MSD_{t=1s}$) for each nucleosome under either 1pN, 3pN, and 10pN were indicated on a scatter plot (Figure S2B). The maximum recorded value of α for a single nucleosome (0.22, 0.22 and 0.20 under 1pN, 3pN and 10pN, respectively) was used as the cut-off threshold for determining whether a tracked H1.0 is immobile (Figure S2C, shown for 1pN only). There was a small fraction (less than 5%) of H1.0 traces that had an α of less than the cut-off threshold but an $MSD_{t=1s}$ that was larger than the maximum $MSD_{t=1s}$ for nucleosomes. Upon visual examination, these traces showed incorrectly tracked positions and were therefore not included (Figure S2C, black squares, shown for 1pN only).

Statistical analysis

In order to report uncertainties associated with each fit parameter, each data set was randomly divided into three subgroups with similar sample size based on selection without replacement statistical analysis. All reported uncertainties are in the mean ± SEM (standard error of the mean) format. The reported *p*-values are based on student's t-test performed in MATLAB.

Molecular Cell, Volume *86*

Supplemental information

Linker histone H1.0 loads onto nucleosomes through multiple pathways that are facilitated by histone chaperones

Ehsan Akbari, Nathaniel L. Burge, Matti Valdimarsson, Aritra Chowdhury, Benjamin Schuler, and Michael G. Poirier

SUPPLEMENTARY INFORMATION

Linker histone H1.0 loads onto nucleosomes through multiple pathways that are facilitated by histone chaperones.

Ehsan Akbari[1], Nathaniel L. Burge[2], Matti Valdimarsson[3], Aritra Chowdhury[3], Benjamin Schuler[3,4], Michael G. Poirier[1,2,5,6,*]

[1]Department of Physics, The Ohio State University, Columbus, OH 43210, USA

[2]Ohio State Biochemistry Graduate Program, The Ohio State University, Columbus, OH 43210, USA

[3]Department of Biochemistry, University of Zurich, 8057 Zurich, Switzerland

[4]Department of Physics, University of Zurich, 8057 Zurich, Switzerland

[5]Department of Chemistry & Biochemistry, The Ohio State University, Columbus, OH 43210, USA

[6]Lead contact

*Correspondence: poirier.18@osu.edu (M.G.P)

Supplementary Figures

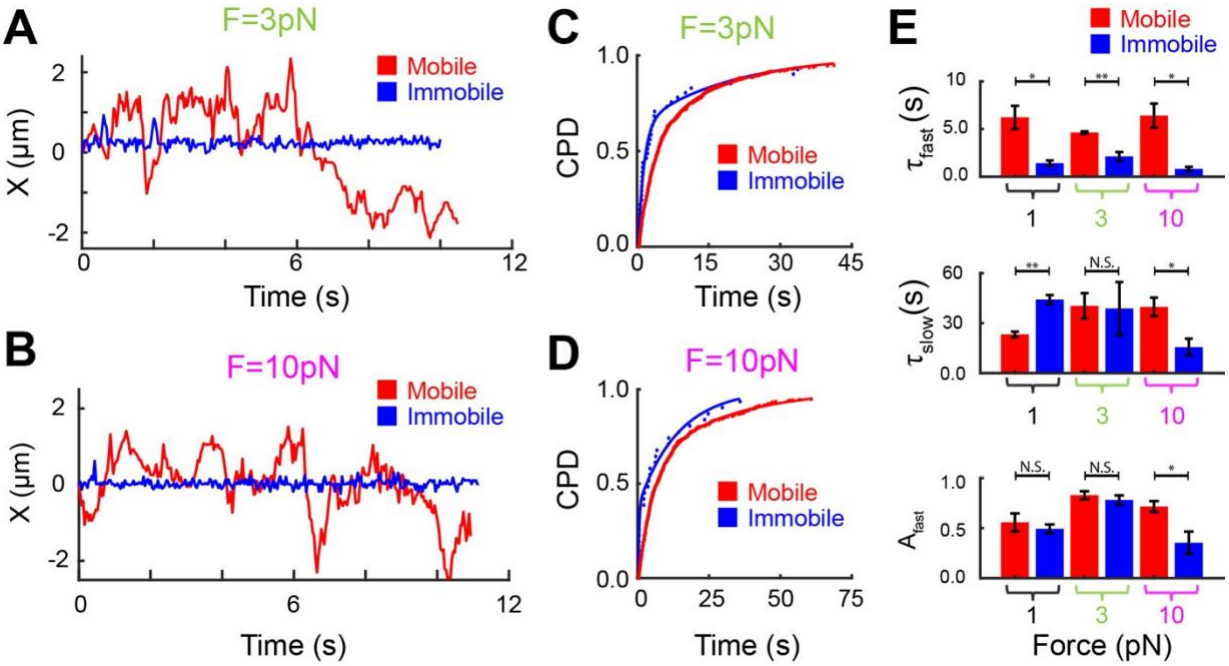


Figure S1: Force dependence of DNA bound H1.0 resident time (related to Figure 1). (**A**) and (**B**) Net displacement of a diffusing (red) versus immobile (blue) trace over time when bound to a tether under 3pN and 10pN of constant force, respectively. (**C**) and (**D**) Dwell time CPDs for immobile (blue) versus diffusing (red) traces that were bound to DNA under 3pN and 10pN of constant force, respectively. All four dwell time CPDs were best fit to a double-exponential model to yield short dwell time (τ_{fast}), long dwell time (τ_{slow}), and short dwell time fraction (A_{fast}). (**E)** Fit parameters τ_{fast}, τ_{slow} and A_{fast} for mobile (red) versus immobile (blue) H1.0 traces under 1pN (black), 3pN (green) and 10pN (magenta) of constant force.

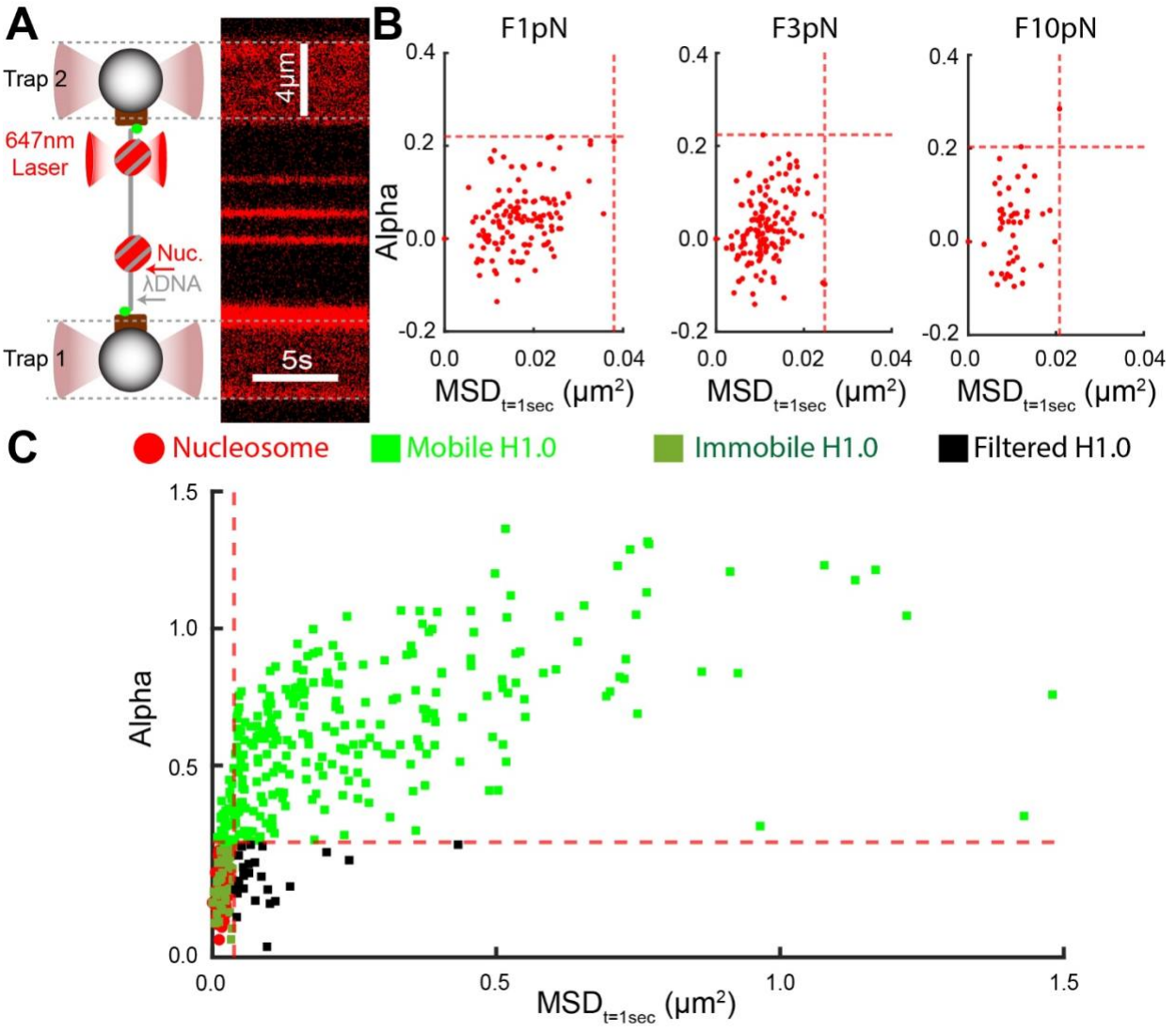


Figure S2: Nucleosome position calibration measurements for differentiating between mobile and immobile H1.0 (related to Figure 1). (**A**) Illustration of the single-molecule assembly along with a kymograph of Cy5-labled nucleosomes sparsely reconstituted along the nucleosome-containing tether. The kymograph is cropped from the original kymograph. (**B**) Scatter plots of $MSD_{t=1sec}$ (mean squared displacement at 1 second) versus α for nucleosomes while the tether was subjected to 1pN, 3pN, or 10pN mechanical force. (**C**) Scatter plot of $MSD_{t=1sec}$ versus α for H1.0 (dark green, bright green and black) on DNA-only tethers and the nucleosomes (red) within nucleosome containing tethers that are subject to a constant force of 1pN. The tracked H1.0 traces were characterized as mobile (bright green), immobile (dark green), or filtered (falsely detected position, black).

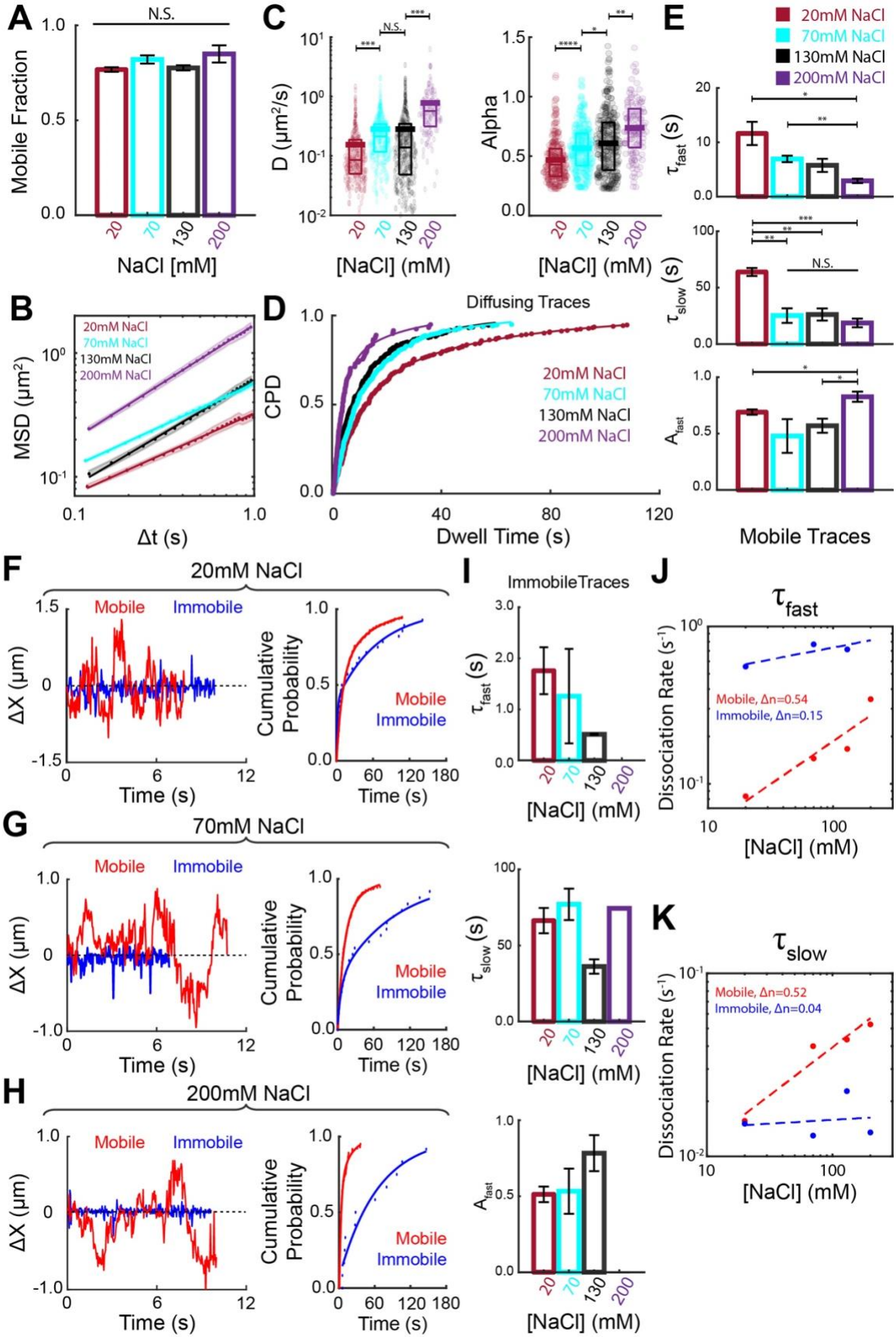

A
Mobile Fraction
N.S.
NaCl [mM]
C
D (μm²/s)
N.S.
[NaCl] (mM)
Alpha
[NaCl] (mM)
E
20mM NaCl
70mM NaCl
130mM NaCl
200mM NaCl
τfast (s)
τslow (s)
N.S.
Afast
Mobile Traces
B
MSD (μm²)
Δt (s)
D
Diffusing Traces
CPD
Dwell Time (s)
F
20mM NaCl
Mobile
Immobile
ΔX (μm)
Time (s)
Cumulative Probability
G
70mM NaCl
H
200mM NaCl
I
ImmobileTraces
J
τfast
Dissociation Rate (s⁻¹)
Mobile, Δn=0.54
Immobile, Δn=0.15
K
τslow
Mobile, Δn=0.52
Immobile, Δn=0.04

Figure S3: Characterization of the influence of Na^+ screening on H1.0-DNA interactions (related to Figure 1). (A) Fraction of H1.0 traces recorded as mobile along DNA-only tethers in 20mM NaCl (dark red), 70mM NaCl (cyan), 130mM NaCl (black), and 200mM NaCl (purple). Increased NaCl concentration does not significantly increase the fraction $H1.0_{Mobile}$. **(B)** Average mean-squared displacement over time, along with **(C)** violin plots of estimated diffusion coefficients and estimated alphas plotted for diffusing H1.0 traces in 20mM NaCl (dark red), 70mM NaCl (cyan), 130mM NaCl (black), and 200mM NaCl (purple). Ionic screening significantly enhanced H1.0 diffusivity along the DNA. In addition, elevated ionic concentration increases the average estimated alpha, indicating near random-walk diffusion. Solid lines indicate the mean. Within each box plot, the center, bottom, and top marks indicate the median, the 25^{th} percentile, and the 75^{th} percentile, respectively. **(D)** Cumulative probability of dwell times for diffusing H1.0 traces in 20mM NaCl (dark red), 70mM NaCl (cyan), 130mM NaCl (black) and 200mM NaCl (purple). The cumulative probabilities were best fit to a double-exponential model to yield the characteristic short dwell time (τ_{fast}), long dwell time (τ_{slow}), and short dwell time fraction (A_{fast}). Na^+ screening significantly decreased the H1.0 dwell time on the DNA. **(E)** Estimated values of τ_{fast}, τ_{slow} and A_{fast} for diffusing H1.0 in 20mM NaCl (dark red), 70mM NaCl (cyan), 130mM NaCl (black) and 200mM NaCl (purple). The characteristic τ_{fast} and τ_{slow} values were significantly reduced by Na^+ screening. **(F-H)** Representative traces of net displacement for immobile (blue) and mobile (red) traces, cumulative probability of dwell times for immobile (blue) and mobile (red) traces, and characteristic dwell times and ratio of fast dissociating traces for immobile traces in 20mM NaCl, 70mM NaCl, and 200mM NaCl, respectively**. (I)** Values of τ_{fast}, τ_{slow} and A_{fast} for $H1.0_{Immobile}$ in 20mM NaCl (dark red), 70mM NaCl (cyan), 130mM NaCl (black) and 200mM NaCl (purple)**. (J-K)** Estimated characteristic counterion release based on weakening of DNA binding interaction for $H1.0_{Mobile}$ and $H1.0_{Immobile}$ under increasing Na^+ concentration. The mobile population exhibits only modest counterion release ($\Delta n \approx 0.54$ fast and 0.52 slow)**,** while the immobile population exhibits near-zero counterion release ($\Delta n \approx 0.15$ fast and 0.04 slow).Note that all tests were performed while the tether was under constant 1pN mechanical force. * denotes $p<0.05$. ** denotes $p<0.01$. *** denotes $p<0.001$. **** denotes $p<0.0001$.

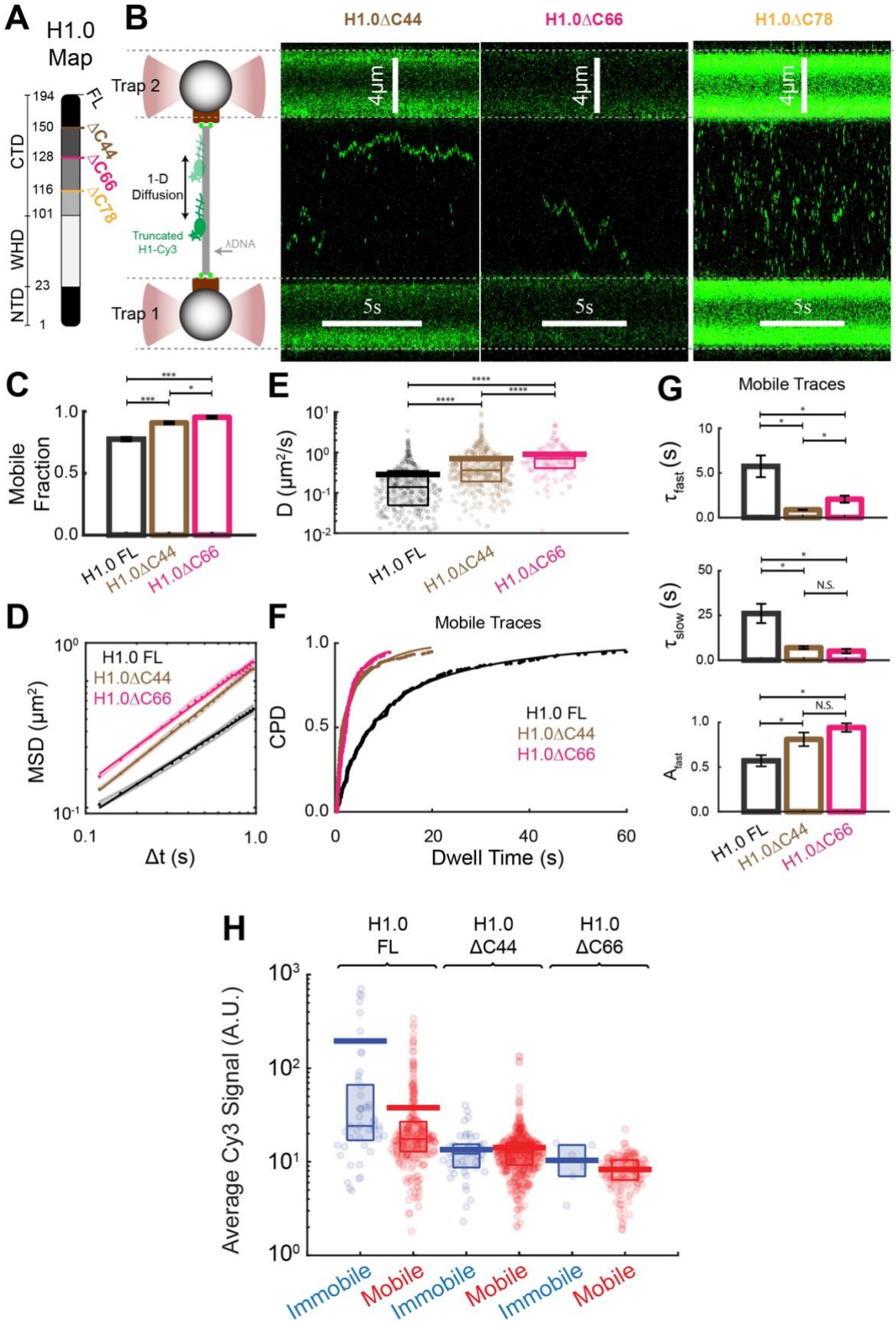

A
H1.0 Map
194
150
128
116
101
23
1
FL
ΔC44
ΔC66
ΔC78
CTD
WHD
NTD
B
H1.0ΔC44
H1.0ΔC66
H1.0ΔC78
Trap 2
Trap 1
1-D Diffusion
Truncated H1-Cy3
λDNA
4μm
5s
C
Mobile Fraction
H1.0 FL
H1.0ΔC44
H1.0ΔC66
E
D (μm²/s)
G
Mobile Traces
τfast (s)
τslow (s)
Afast
N.S.
D
MSD (μm²)
Δt (s)
F
Mobile Traces
CPD
Dwell Time (s)
H
Average Cy3 Signal (A.U.)
Immobile
Mobile

Figure S4: The influence of linker histone truncations on H1.0-DNA interactions (related to Figure 1). (A) Domain Map of the H1.0 full-length (FL): disordered N-terminal domain (NTD) (residues 1-22), winged helix domain (WHD) (residues 23-100), and disordered C-terminal domain (CTD) (residues 101-194). H1.0s with a truncated CTD contained either 44 (ΔC44, brown), 66 (ΔC66, pink) and 78 (ΔC78, orange) residues deleted from the C-terminus. The kymographs shown are cropped from original kymographs. **(B**) Schematic of the single-molecule experimental setup along with representative kymographs of H1.0 with different CTD truncations bound to DNA-only tethers. While H1.0ΔC44 and H1.0ΔC66 exhibited high mobility along the dsDNA, H1.0ΔC78 exhibited mostly short-lived binding (~100ms) to dsDNA. **(C**) Bar plots of the fraction of mobile H1.0 FL (black), H1.0ΔC44 (brown) and H1.0 ΔC66 (pink) on DNA-only tethers. Unlike H1.0 FL, nearly all H1.0 ΔC44 and H1.0 ΔC66 were designated as mobile. **(D**) Average mean-squared displacement over time. (**E**) Violin plots of the diffusion coefficient for each H1.0 FL (black), H1.0 ΔC44 (brown), and H1.0 ΔC66 (pink). H1.0 ΔC44 and H1.0 ΔC66 exhibited significantly larger D as compared to H1.0 FL. Solid lines indicate the mean. Within each box plot, the center, bottom, and top lines indicate the median, the 25th percentile, and the 75th percentile, respectively. **(F)** Cumulative probability of dwell times for mobile H1.0. They were best fit to a double-exponential model with a short dwell time (τ_1), a long dwell time (τ_2), and a short dwell time fraction (A_1). H1.0 ΔC44 and H1.0 ΔC66 exhibited significantly smaller dwell times compared to H1.0 FL. **(G)** τ_{fast}, τ_{slow} and A_{fast} values for mobile H1.0 FL (black), H1.0 ΔC44 (brown) and H1.0 ΔC66 (pink). **(H)** Average Cy3 signal for immobile versus mobile population on DNA-only tethers of full-length (FL) H1.0 compared to H1.0 with truncated CTD. The measured Cy3 signal within up to the first 1s of being loaded onto the tether was averaged per molecule. Solid lines indicate the mean. Within each box plot, the center, bottom, and top lines indicate the median, the 25th percentile, and the 75th percentile, respectively. Note that all tests were performed in a buffer containing 130mM NaCl and the tether was held under a 1pN constant force. * denotes $p<0.05$. ** denotes $p<0.01$. **** denotes $p<0.0001$.

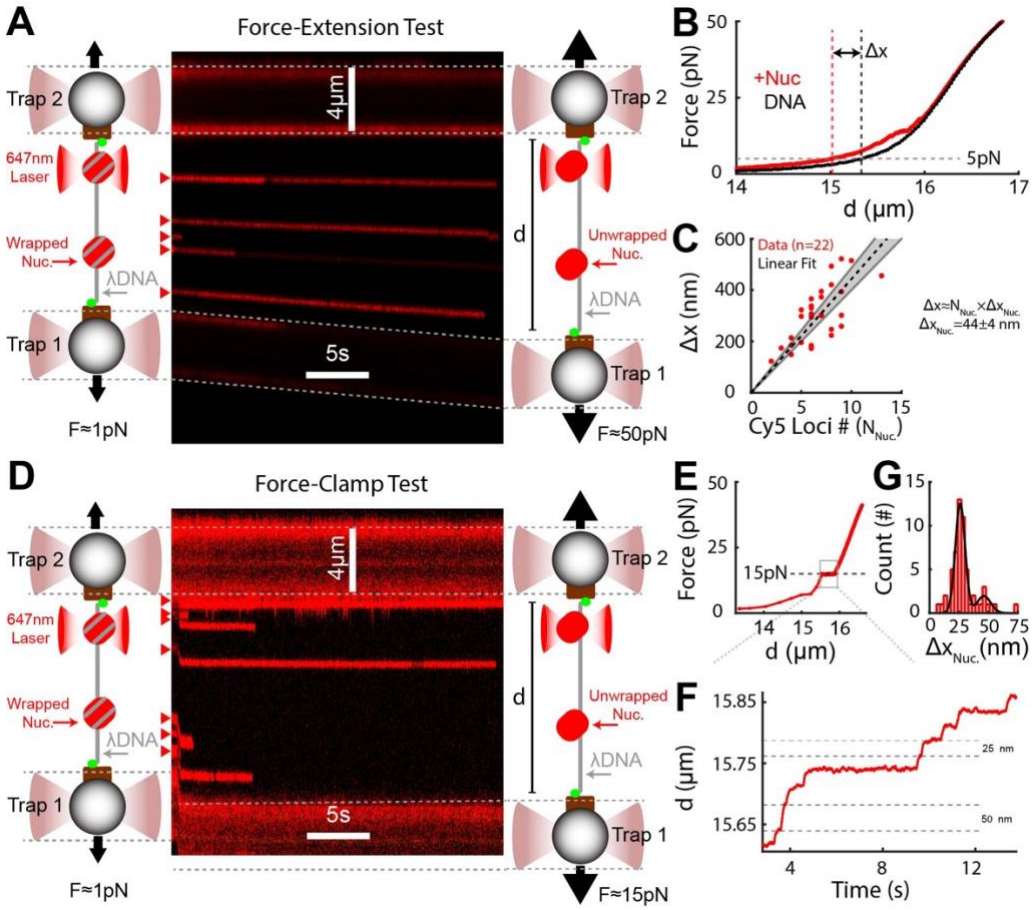


Figure S5: Characterization of nucleosome-containing lambda DNA tethers (related to STAR Methods). (A) Representative kymographs with schematics of the beginning and end of the force-extension measurements performed with tethers containing Cy5-labeled nucleosomes. The observed Cy5 loci were used to determine the numbers and position of nucleosomes along the tether (red arrowheads). **(B)** Representative force-extension plot of a tether containing nucleosomes (red) compared to the tether after the nucleosomes are removed (black). The vertical lines indicate the difference in the tether's end-to-end distance at 5pN with and without nucleosomes. **(C)** The measured reduction in tether end-to-end distance (Δx) at 5pN compared to the number of detected Cy5 loci. Each Cy5 locus reduced the tether end-to-end distance by $\Delta x_{.}$ = 44±4 nm. **(D)** Representative kymographs with schematics of the beginning and end of the force-clamp measurements performed on a tether with Cy5-labeled nucleosomes. **(E)** Representative force-extension curve to a period of constant force at 15pN. **(F)** A zoom-in of the trace in (E) when the force is held constant at 15pN. This reveals the characteristic ~25nm lengthening per nucleosome unwrapping (Δx_{Nuc}) events that have been previously reported. **(G)** Probability distribution of the Δx_{Nuc} steps due to nucleosome unwrapping while applying 15pN of force. The most probable Δx_{Nuc} was 25nm, which is characteristic of single nucleosome unwrapping at this force. The second most probable lengthening size was 50nm, which is indicative of two nucleosomes unwrapping events occurring nearly simultaneously. The kymographs shown in A and D are cropped from original kymographs.

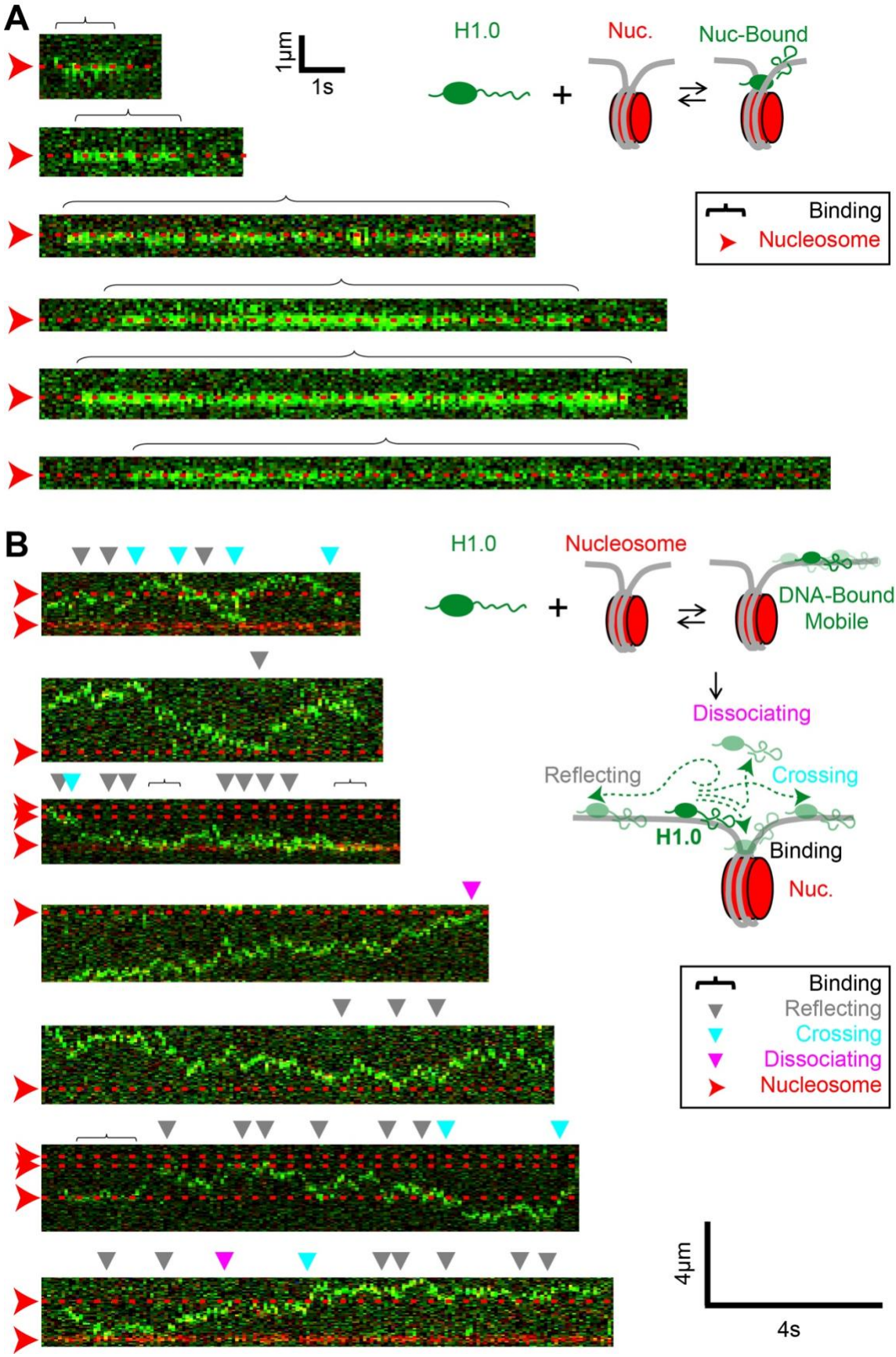

A
1μm
1s
H1.0
Nuc.
Nuc-Bound
Binding
Nucleosome
B
H1.0
Nucleosome
DNA-Bound
Mobile
Dissociating
Reflecting
Crossing
H1.0
Binding
Nuc.
Binding
Reflecting
Crossing
Dissociating
Nucleosome
4μm
4s

Figure S6: Gallery of H1.0 kymographs bound to tether with nucleosomes (related to Figures 2 and 3). (A) Representative kymographs of H1.0 that directly load onto nucleosomes when first binding a nucleosome-containing tether. The nucleosome positions are indicated with the red arrowhead along with the red dashed lines. The illustration provides a visual description of the observed binding events. H1.0 is immobile upon direct binding to a nucleosome. All measurements were done while the tether was under a constant force of 1pN. **(B)** Representative kymographs of $H1.0_{Mobile}$ that directly load onto DNA when first binding a nucleosome-containing tether. The nucleosome positions are indicated with the red arrowhead along with the red dashed lines. The illustration provides a visual description of the observed binding events. Following $H1.0_{Mobile}$ colocalization with a nucleosome, $H1.0_{Mobile}$ can bind to (black bracket), reflect off (grey arrow), cross over (cyan arrow), or dissociate from (magenta arrow) the nucleosome. $H1.0_{Mobile}$ reflects off nucleosomes more often than binding to, crossing over or dissociating from nucleosomes. All measurements were done while the tether was under a constant force of 1pN. The kymographs shown are cropped from original kymographs.

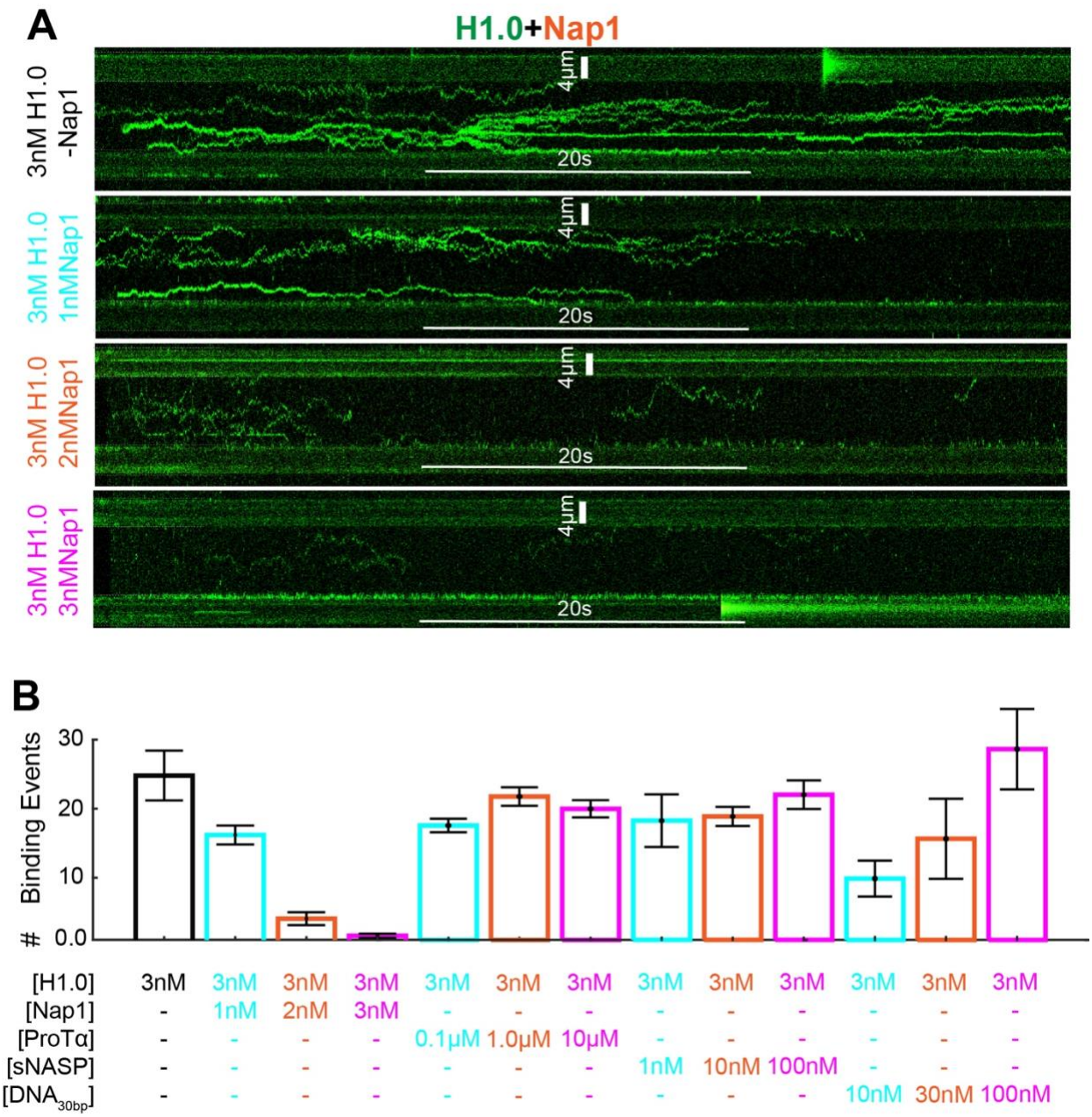


Figure S7: **Characterization of the influence of linker histone chaperones on H1.0 binding to dsDNA (related to Figure 4). (A)** Representative kymographs of H1.0 that directly load onto DNA-only tethers at Nap1 concentrations of 0nM (black), 1nM (cyan), 2nM (orange), and 3 nM (magenta). Elevating Nap1 concentrations reduces H1.0 occupancy on the DNA-only tether. The kymographs shown are cropped from original kymographs. **(B)** Number of binding events to the DNA-only tether over a period of 3min in the presence of increasing concentrations of Nap1, ProTα, sNASP, or DNA_{30bp}. The number of H1.0 binding events to the DNA-only tether systematically reduced with increased NAP1 concentration. However, the other chaperones did not prevent loading of H1.0 onto DNA-only tethers. All measurements were done while the tether was under a constant force of 1pN.

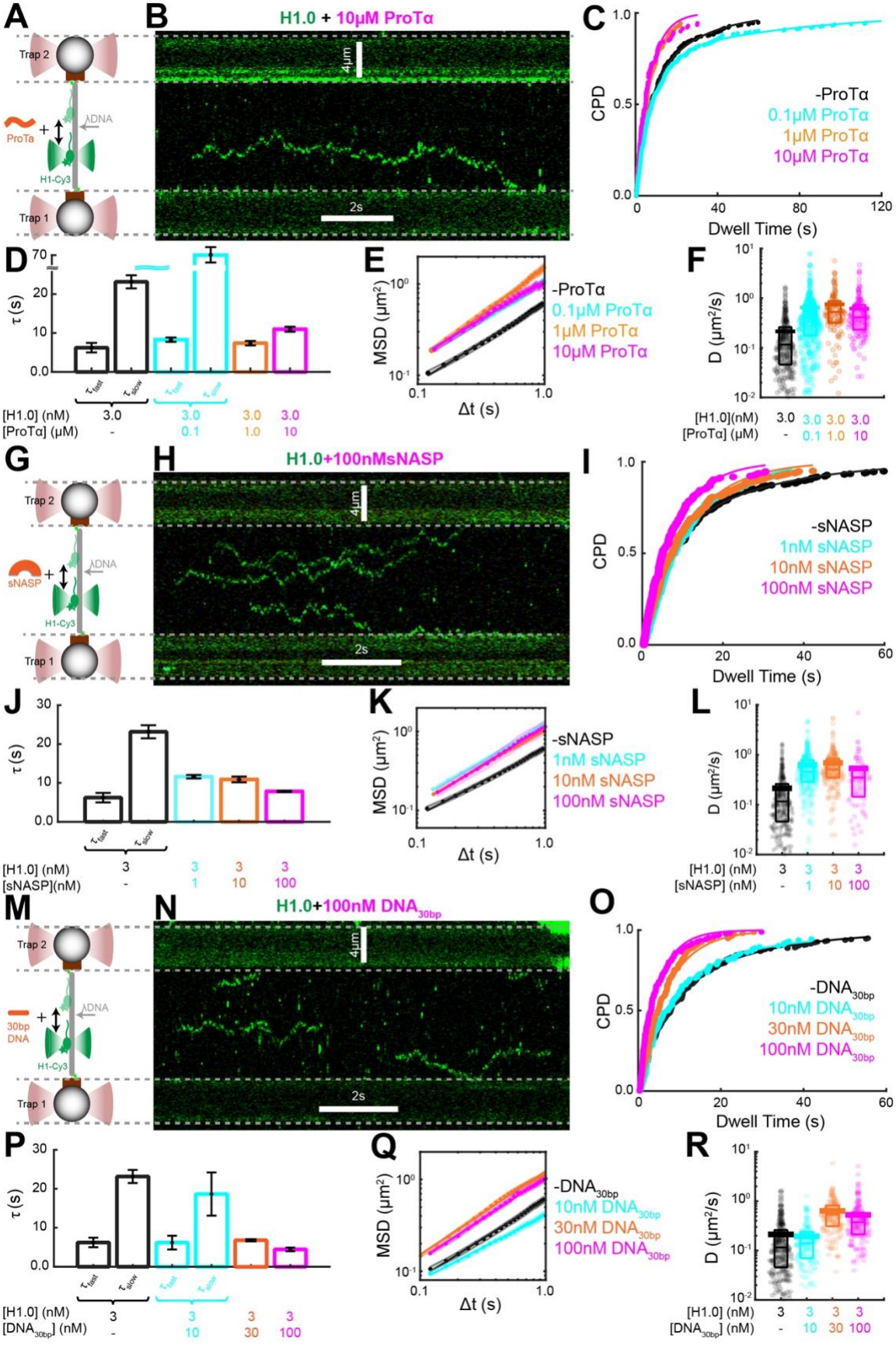

A
B
H1.0 + 10μM ProTα
Trap 2
Trap 1
ProTα
λDNA
H1-Cy3
4μm
2s
C
CPD
Dwell Time (s)
-ProTα
0.1μM ProTα
1μM ProTα
10μM ProTα
D
τ (s)
[H1.0] (nM) 3.0 3.0 3.0 3.0
[ProTα] (μM) - 0.1 1.0 10
E
MSD (μm²)
Δt (s)
F
D (μm²/s)
[H1.0](nM) 3.0 3.0 3.0 3.0
[ProTα] (μM) - 0.1 1.0 10
G
H1.0+100nMsNASP
sNASP
I
-sNASP
1nM sNASP
10nM sNASP
100nM sNASP
J
[H1.0] (nM) 3 3 3 3
[sNASP](nM) - 1 10 100
K
L
[H1.0] (nM) 3 3 3 3
[sNASP] (nM) - 1 10 100
M
N
H1.0+100nM DNA30bp
30bp DNA
O
-DNA30bp
10nM DNA30bp
30nM DNA30bp
100nM DNA30bp
P
[H1.0] (nM) 3 3 3 3
[DNA30bp] (nM) - 10 30 100
Q
R
[H1.0] (nM) 3 3 3 3
[DNA30bp] (nM) - 10 30 100

Figure S8: Characterization of the influence of ProTα, sNASP and DNA_{30bp} on H1.0 mobility and residence time on DNA (related to Figure 4). (A) Illustration of the single-molecule experimental setup with ProTα. **(B)** A representative kymograph of a Cy3-labeled H1.0 (green) diffusing along a DNA-only tether in the presence of ProTα. **(C)** Dwell time CPD of DNA-bound H1.0 in the presence of increasing concentrations of ProTα. The CPDs were best fit with two exponentials for 0 and 0.1 μM ProTα and with a single exponential for 1.0 μM and 10 μM ProTα. Increasing the concentration of ProTα systematically reduces the H1.0 dwell time on DNA-only tethers. **(D)** Summary of the characteristic dwell times (τ) from the exponential fits of the CPDs in (C). The double exponential fits provide two characteristic dwell times (τ_{fast} and τ_{slow}), while the single exponential fits provide one characteristic dwell time. **(E)** Average MSD versus time for increasing concentrations of ProTα. **(F)** Violin plots of $H1.0_{Mobile}$ diffusion coefficients in the presence of increasing concentrations of ProTα. ProTα increased the mobility of DNA-bound H1.0. Solid lines indicate the mean. Within each box plot, the center, bottom, and top lines indicate the median, the 25th percentile and the 75th percentile, respectively. **(G)** Illustration of the single-molecule experimental setup with sNASP. **(H)** Representative kymograph of a single Cy3-labeled H1.0 (green) diffusing along a DNA-only tether in the presence of sNASP. The kymograph is cropped from the original kymograph. **(I)** Dwell time CPD of DNA-bound H1.0 in the presence of increasing concentrations of sNASP. The CPDs were best fit with two exponentials for 0 sNASP, and with a single exponential for 1.0nμM, 10nM, and 100nM sNASP. Increasing the concentration of sNASP reduces the H1.0 dwell time on DNA-only tethers. **(J)** Summary of the characteristic dwell times (τ) from the exponential fits of the CPDs in (C). The double exponential fits provide two characteristic dwell times (τ_{fast} and τ_{slow}), while the single exponential fits provide one characteristic dwell time. **(K)** Average MSD versus time for increasing concentrations of sNASP. **(L)** Violin plots of $H1.0_{Mobile}$ diffusion coefficients in the presence of increasing concentrations of sNASP. sNASP increased the mobility of DNA-bound H1.0. Solid lines indicate the mean. Within each box plot, the center, bottom, and top lines indicate the median, the 25th percentile, and the 75th percentile, respectively. **(M)** Illustration of the single-molecule experimental setup with DNA_{30bp}. **(N)** Representative kymograph of a single Cy3-labeled H1.0 (green) diffusing along a DNA-only tether in the presence of DNA_{30bp}. The kymograph is cropped from the original kymograph. **(O)** Dwell time CPD of DNA-bound H1.0 in the presence of increasing concentrations of DNA_{30bp}. The CPDs were best fit with two exponentials for 0 and 10nM DNA_{30bp}, and with a single exponential for 30nM and 100nM DNA_{30bp}. Increasing the concentration of DNA_{30bp} reduces the H1.0 dwell time on DNA-only tethers. **(P)** Summary of the characteristic dwell times (τ) from the exponential fits of the CPDs in (D). The double exponential fits provide two characteristic dwell times (τ_{fast} and τ_{slow}), while the single exponential fits provide one characteristic dwell time. **(Q)** Average MSD versus time for increasing concentrations of DNA_{30bp}. **(R)** Violin plots of $H1.0_{Mobile}$ diffusion coefficients in the presence of increasing concentrations of DNA_{30bp}. DNA_{30bp} increased the mobility of DNA-bound H1.0. All measurements were done with a constant force of 1pN. Solid lines indicate the mean. Within each box plot, the center, bottom, and top lines indicate the median, the 25th percentile, and the 75th percentile, respectively. The kymographs shown in B, H and N are cropped from the original kymograph. All measurements were done with a constant force of 1pN.

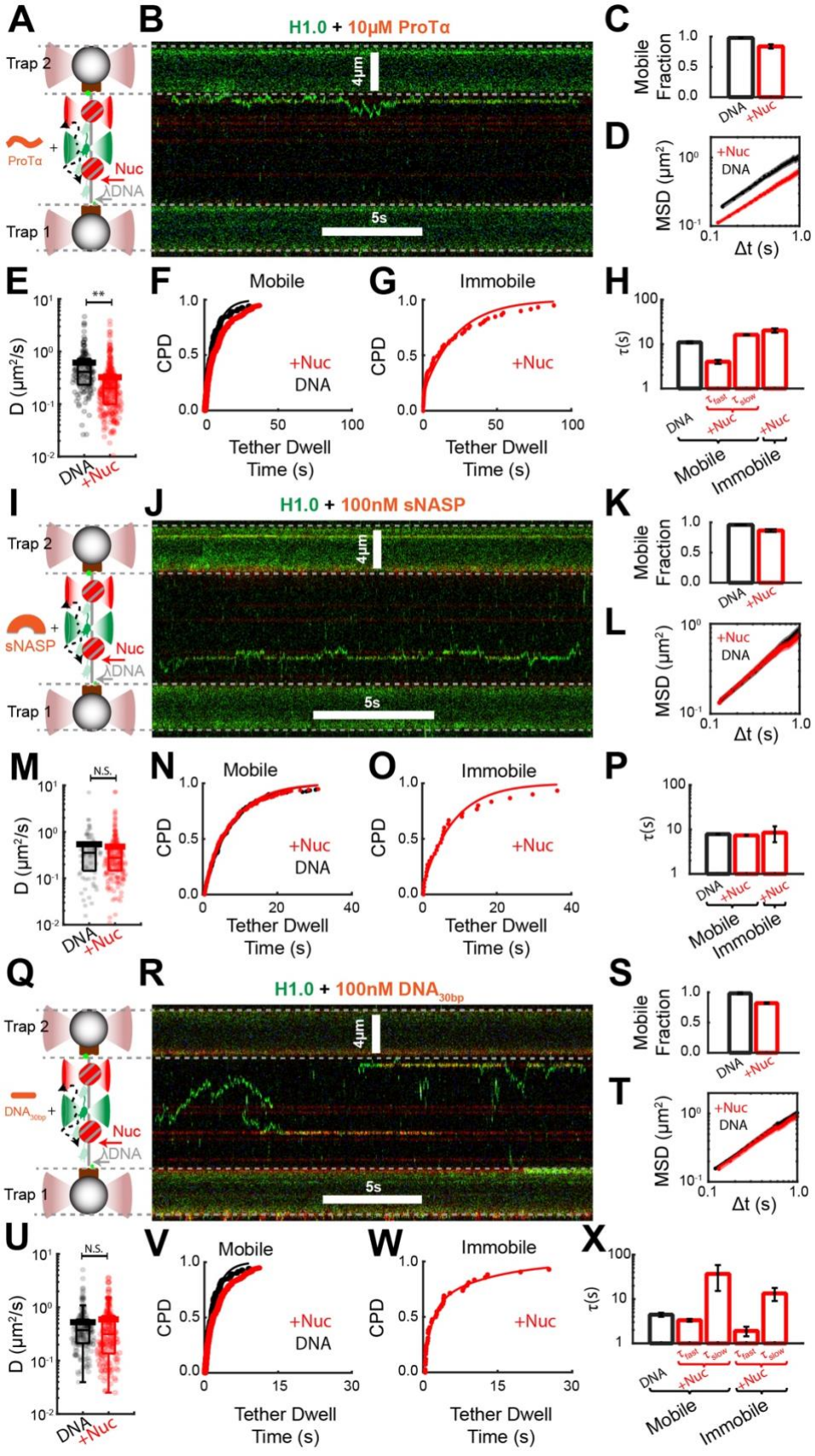

A
B
H1.0 + 10μM ProTα
Trap 2
Trap 1
ProTα
Nuc
λDNA
4μm
5s
C
Mobile Fraction
DNA
+Nuc
D
MSD (μm²)
Δt (s)
E
D (μm²/s)
**
F
Mobile
CPD
Tether Dwell Time (s)
G
Immobile
H
τ(s)
Mobile
Immobile
I
H1.0 + 100nM sNASP
sNASP
J
K
L
M
N.S.
N
O
P
Q
R
H1.0 + 100nM DNA30bp
DNA30bp
S
T
U
V
W
X

Figure S9: Characterization of H1.0 dynamics on nucleosome-containing tethers in the presence of ProTα, sNASP and DNA_{30bp} (related to Figure 5). (A) Illustration of the single-molecule experiment with ProTα. **(B)** Representative kymograph of H1.0 (green) bound to a nucleosome-containing tether in the presence of ProTα. Red indicates the locations of the nucleosomes along the DNA tether. **(C)** Fraction of mobile DNA-bound H1.0 in the presence of ProTα when bound to DNA-only (black) and nucleosome-containing (red) tethers. **(D)** Average MSD versus time of $H1.0_{Mobile}$ traces when diffusing along nucleosome-containing (red) and DNA-only (black) tethers. **(E)** Violin plots of diffusion coefficients for $H1.0_{mobile}$ along DNA-only (black) and nucleosome-containing (red) tethers in the presence of ProTα. Solid lines indicate the mean. Within each box plot, the center, bottom, and top marks indicate the median, the 25^{th} percentile and the 75^{th} percentile, respectively. **(F)** and **(G)** Dwell time CPD for $H1.0_{Mobile}$ and $H1.0_{Immobile}$, respectively, bound to DNA-only (black) and nucleosome-containing (red) tethers in the presence of ProTα. There were no $H1.0_{Immobile}$ traces detected on DNA-only tethers in the presence of ProTα, so it is not included in (G). **(H)** In the presence of ProTα, characteristic dwell times for $H1.0_{Mobile}$ and $H1.0_{Immobile}$ when bound to DNA-only (DNA, black) and nucleosomes-containing (+Nuc, red) tethers. The CPD of $H1.0_{Mobile}$ on DNA-only tethers and $H1.0_{Immobile}$ on +Nuc tethers fit best to a single exponential. The CPD of $H1.0_{Mobile}$ on +Nuc tethers fit best to a double exponential, resulting in τ_{fast} and τ_{slow} (A_{fast}=0.40±0.07). **(I)** Illustration of the single-molecule experiment with sNASP. **(J)** Representative kymograph of H1.0 (green) bound to a nucleosome-containing tether in the presence of sNASP. Red indicates the locations of the nucleosomes along the DNA tether. **(K)** Fraction of mobile DNA-bound H1.0 in the presence of sNASP when bound to DNA-only (black) and nucleosome-containing (red) tethers. **(L)** Average MSD versus time of $H1.0_{Mobile}$ traces when diffusing along nucleosome-containing (red) and DNA-only (black) tethers. **(M)** Violin plots of diffusion coefficients for $H1.0_{Mobile}$ along DNA-only (black) and nucleosome-containing (red) tethers in the presence of sNASP. Solid lines indicate the mean. Within each box plot, the center, bottom, and top marks indicate the median, the 25^{th} percentile and the 75^{th} percentile, respectively. **(N)** and **(O)** Dwell time CPD for $H1.0_{Mobile}$ and $H1.0_{Immobile}$, respectively, bound to DNA-only (black) and nucleosome-containing (red) tethers in the presence of sNASP. There were no $H1.0_{Immobile}$ traces detected on DNA-only tethers in the presence of sNASP, so it is not included in (G). **(P)** In the presence of sNASP, characteristic dwell times for $H1.0_{Mobile}$ and $H1.0_{Immobile}$ when bound to DNA-only (DNA, black) and nucleosomes-containing (+Nuc, red) tethers. All CPDs of dwell times fit best to a single exponential. **(Q)** Illustration of the single-molecule experiment with DNA_{30bp}. **(R)** Representative kymograph of H1.0 (green) bound to a nucleosome-containing tether in the presence of 30bpDNA. Red indicates the locations of the nucleosomes along the DNA tether. **(S)** Fraction of mobile DNA-bound H1.0 in the presence of DNA_{30bp} when bound to DNA-only (black) and nucleosome-containing (red) tethers. **(T)** Average MSD versus time of $H1.0_{Mobile}$ traces when diffusing along nucleosome-containing (red) and DNA-only (black) tethers. **(U)** Violin plots of diffusion coefficients for $H1.0_{Mobile}$ along DNA-only (black) and nucleosome-containing (red) tethers in the presence of DNA_{30bp}. Solid lines indicate the mean. Within each box plot, the center, bottom, and top marks indicate the median, the 25^{th} percentile, and the 75^{th} percentile, respectively. **(V)** and **(W)** Dwell time CPD for $H1.0_{Mobile}$ and $H1.0_{Immobile}$, respectively, bound to DNA-only (black) and nucleosome-containing (red) tethers in the presence of DNA_{30bp}. There were no $H1.0_{Immobile}$ traces detected on DNA-only tethers in the presence of DNA_{30bp}, so it is not included in (G). **(X)** In the presence of DNA_{30bp}, characteristic dwell times for $H1.0_{mobile}$ and $H1.0_{Immobile}$ when bound to DNA-only (DNA, black) and nucleosomes-containing (+Nuc, red) tethers. The CPD of $H1.0_{Mobile}$ on DNA-only tethers fit best to a single exponential. The CPD of $H1.0_{Mobile}$ and $H1.0_{Immobile}$ on +Nuc tethers fit best to a double exponential, resulting in τ_{fast} and τ_{slow} (A_{fast}=0.6±0.3 for $H1.0_{Mobile}$ and A_{fast}=0.64±0.03 for $H1.0_{Immobile}$). The kymographs shown in B, J and R are cropped from the original kymograph. All measurements were done with a constant force of 1 pN.

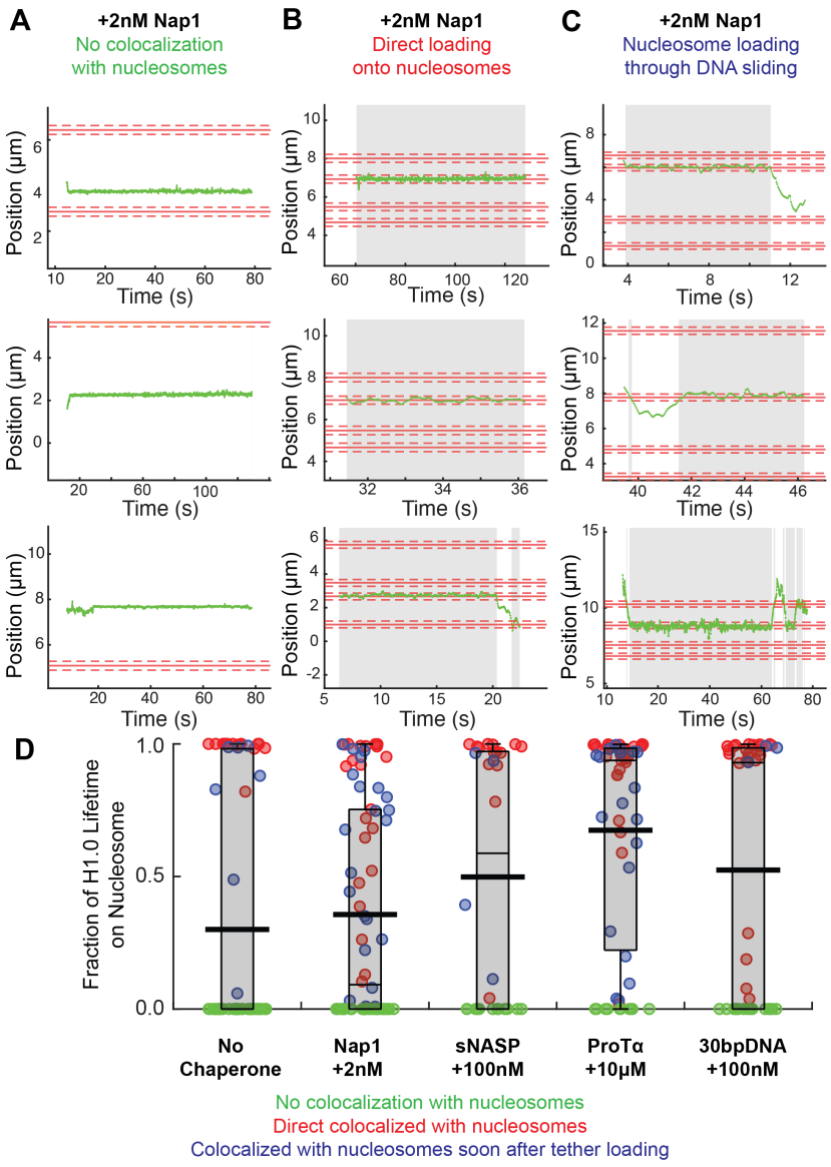


Figure S10: Analysis of the fraction of H1.0$_{Immobile}$ that colocalizes with nucleosomes without and with linker histone chaperones (related to Figures 5 and 6). Representative H1.0$_{Immobile}$ traces that loaded onto tethers with nucleosomes in the presence of 2nM Nap1 and **(A)** did not colocalize with a nucleosome, **(B)** directly loaded onto a nucleosome, and **(C)** loaded onto nucleosomes soon after loading onto the DNA, so it was categorized as immobile. **(D)** Fraction of the H1.0$_{Immobile}$ lifetime that colocalized with a detected nucleosome for each tether-binding event. A value of zero indicates the H1.0 never colocalized with a detected nucleosome. A value of one indicates the H1.0 colocalized with a detected nucleosome during the entire lifetime of the molecule. Solid lines indicate the mean. Within each box plot, the center, bottom, and top lines indicate the median, the 25th percentile, and the 75th percentile, respectively. In the presence of each linker histone chaperone at the concentration used with nucleosome-containing tethers, the immobile fraction of H1.0 on DNA-only tethers was below 4%. Therefore, the immobile H1.0 that do not colocalize with a Cy5-labeled nucleosome are most likely interacting with unlabeled or photobleached nucleosomes.

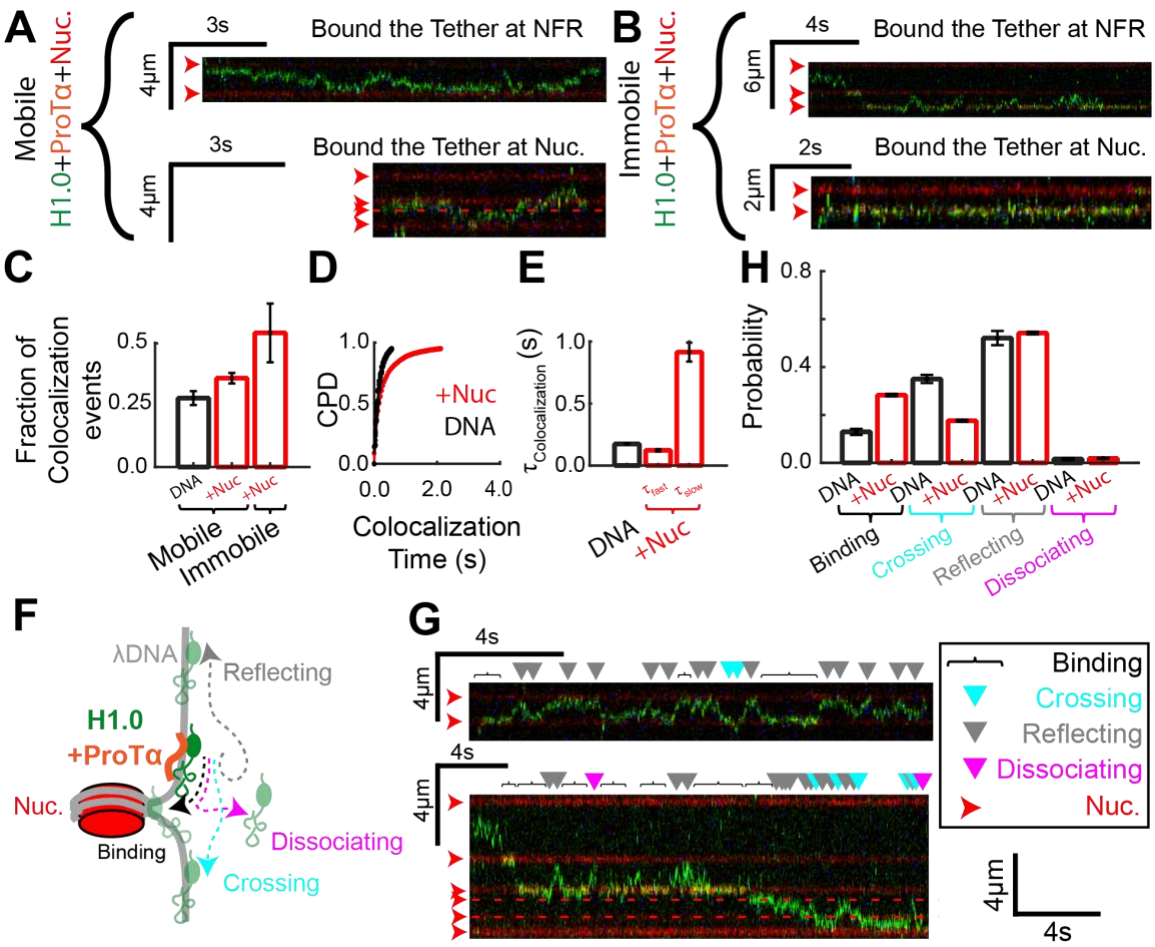


Figure S11: Characterization of the influence of ProTα on H1.0 loading onto nucleosomes (related to Figure 6). Representative kymographs of **(A)** $H1.0_{Immobile}$ and **(B)** $H1.0_{Mobile}$ bound to a nucleosome-free region (Bound the Tether at NFR) versus bound to a nucleosome (Bound the Tether at Nuc.) when first loaded onto a nucleosome-containing tether in the presence of ProTα. **(C)** With ProTα, the probability that an H1.0 binding event to a nucleosome-containing tether is colocalized with a nucleosome (+Nuc, red) when first loaded onto the tether. This is compared to the probability of an H1.0 binding event to a DNA-only tether that is colocalized with randomly selected points at the same density as the nucleosome density (DNA, black). **(D)** In the presence of ProTα, the CPD of $H1.0_{Mobile}$-nucleosome colocalization events (red) was compared to the CPD of $H1.0_{Mobile}$ colocalization events at randomly selected points along DNA-only tethers (black). The CPD at random positions on DNA-only tethers was best fit to a single exponential model, while the CPD at nucleosomes was best fit to a double exponential. **(E)** A summary of the characteristic dwell times, $\tau_{colocalization}$, from the exponential fits of the CPDs in (D). The addition of ProTα resulted in a second characteristic time, τ_{slow}, suggesting that ProTα facilitates stable loading of H1.0 onto nucleosomes. **(F)** Illustration of the four possible outcomes following a colocalization event between an $H1.0_{Mobile}$ and a nucleosome: binding, crossing, reflecting, and dissociating. **(G)** Representative kymographs of $H1.0_{Mobile}$ (green) bound to nucleosome containing tethers. The nucleosome locations are indicated by dotted red lines. **(H)** Summary of the probability of binding (0.4s < colocalization time), crossing, reflecting, and dissociating events for $H1.0_{Mobile}$-nucleosome colocalization events (red) and $H1.0_{Mobile}$ colocalization events at randomly selected points along DNA-only tethers (black). All measurements were done with a constant force of 1 pN and 10 μM ProTα. The kymographs in A, B, and G are cropped from original kymographs.

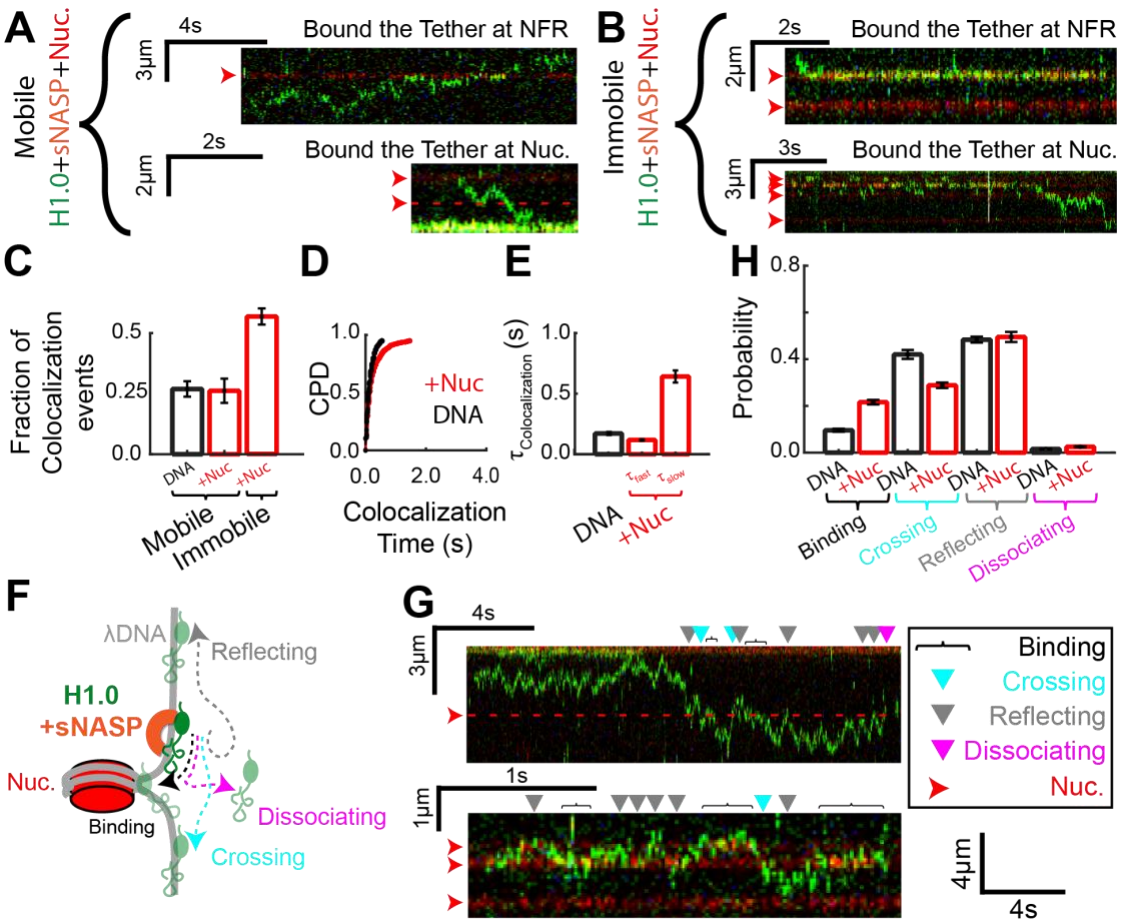


Figure S12: Characterization of the influence of sNASP on H1.0 loading onto nucleosomes (related to Figure 6). Representative kymographs of **(A)** $H1.0_{immobile}$ and **(B)** $H1.0_{mobile}$ bound to a nucleosome-free region (Bound the Tether at NFR) versus bound to a nucleosome (Bound the Tether at Nuc.) when first loaded onto a nucleosome-containing tether in the presence of sNASP. **(C)** With sNASP, the probability that an H1.0 binding event to a nucleosome-containing tether is colocalized with a nucleosome (+Nuc, red) when first loaded onto the tether. This is compared to the probability of an H1.0 binding event to a DNA-only tether that is colocalized with randomly selected points at the same density as the nucleosome density (DNA, black). **(D)** In the presence of sNASP, the CPD of $H1.0_{Mobile}$-nucleosome colocalization events (red) was compared to the CPD of $H1.0_{Mobile}$ colocalization events at randomly selected points along DNA-only tethers (black). The CPD at random positions on DNA-only tethers was best fit to a single exponential model, while the CPD at nucleosomes was best fit to a double exponential. **(E)** A summary of the characteristic dwell times, $\tau_{colocalization}$, from the exponential fits of the CPDs in (D). The addition of sNASP resulted in a second characteristic time, τ_{slow}, suggesting that sNASP facilitates stable loading of H1.0 onto nucleosomes. **(F)** Illustration of the four possible outcomes following a colocalization event between an $H1.0_{Mobile}$ and a nucleosome: binding, crossing, reflecting, and dissociating. **(G)** Representative kymographs of $H1.0_{Mobile}$ (green) bound to nucleosome containing tethers. The nucleosome locations are indicated by dotted red lines. **(H)** Summary of the probability of binding (0.4s < colocalization time), crossing, reflecting, and dissociating events for $H1.0_{Mobile}$-nucleosome colocalization events (red) and $H1.0_{Mobile}$ colocalization events at randomly selected points along DNA-only tethers (black). All measurements were done with a constant force of 1 pN and 100nM sNASP. The kymographs in A, B, and G are cropped from original kymographs.

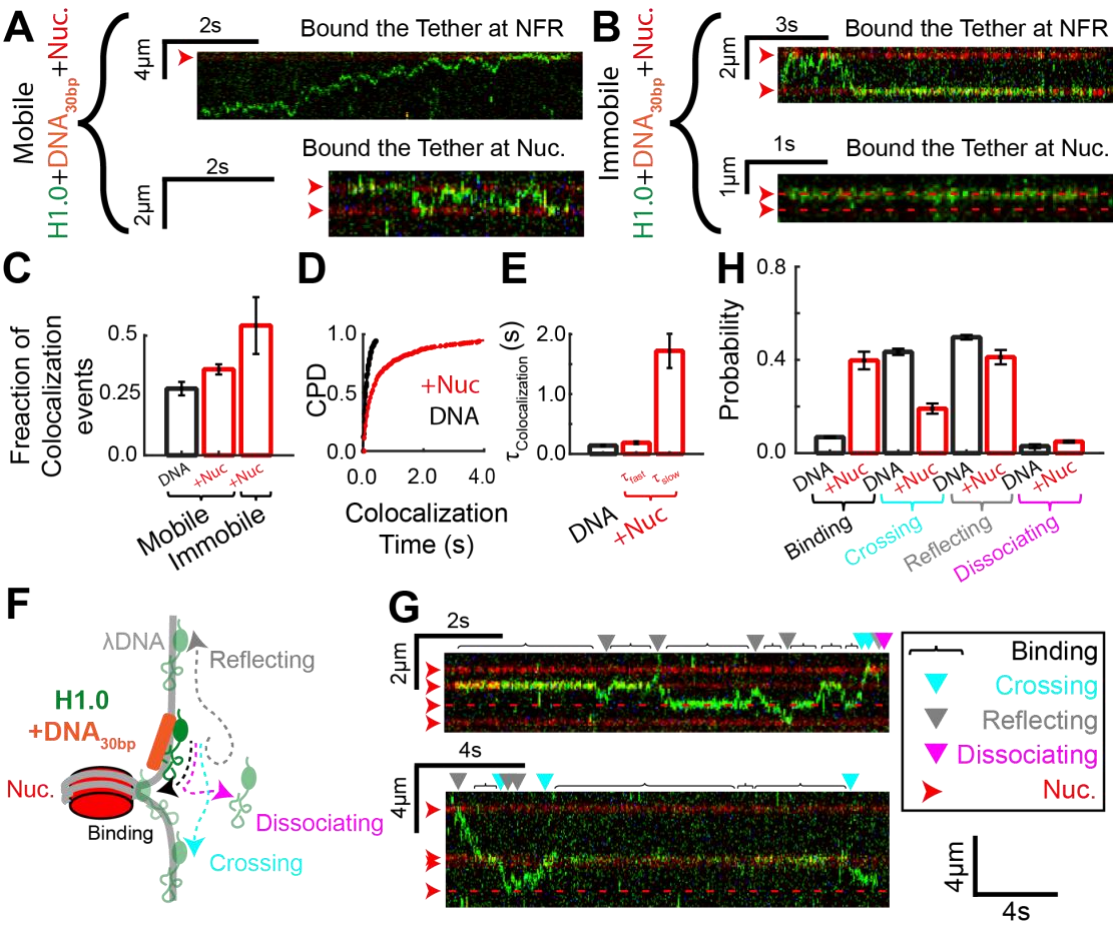


Figure S13: Characterization of the influence of DNA_{30bp} on H1.0 loading onto nucleosomes (related to Figure 6). Representative kymographs of **(A)** $H1.0_{Immobile}$ and **(B)** $H1.0_{Mobile}$ bound to a nucleosome-free region (Bound the Tether at NFR) versus bound to a nucleosome (Bound the Tether at Nuc.) when first loaded onto a nucleosome-containing tether in the presence of 30bpDNA. **(C)** With DNA_{30bp}, the probability that an H1.0 binding event to a nucleosome-containing tether is colocalized with a nucleosome (+Nuc, red) when first loaded onto the tether. This is compared to the probability of an H1.0 binding event to a DNA-only tether that is colocalized with randomly selected points at the same density as the nucleosome density (DNA, black). **(D)** In the presence of DNA_{30bp}, the CPD of $H1.0_{Mobile}$-nucleosome colocalization events (red) was compared to the CPD of $H1.0_{Mobile}$ colocalization events at randomly selected points along DNA-only tethers (black). The CPD at random positions on DNA-only tethers was best fit to a single exponential model, while the CPD at nucleosomes was best fit to a double exponential. **(E)** A summary of the characteristic dwell times, $\tau_{colocalization}$, from the exponential fits of the CPDs in (D). The addition of DNA_{30bp} resulted in a second characteristic time, τ_{slow}, suggesting that DNA_{30bp} facilitates stable loading of H1.0 onto nucleosomes. **(F)** Illustration of the four possible outcomes following a colocalization event between an $H1.0_{Mobile}$ and a nucleosome: binding, crossing, reflecting, and dissociating. **(G)** Representative kymographs of $H1.0_{mobile}$ (green) bound to nucleosome containing tethers. The nucleosome locations are indicated by dotted red lines. **(H)** Summary of the probability of binding (0.4s < colocalization time), crossing, reflecting, and dissociating events for $H1.0_{Mobile}$-nucleosome colocalization events (red) and $H1.0_{Mobile}$ colocalization events at randomly selected points along DNA-only tethers (black). All measurements were done with a constant force of 1 pN and 100nM DNA_{30bp}. The kymographs in A, B, and G are cropped from original kymographs.

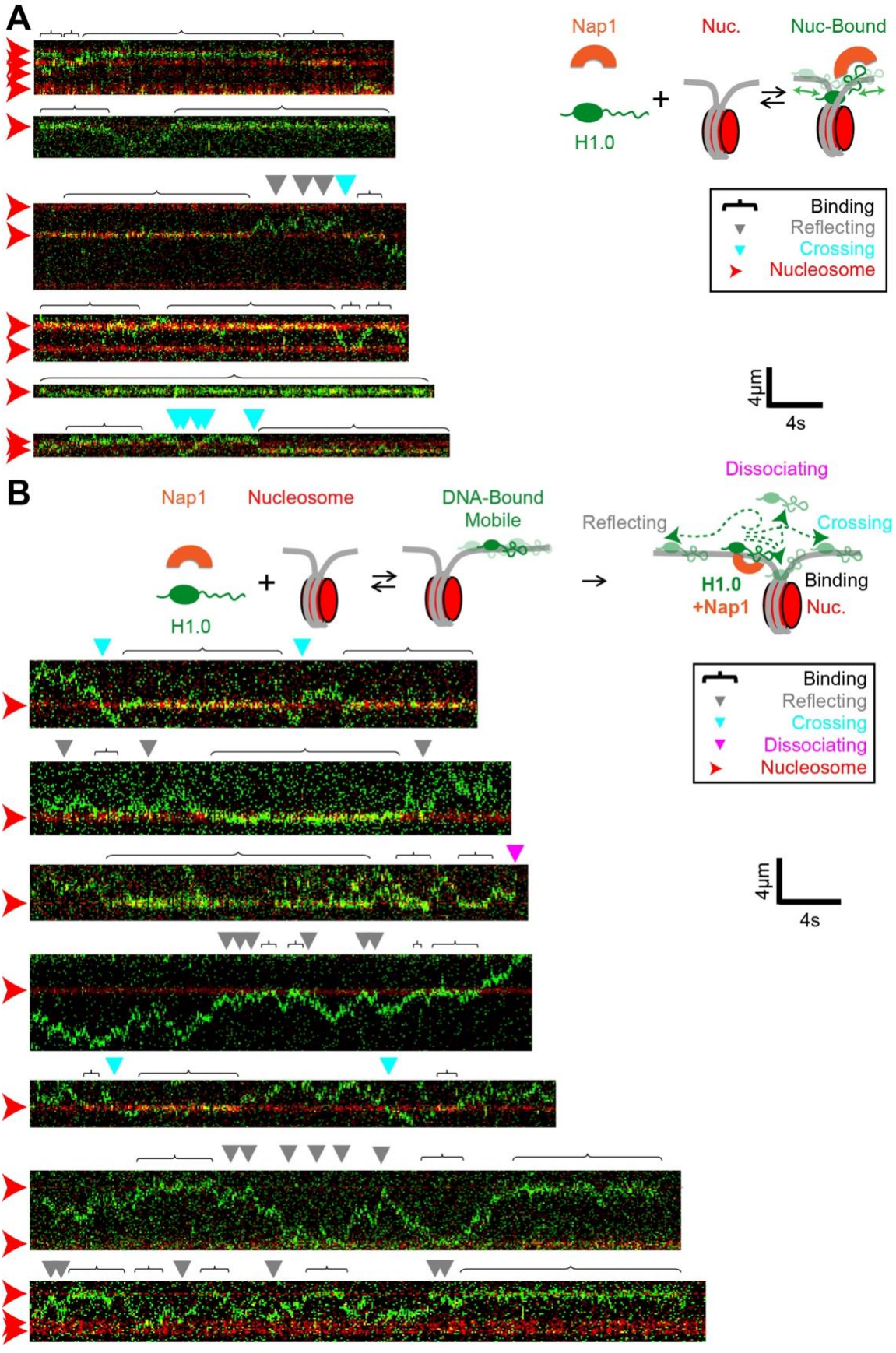

A
Nap1
Nuc.
Nuc-Bound
H1.0
Binding
Reflecting
Crossing
Nucleosome
4μm
4s
B
Nap1
Nucleosome
DNA-Bound
Mobile
H1.0
Dissociating
Reflecting
Crossing
H1.0
+Nap1
Binding
Nuc.
Binding
Reflecting
Crossing
Dissociating
Nucleosome
4μm
4s

Figure S14: Kymograph gallery of H1.0 bound to tethers with nucleosomes in the presence of Nap1 (related to Figures 5 and 6). (A) Representative kymographs of H1.0 that directly load onto nucleosomes when first binding a nucleosome-containing tether in the presence of Nap1. The nucleosome positions are indicated with the red arrowhead along with the red dash lines. The illustration provides a visual description of the observed binding events. Following $H1.0_{Mobile}$ colocalization with a nucleosome, $H1.0_{Mobile}$ is observed to bind to (black bracket), reflect off (grey arrow), or cross over (cyan arrow) the nucleosome. H1.0 remains bound to the nucleosome for many seconds but also transitions to DNA and then either rebinds the same nucleosome or a neighboring nucleosome. **(B)** Representative kymographs of $H1.0_{Mobile}$ that directly load onto DNA when first binding a nucleosome-containing tether in the presence of Nap1. The nucleosome positions are indicated with the red arrowhead along with the red dash lines. The illustration provides a visual description of the observed binding events and the outcomes following an $H1.0_{Mobile}$-nucleosome colocalization event. Following $H1.0_{Mobile}$ colocalization with a nucleosome, $H1.0_{Mobile}$ can bind to (black bracket), reflect off (grey arrow), cross over (cyan arrow), or dissociate from (magenta arrow) the nucleosome. In the presence of Nap1, $H1.0_{mobile}$ largely binds to or reflects off nucleosomes. All measurements were done while the tether was under a constant force of 1pN. The kymographs shown are cropped from original kymographs. All measurements were done while the tether was under a constant force of 1pN and in the presence of 2nM Nap1.

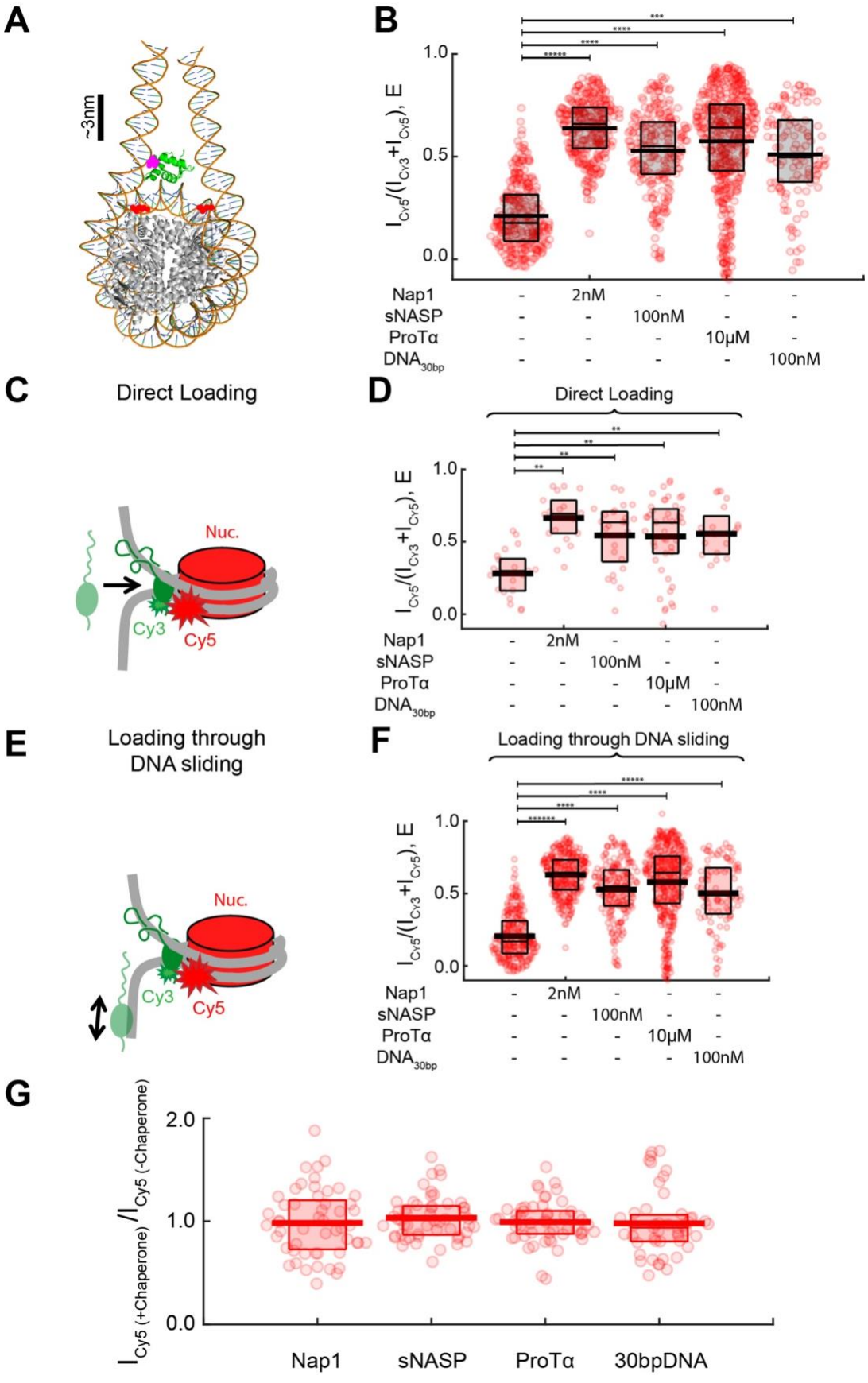

A
~3nm
B
1.0
0.5
0.0
$I_{Cy5}/(I_{Cy3}+I_{Cy5})$, E
Nap1 - 2nM - - -
sNASP - - 100nM - -
ProTα - - - 10μM -
DNA_{30bp} - - - - 100nM
C
Direct Loading
Nuc.
Cy3
Cy5
D
Direct Loading
E
Loading through DNA sliding
F
Loading through DNA sliding
G
$I_{Cy5\ (+Chaperone)}/I_{Cy5\ (-Chaperone)}$
2.0
1.0
0.0
Nap1
sNASP
ProTα
30bpDNA

Figure S15: FRET measurements of H1.0 loading near the nucleosome dyad without and with linker histone chaperones (related to Figures 5 and 6). (A) Structural model of human H1.0 (green, PDB: 7K5X) bound to the nucleosome with the locations of Cy3 on H1.0 S22C (magenta) and Cy5 on H2A K119C (red). The histone octamer is depicted in gray, while the DNA backbone is depicted in light brown. **(B)** Violin plots of the average FRET efficiency during H1.0-nucleosome colocalization events without and with different linker histone chaperones. Presence of each chaperone resulted in a significant increase in the average FRET between H1.0 and nucleosomes. All experiments were performed in 130mM NaCl under 1pN of constant force. Solid lines indicate the mean. Within each box plot, the center, bottom, and top lines indicate the median, the 25th percentile and the 75th percentile, respectively. **(C)** Illustration of H1.0 directly loading onto nucleosomes. **(D)** Violin plots of the average FRET efficiency during H1.0-Nucleosome colocalization events in presence of different linker histone chaperones compared to H1.0 directly loaded onto nucleosomes without a chaperone. **(E)** Illustration of H1.0 loading onto nucleosomes following DNA binding and then loading onto the nucleosome through DNA sliding. **(F)** Violin plots of the average FRET efficiency during H1.0-nucleosome colocalization events in the presence of different linker histone chaperones compared to H1.0 loading onto nucleosomes through DNA sliding without a chaperone. The presence of each chaperone resulted in a significant increase in average FRET between H1.0 and nucleosomes for either loading mechanism. All experiments were performed in 130mM NaCl under 1pN of constant force. Solid lines indicate the mean. Within each box plot, the center, bottom and top lines indicate the median, the 25th percentile and the 75th percentile, respectively. Both mechanisms of H1.0 loading onto nucleosomes (direct loading and via DNA sliding) result in H1.0 loading near the dyad when linker histone chaperones are present. **(G)** The influence of different linker histone chaperones on Cy5 emission when excited with the 532nm laser. Each data point is the average Cy5 emission of a single nucleosome in the presence of the indicated chaperone when excited by a 532nm laser normalized by the average Cy5 emission from a nucleosome without the histone chaperone. Solid lines indicate the mean. Within each box plot, the center, bottom, and top lines indicate the median, the 25th percentile and the 75th percentile, respectively. ** denotes p<0.01. *** denotes p<0.001. **** denotes p<0.0001. ***** denotes p<0.00001. ****** denotes p<0.000001.

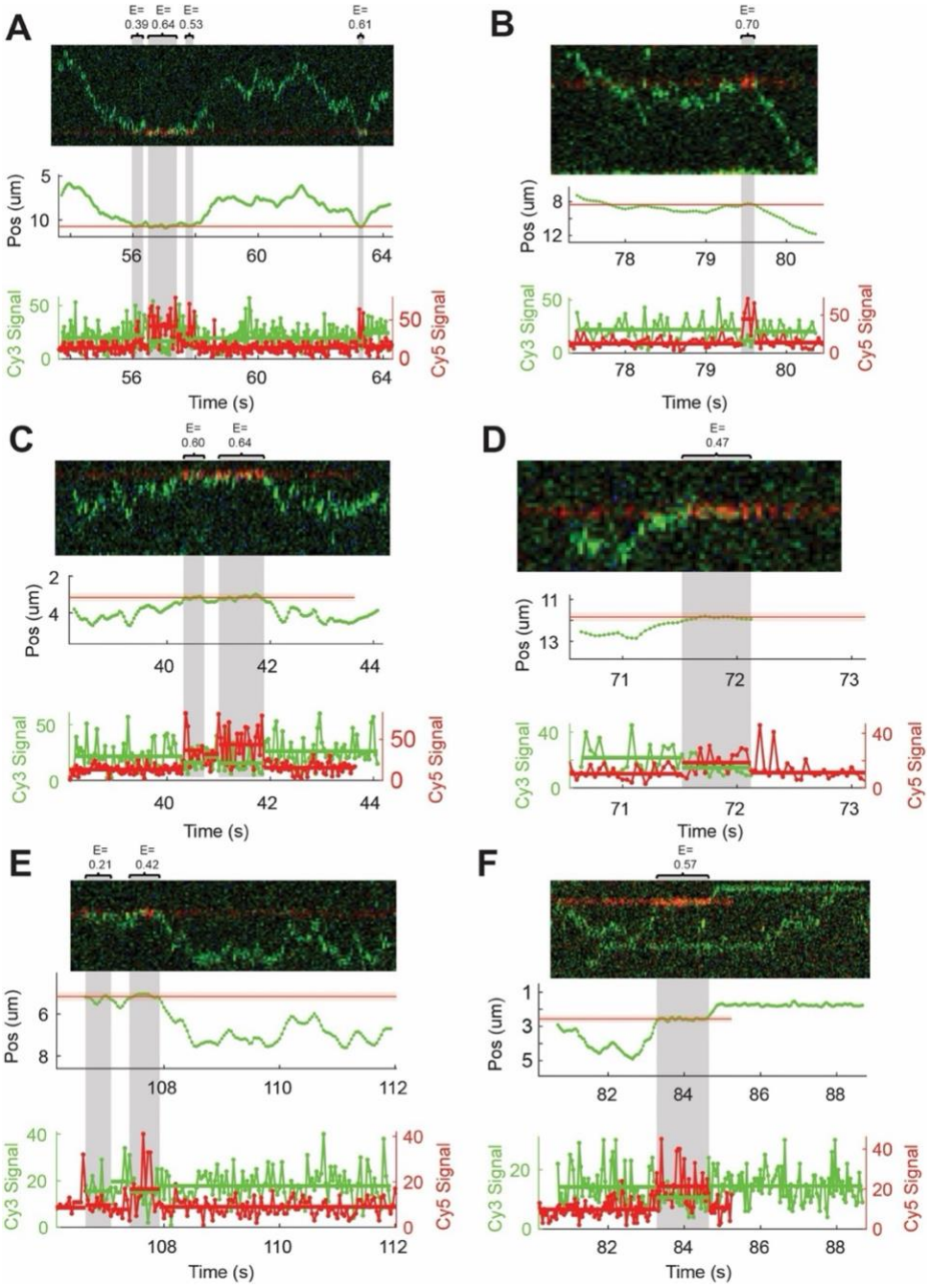


Figure S16: Examples of single-molecule FRET measurements of H1.0-nucleosome colocalization in the absence of a chaperone (related to Figures 5 and 6). (A-F) Six representative kymographs of H1.0 bound to nucleosome-containing tethers that include a colocalization event. The position of H1.0 along the tether versus time is plotted below. The location of the nucleosome is indicated by a black horizontal line, with orange indicating the uncertainty of the nucleosome position. The vertical horizontal bars indicate when H1.0 is colocalized with the nucleosome. The Cy3 and Cy5 intensities are shown below the position plot with horizontal lines to indicate the average fluorescence before, during, and after the colocalization event. Many of these events show Cy3 and Cy5 signal are anticorrelated indicating an increase in the FRET efficiency occurs. The kymographs shown are cropped from original kymographs.

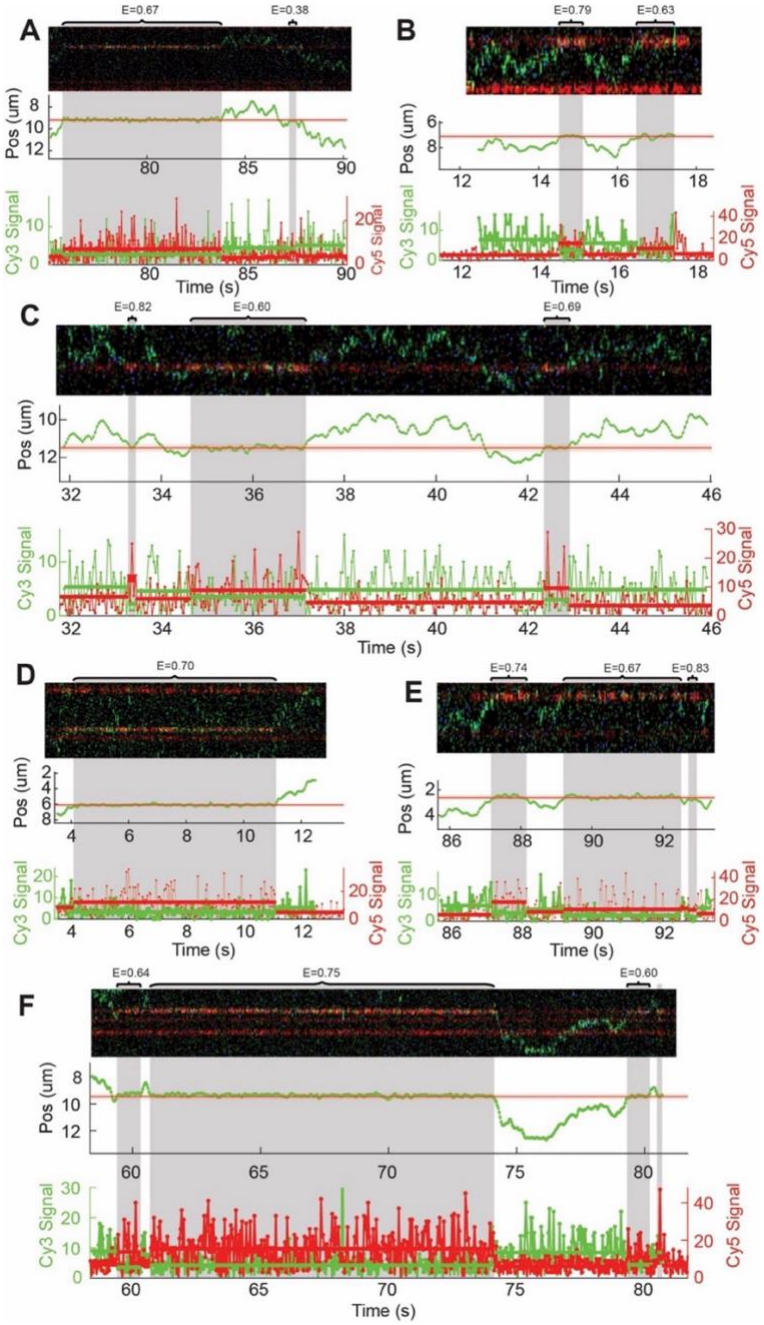


Figure S17: Examples of single-molecule FRET measurements of H1.0-nucleosome colocalization in the presence of Nap1 (related to Figures 5 and 6). (A-F) Six representative kymographs that include a colocalization event of H1.0 bound to nucleosome-containing tethers in the presence of 2nM Nap1. The position of H1.0 along the tether versus time is plotted below. The location of the nucleosome is indicated by a black horizontal line, with orange indicating the uncertainty of the nucleosome position. The vertical horizontal bars indicate when H1.0 is colocalized with the nucleosome. The Cy3 and Cy5 intensities are shown below the position plot with horizontal lines to indicate the average fluorescence before, during, and after the colocalization event. Many of these events show Cy3 and Cy5 signal are anticorrelated indicating an increase in the FRET efficiency occurs. The kymographs shown are cropped from original kymographs.

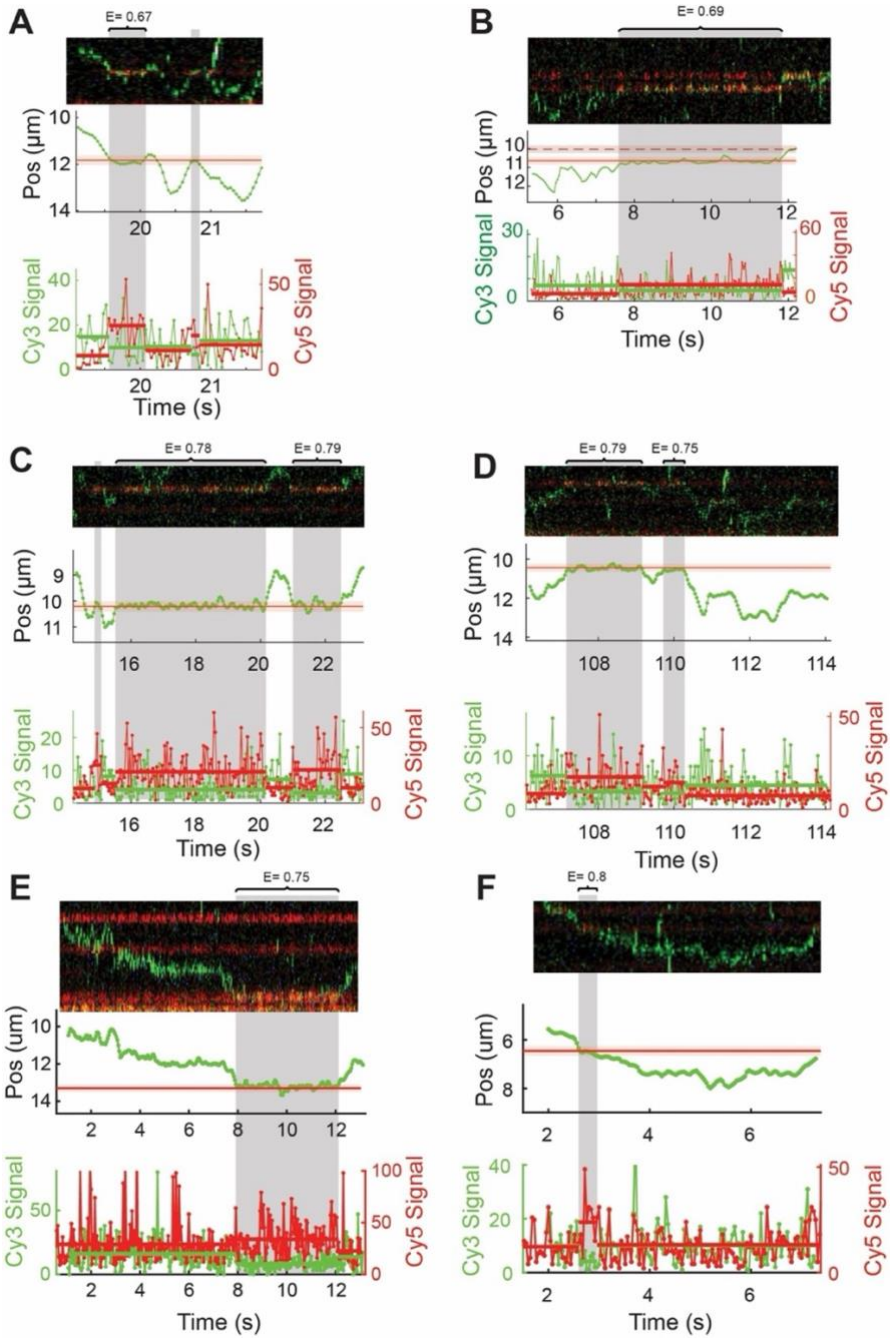


Figure S18: Examples of single-molecule FRET measurements of H1.0-nucleosome colocalization in the presence of sNASP (related to Figures 5 and 6). (A-F) Six representative kymographs that include a colocalization event of H1.0 bound to nucleosome-containing tethers in the presence of 100nM sNASP. The position of H1.0 along the tether versus time is plotted below. The location of the nucleosome is indicated by a black horizontal line, with orange indicating the uncertainty of the nucleosome position. The vertical horizontal bars indicate when H1.0 is colocalized with the nucleosome. The Cy3 and Cy5 intensities are shown below the position plot with horizontal lines to indicate the average fluorescence before, during, and after the colocalization event. Many of these events show Cy3 and Cy5 signal are anticorrelated indicating an increase in the FRET efficiency occurs. The kymographs shown are cropped from original kymographs.

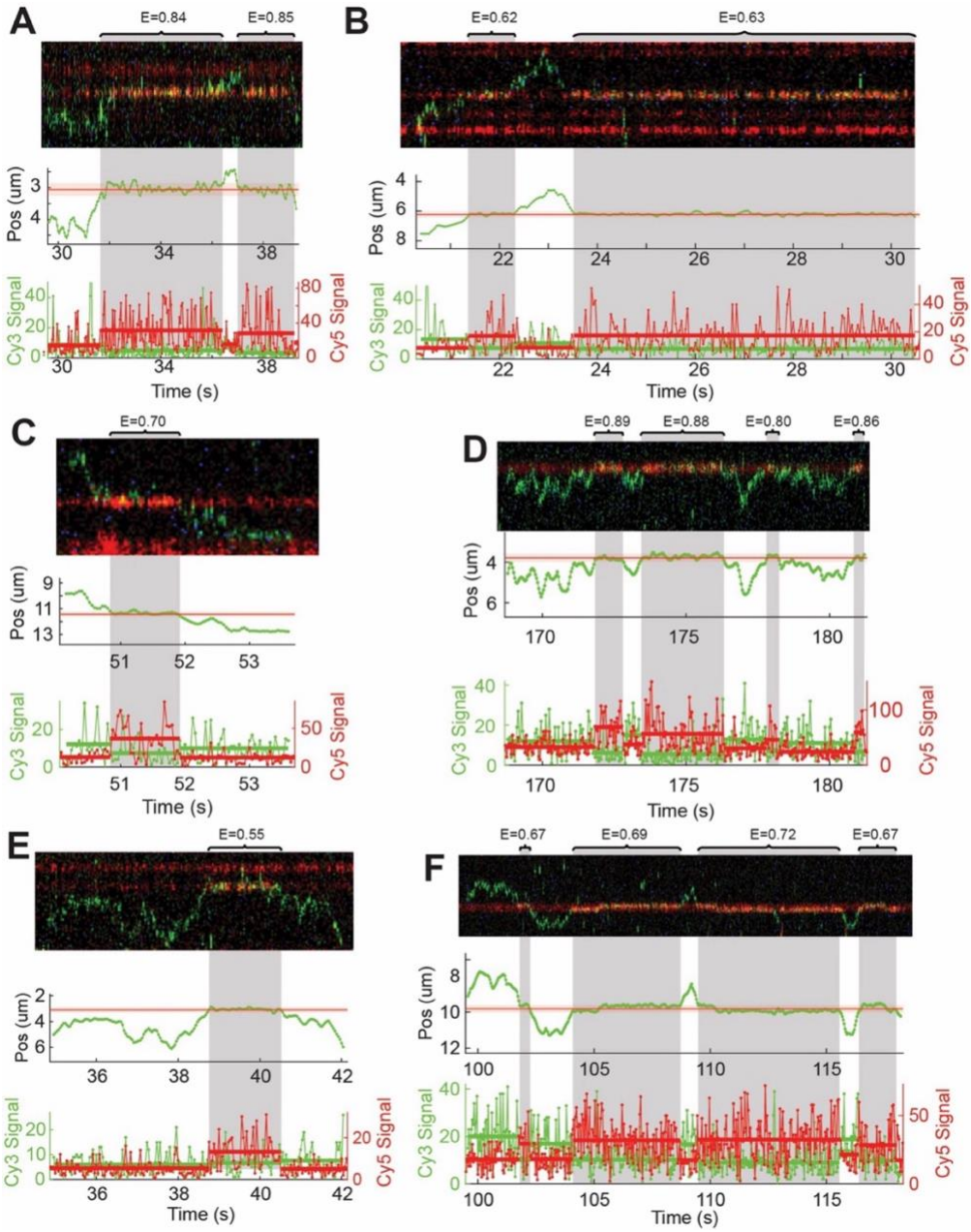


Figure S19: Example of single-molecule FRET measurements of H1.0-nucleosome colocalization in the presence of ProTα (related to Figures 5 and 6). (A-F) Six representative kymographs that include a colocalization event of H1.0 bound to nucleosome-containing tethers in the presence of 10μM ProTα. The position of H1.0 along the tether versus time is plotted below. The location of the nucleosome is indicated by a black horizontal line, with orange indicating the uncertainty of the nucleosome position. The vertical horizontal bars indicate when H1.0 is colocalized with the nucleosome. The Cy3 and Cy5 intensities are shown below the position plot with horizontal lines to indicate the average fluorescence before, during, and after the colocalization event. Many of these events show Cy3 and Cy5 signal are anticorrelated indicating an increase in the FRET efficiency occurs. The kymographs shown are cropped from original kymographs.

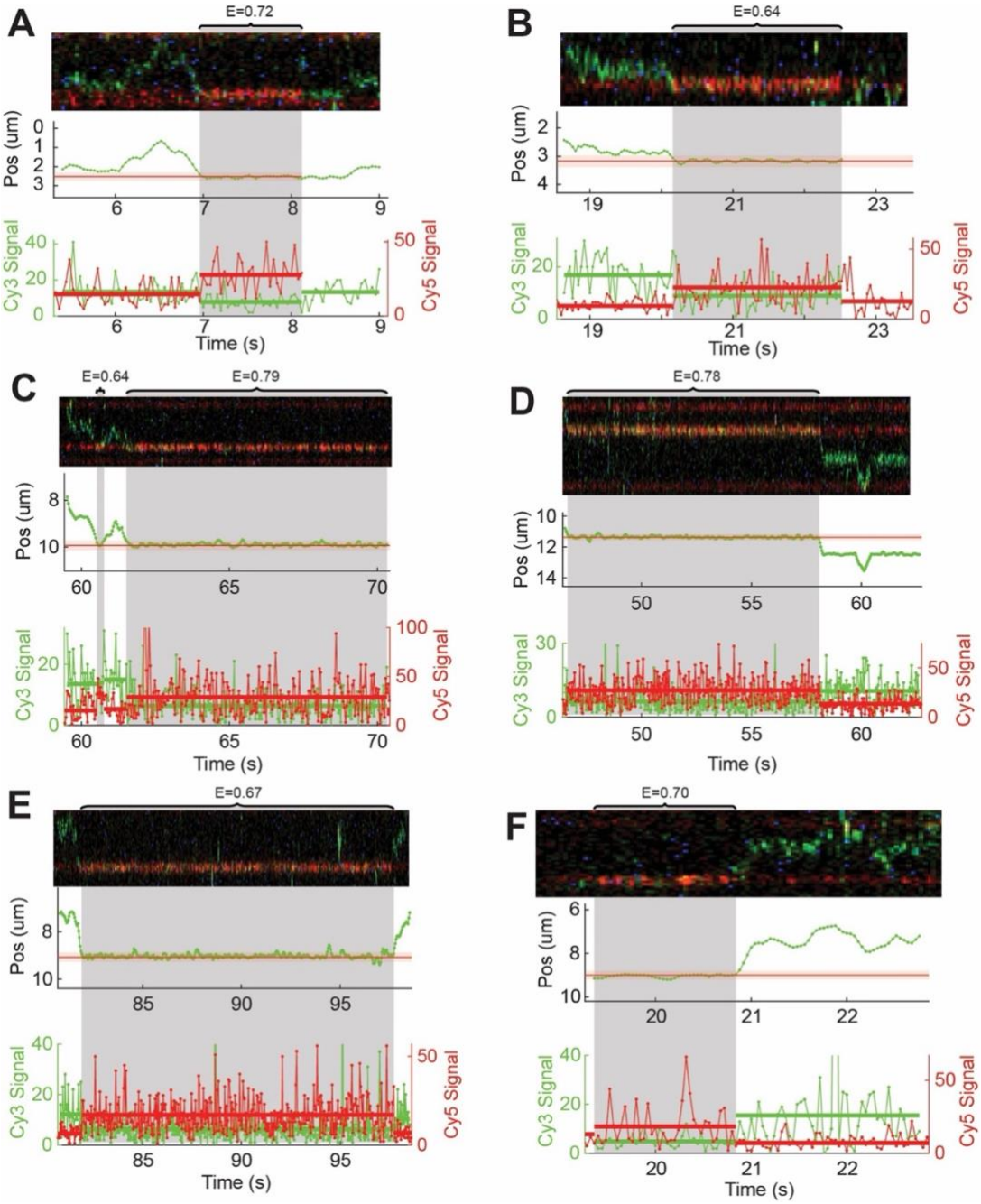


Figure S20: Examples of single-molecule FRET measurements of H1.0-nucleosome colocalization in the presence of DNA_{30bp} (related to Figures 5 and 6). (A-F) Six representative kymographs that include a colocalization event of H1.0 bound to nucleosome-containing tethers in the presence of 100nM DNA_{30bp}. The position of H1.0 along the tether versus time is plotted below. The location of the nucleosome is indicated by a black horizontal line, with orange indicating the uncertainty of the nucleosome position. The vertical horizontal bars indicate when H1.0 is colocalized with the nucleosome. The Cy3 and Cy5 intensities are shown below the position plot with horizontal lines to indicate the average fluorescence before, during, and after the colocalization event. Many of these events show Cy3 and Cy5 signal are anticorrelated indicating an increase in the FRET efficiency occurs. The kymographs shown are cropped from original kymographs.

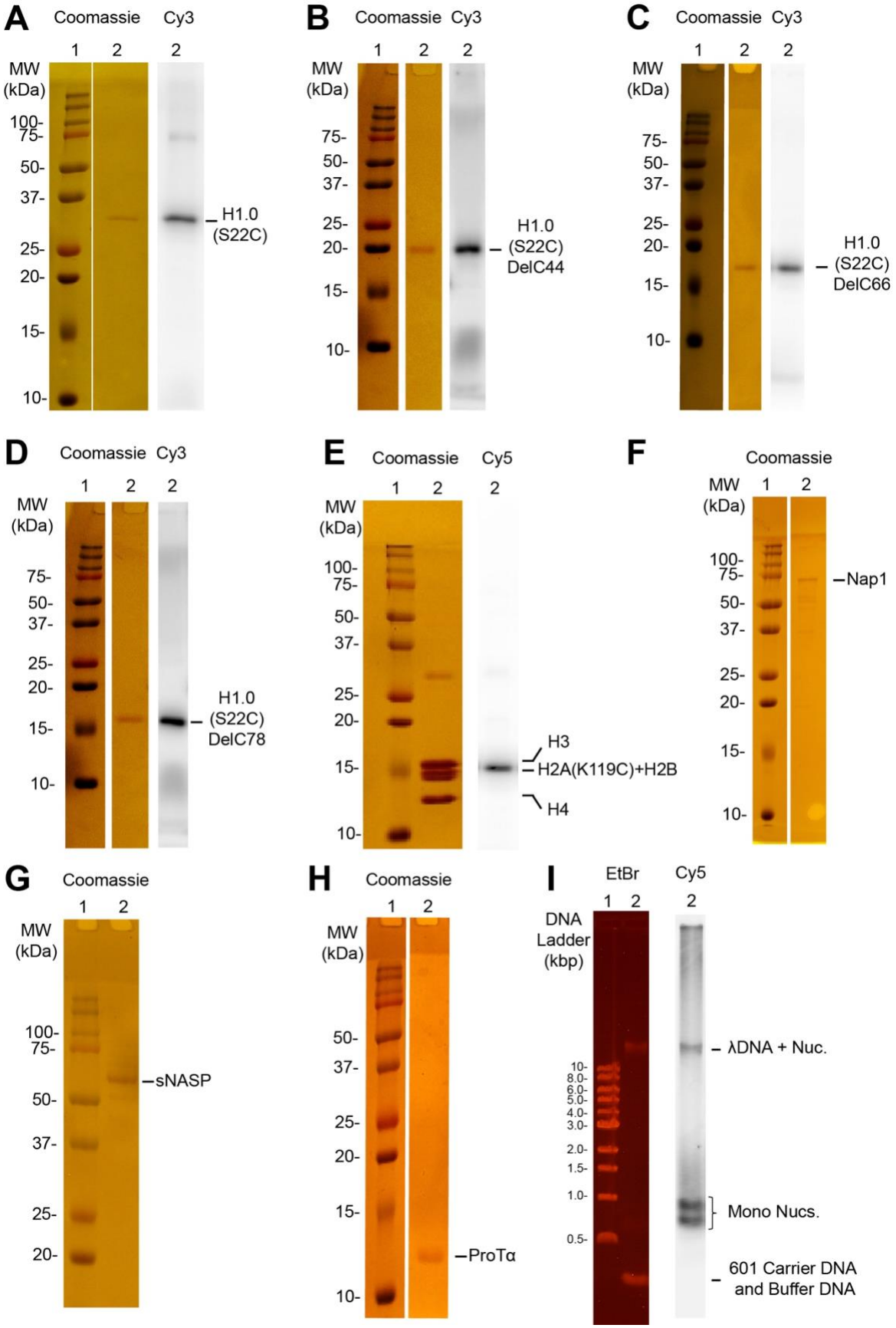

A
Coomassie
Cy3
1
2
2
MW (kDa)
100-
75-
50-
37-
25-
20-
15-
10-
H1.0 (S22C)
B
Coomassie
Cy3
1
2
2
MW (kDa)
75-
50-
37-
25-
20-
15-
10-
H1.0 (S22C) DelC44
C
Coomassie
Cy3
1
2
2
MW (kDa)
75-
50-
37-
25-
20-
15-
10-
H1.0 (S22C) DelC66
D
Coomassie
Cy3
1
2
2
MW (kDa)
75-
50-
37-
25-
20-
15-
10-
H1.0 (S22C) DelC78
E
Coomassie
Cy5
1
2
2
MW (kDa)
100-
75-
50-
37-
25-
20-
15-
10-
H3
H2A(K119C)+H2B
H4
F
Coomassie
MW (kDa)
1
2
100-
75-
50-
37-
25-
20-
15-
10-
Nap1
G
Coomassie
1
2
MW (kDa)
100-
75-
50-
37-
25-
20-
sNASP
H
Coomassie
1
2
MW (kDa)
50-
37-
25-
20-
15-
10-
ProTα
I
EtBr
Cy5
1
2
2
DNA Ladder (kbp)
10-
8.0-
6.0-
5.0-
4.0-
3.0-
2.0-
1.5-
1.0-
0.5-
λDNA + Nuc.
Mono Nucs.
601 Carrier DNA and Buffer DNA

Figure S21: Characterization of purified proteins and nucleosome reconstitutions (related to STAR Methods). (A-D) SDS-PAGE analysis of H1.0(S22C) along with H1.0 with truncated CTD (H1.0ΔC44, H1.0ΔC66 and H1.0ΔC78) by Coomassie Brilliant Blue imaging. Lane 1: standard protein molecular weights in kDa. Lane 2: Purified human H1.0 visualized on SDS acrylamide gel. The Cy3 labeling of H1.0(S22C) was confirmed by Cy3 fluorescence (Lane 2, Cy3). **(E)** SDS-PAGE analysis of the histone octamer by Coomassie Brilliant Blue imaging. Lane 1: standard protein molecular weights in kDa. Lane 2: Purified human histone octamer visualized on SDS acrylamide gel. The Cy5 labeling of H2A(K119C) was confirmed by Cy5 fluorescence (Lane 2, Cy5). **(F)** SDS-PAGE analysis of Nap1 by Coomassie Brilliant Blue imaging. Lane 1: standard protein molecular weights in kDa. Lane 2: Purified mouse Nap1 visualized on SDS acrylamide gel. **(G)** SDS-PAGE analysis of sNASP by Coomassie Brilliant Blue imaging. Lane 1: standard protein molecular weights in kDa. Lane 2: Purified sNASP visualized on SDS acrylamide gel. **(H)** SDS-PAGE analysis of ProTα by Coomassie Brilliant Blue imaging. Lane 1: standard protein molecular weights in kDa. Lane 2: Purified human ProTα visualized on SDS acrylamide gel. **(I)** Agarose gel electrophoresis analysis with ethidium bromide imaging of the nucleosome reconstitutions onto lambda DNA in the presence of excess 601 carrier DNA and low-affinity carrier DNA. Lane 1: Standard 1kb DNA ladder. Lane 2: Nucleosomes reconstituted along lambda DNA in the presence of excess short carrier DNA. Lambda DNA tether and excess unconverted carrier DNA were visualized using EtBr staining. Fluorescence signal from H2A(K119C)-Cy5 was used to confirm the presence of nucleosomes reconstituted along the lambda DNA tether (Lane 2, Cy5). All gel images shown are cropped from larger original images.

Supplementary Tables

Tether Type	Force	Mobile Fraction	Alpha (α)	Diffusion Coefficient (D)
DNA-only	1pN	0.84 ± 0.01	0.80 ± 0.02	0.281 ± 0.002 $\mu m^2/s$
DNA-only	3pN	0.91 ± 0.01	0.79 ± 0.02	0.31 ± 0.01 $\mu m^2/s$
DNA-only	10pN	0.91 ± 0.01	0.79 ± 0.02	0.368 ± 0.003 $\mu m^2/s$
Nucleosome-containing	1pN	0.88 ± 0.01	0.84 ± 0.01	0.344 ± 0.02 $\mu m^2/s$

Table S1: Summary of mobility analysis of H1.0 bound to DNA-only tethers under different force and to nucleosome-containing tethers at 1pN (related to Figures 1 and 2).

Tether Type	Force	Mobility	τ_{fast} (s)	τ_{slow} (s)	A_{fast}
DNA-only	1pN	Mobile	6 ± 1	23 ± 2	0.55 ± 0.09
DNA-only	1pN	Immobile	1.4 ± 0.3	44 ± 3	0.49 ± 0.04
DNA-only	3pN	Mobile	4.6 ± 0.1	40 ± 8	0.83 ± 0.04
DNA-only	3pN	Immobile	2.1 ± 0.5	40 ± 20	0.78 ± 0.04
DNA-only	10pN	Mobile	6 ± 1	40 ± 6	0.71 ± 0.05
DNA-only	10pN	Immobile	0.8 ± 0.2	16 ± 5	0.4 ± 0.1
Nucleosome-containing	1pN	Mobile	6 ± 1	22 ± 2	0.6 ± 0.1
Nucleosome-containing	1pN	Immobile	7 ± 1	80 ± 20	0.62 ± 0.05

Table S2: Summary of dwell-time analysis of H1.0 bound to DNA-only tethers under different forces and to nucleosome-containing tethers at 1pN (related to Figures 1 and 2).

[NaCl]	Mobility	τ_{fast} (s)	τ_{slow} (s)	A_{fast}
20mM	Mobile	12±2	64±4	0.69±-0.02
70mM	Mobile	6.9±0.6	25±7	0.48±0.15
130mM	Mobile	6 ± 1	23 ± 2	0.55 ± 0.09
200mM	Mobile	2.9±0.4	19±4	0.83±0.04
20mM	Immobile	1.8±0.5	66.3±8.3	0.51±0.05
70mM	Immobile	1.3±0.9	77±10	0.53±0.15
130mM	Immobile	1.4 ± 0.3	44 ± 3	0.49 ± 0.04
200mM	Immobile	N.A.	~74	0.0

Table S3: Summary of dwell-time analysis of H1.0 bound to DNA-only tethers under 1 pN of force in different concentrations of NaCl (related to Figure 1).

[NaCl]	Mobile Fraction	Alpha (α)	Diffusion Coefficient (D)
20mM	76.7±1.2%	0.65±0.02	0.154±0.009 $\mu m^2/s$
70mM	82.0±2.2%	0.72±0.01	0.280±0.004 $\mu m^2/s$
130mM	84±1%	0.80±0.02	0.281±0.002 $\mu m^2/s$
200mM	85.0±4.5%	0.92±0.01	0.78±0.03 $\mu m^2/s$

Table S4: Summary of mobility analysis of H1.0 bound to DNA-only tethers under 1 pN of force in different concentrations of NaCl (related to Figure 1).

H1.0 truncation	Mobile Fraction	Alpha (α)	Diffusion Coefficient (D)
H1.0	84±1%	0.80±0.02	0.281±0.002 $\mu m^2/s$
H1.0 ΔC44	90.8±0.7%	1.06±0.01	0.697±0.007 $\mu m^2/s$
H1.0 ΔC66	95.4±0.7%	0.99±0.02	0.90±0.02 $\mu m^2/s$

Table S5: Summary of mobility analysis of H1.0 truncations bound to DNA-only tethers under 1 pN of force compared to H1.0 with truncated C-terminal tail (related to Figure 1).

H1.0 truncation	τ_{fast} (s)	τ_{slow} (s)	A_{fast}
H1.0	6 ± 1	23 ± 2	0.55 ± 0.09
H1.0 ΔC44	0.87 ± 0.02	7.0 ± 0.7	0.81 ± 0.08
H1.0 ΔC66	2.1 ± 0.4	5.1 ± 1.3	0.94 ± 0.05

Table S6: Summary of dwell-time analysis of H1.0 bound to DNA-only tethers under 1 pN of force compared to H1.0 with a truncated C-terminal tail (related to Figure 1).

H1.0 truncation	Mobility	Average Cy3 (A.U.)	*p*_value
H1.0	Immobile	180 ± 50	0.04
H1.0	Mobile	38 ± 3	
H1.0 ΔC44	Immobile	13 ± 2	0.62
H1.0 ΔC44	Mobile	14.1 ± 0.7	
H1.0 ΔC66	Immobile	11 ± 1	0.12
H1.0 ΔC66	Mobile	8.5 ± 0.3	

Table S7: Summary of average Cy3 signal of H1.0 bound to DNA-only tethers under 1 pN of force compared to H1.0 with truncated C-terminal tail (related to Figure 1).

Anionic Molecule	Concentration	Mobile Fraction	Alpha (α)	Diffusion Constant (D)
None	N.A.	0.88 ± 0.01	0.84±0.01	0.344±0.02 $\mu m^2/s$
Nap1	2 nM	0.84 ± 0.01	0.81±0.01	0.49±0.02 $\mu m^2/s$
ProTα	10 μM	0.84 ± 0.04	0.83±0.01	0.32±0.0 $\mu m^2/s$
sNASP	100 nM	0.86 ± 0.02	0.82±0.03	0.48±0.06 $\mu m^2/s$
DNA_{30bp}	100 nM	0.82 ± 0.01	0.87±0.03	0.6 ± 0.1 $\mu m^2/s$

Table S8: Summary of mobility analysis of H1.0 bound to nucleosome-containing tethers under 1 pN of force (related to Figures 2 and 5).

Anionic Molecule	Conc.	Mobility	Exponential	τ_{fast} (s)	τ_{slow} (s)	τ (s)	A_{fast}
None	0	Mobile	Double	6 ± 1	22 ± 2	N.A.	0.6 ± 0.1
Nap1	2nM	Mobile	Single	N.A.	N.A.	16 ± 1	N.A.
ProTα	10 μM	Mobile	Double	4.0 ± 0.4	16.2 ± 0.3	N.A.	0.40 ± 0.07
sNASP	100nM	Mobile	Single	N.A.	N.A.	7.4 ± 0.3	N.A.
DNA_{30bp}	100 nM	Mobile	Double	3.3 ± 0.2	40 ± 20	N.A.	0.6 ± 0.3
None	0	Immobile	Double	7 ± 1	80 ± 20	N.A.	0.62 ± 0.05
Nap1	2nM	Immobile	Double	4.5 ± 0.4	40 ± 10	N.A.	0.4 ± 0.1
ProTα	10 μM	Immobile	Single	N.A.	N.A.	20 ± 2	N.A.
sNASP	100nM	Immobile	Single	N.A.	N.A.	8 ± 3	N.A.
DNA_{30bp}	100 nM	Immobile	Double	1.9 ± 0.5	13 ± 4	N.A.	0.64 ± 0.03

Table S9: Summary of dwell-time analysis of H1.0 bound to nucleosome-containing tethers (related to Figures 2 and 5).

Anionic Molecule	Conc.	Tether Type	Exponential	τ_{fast} (s)	τ_{slow} (s)	τ (s)	A_{fast}
None	N.A.	DNA-Only	Single	N.A.	N.A.	0.18 ± 0.01	N.A.
None	N.A.	Nucleosome-Containing	Single	N.A.	N.A.	0.20 ± 0.01	N.A.
Nap1	2nM	DNA-Only	Single	N.A.	N.A.	0.134 ± 0.008	N.A.
Nap1	2nM	Nucleosome-Containing	Double	0.17 ± 0.01	1.14 ± 0.08	N.A.	0.80 ± 0.01
ProTa	10 μM	DNA-Only	Single	N.A.	N.A.	0.171 ± 0.002	N.A.
ProTa	10 μM	Nucleosome-Containing	Double	0.123 ± 0.009	0.91 ± 0.08	N.A.	0.62 ± 0.02
sNASP	100 nM	DNA-Only	Single	N.A.	N.A.	0.162 ± 0.006	N.A.
sNASP	100 nM	Nucleosome-Containing	Double	0.118 ± 0.004	0.64 ± 0.05	N.A.	0.63 ± 0.01
DNA_{30bp}	100 nM	DNA-Only	Single	N.A.	N.A.	0.14 ± 0.01	N.A.
DNA_{30bp}	100 nM	Nucleosome-Containing	Double	0.19 ± 0.02	1.7 ± 0.3	N.A.	0.59 ± 0.02

Table S10: Summary of H1.0-nucleosome colocalization time analysis (related to Figures 3 and 6).

Anionic Molecule	Concentration	Tether Type	Binding Probability	Crossing Probability	Reflecting Probability	Dissociating Probability
None	N.A.	DNA-only	0.14 ± 0.02	0.41 ± 0.01	0.40 ± 0.01	0.024 ± 0.001
None	N.A.	Nucleosome-Containing	0.162 ± 0.002	0.16 ± 0.01	0.650 ± 0.004	0.014 ± 0.004
Nap1	2nM	DNA-only	0.087 ± 0.002	0.53 ± 0.03	0.35 ± 0.02	0.014 ± 0.004
Nap1	2nM	Nucleosome-Containing	0.224 ± 0.006	0.324 ± 0.005	0.45 ± 0.01	0.009 ± 0.001
ProTa	10 μM	DNA-only	0.13 ± 0.01	0.35 ± 0.02	0.52 ± 0.03	0.016 ± 0.004
ProTa	10 μM	Nucleosome-Containing	0.283 ± 0.005	0.176 ± 0.004	0.541 ± 0.006	0.018 ± 0.002
sNASP	100 nM	DNA-only	0.096 ± 0.007	0.42 ± 0.02	0.48 ± 0.01	0.016 ± 0.002
sNASP	100 nM	Nucleosome-Containing	0.22 ± 0.01	0.29 ± 0.01	0.50 ± 0.02	0.025 ± 0.001
DNA_{30bp}	100 nM	DNA-only	0.069 ± 0.003	0.43 ± 0.01	0.50 ± 0.01	0.030 ± 0.008
DNA_{30bp}	100 nM	Nucleosome-Containing	0.40 ± 0.04	0.19 ± 0.02	0.41 ± 0.03	0.050 ± 0.005

Table S11: Summary of the probability of binding (0.4s < colocalization time), crossing, reflecting, and dissociating events for $H1.0_{Mobile}$-nucleosome colocalization events and $H1.0_{Mobile}$ colocalization events at randomly selected points along DNA-only tethers (related to Figures 3 and 6).

Anionic Molecule	Concentration	Mobile Fraction	Alpha (α)	Diffusion Constant (D)
None	0	0.84 ± 0.01	0.80 ± 0.02	0.281 ± 0.002 $\mu m^2/s$
Nap1	1 nM	1	0.68 ± 0.02	0.40±0.02 $\mu m^2/s$
Nap1	2 nM	1	0.92 ± 0.01	0.60±0.06 $\mu m^2/s$
Nap1	3 nM	1	1.10 ± 0.01	1.0±0.3 $\mu m^2/s$
ProTα	0.1 μM	0.93 ± 0.01	0.85 ± 0.01	0.64±0.03 $\mu m^2/s$
ProTα	1 μM	0.92 ± 0.01	1.01 ± 0.02	0.71±0.04 $\mu m^2/s$
ProTα	10 μM	0.98 ± 0.01	0.84 ± 0.03	0.62±0.06 $\mu m^2/s$
sNASP	1 nM	0.97 ± 0.01	0.96 ± 0.01	0.62±0.04 $\mu m^2/s$
sNASP	10 nM	0.98 ± 0.01	0.95 ± 0.01	0.70±0.01 $\mu m^2/s$
sNASP	100 nM	0.96 ± 0.01	1.02 ± 0.02	0.54±0.08 $\mu m^2/s$
DNA_{30bp}	10nM	0.92 ± 0.04	0.71 ± 0.01	0.19±0.01 $\mu m^2/s$
DNA_{30bp}	30 nM	0.99 ± 0.01	0.91 ± 0.02	0.64 ±0.06 $\mu m^2/s$
DNA_{30bp}	100nM	0.98 ± 0.02	0.90 ± 0.02	0.52 ±0.03 $\mu m^2/s$

Table S12: Summary of mobility analysis of H1.0 bound to DNA-only tethers under 1 pN of force (related to Figure 4).

Anionic Molecule	Conc.	Exponential	τ_{fast} (s)	τ_{slow} (s)	τ (s)	A_{fast}
None	0	Double	6 ± 1	23 ± 2	N.A.	0.55 ± 0.09
Nap1	1 nM	Double	6 ± 2	14 ± 3	N.A.	0.7 ± 0.2
Nap1	2 nM	Single	N.A.	N.A.	10.7 ± 0.8	N.A.
Nap1	3 nM	Single	N.A.	N.A.	3.8 ± 0.6	N.A.
ProTα	0.1 μM	Double	8.3 ± 0.6	70 ± 2	N.A.	0.75 ± 0.02
ProTα	1 μM	Single	N.A.	N.A.	7.4 ± 0.6	N.A.
ProTα	10 μM	Single	N.A.	N.A.	11.0 ± 0.7	N.A.
sNASP	1 nM	Single	N.A.	N.A.	11.6 ± 0.4	N.A.
sNASP	10 nM	Single	N.A.	N.A.	10.9 ± 0.8	N.A.
sNASP	100 nM	Single	N.A.	N.A.	7.8 ± 0.2	N.A.
DNA_{30bp}	10 nM	Double	6 ± 1	18 ± 6	N.A.	0.6 ± 0.2
DNA_{30bp}	30 nM	Single	N.A.	N.A.	6.8 ± 0.3	N.A.
DNA_{30bp}	100 nM	Single	N.A.	N.A.	4.4 ± 0.5	N.A.

Table S13: Summary of dwell-time analysis of mobile H1.0 bound to DNA-only tethers under 1 pN of force (related to Figure 4).

Anionic Molecule	Concentration	Nucleosome Loading Mode	Occurance Percentage
None	N.A.	No Loading	67 ± 4 %
		Direct Loading	23 ± 4 %
		Loading through DNA sliding	10 ± 4 %
Nap1	2nM	No Loading	33 ± 4 %
		Direct Loading	31 ± 4 %
		Loading through DNA sliding	35 ± 4 %
sNASP	100 nM	No Loading	40 ± 3 %
		Direct Loading	47 ± 4 %
		Loading through DNA sliding	13 ± 2 %
ProTa	10 μM	No Loading	17 ± 3 %
		Direct Loading	51 ± 5 %
		Loading through DNA sliding	32 ± 4 %
DNA_{30bp}	100 nM	No Loading	38 ± 4 %
		Direct Loading	55 ± 5 %
		Loading through DNA sliding	7 ± 2 %

Table S14: Summary of percentage of visualized $H1.0_{Immobile}$ traces that bound nucleosome-containing tethers and did not colocalize with nucleosomes, directly loaded onto nucleosomes, or loaded onto nucleosomes through DNA sliding (related to Figures 3 and 6).

Anionic Molecule	Concentration	Number of events	Average Fret	*p*_value
None	N.A.	291	0.211 ± 0.008	N.A.
Nap1	2nM	267	0.628 ± 0.009	$3.9x10^{-6}$
sNASP	100 nM	484	0.529 ± 0.009	$1.5x10^{-5}$
ProTa	10 μM	232	0.575 ± 0.009	$1.1x10^{-5}$
DNA_{30bp}	100 nM	121	0.51 ± 0.03	$3.5x10^{-4}$

Table S15: Summary of H1.0-nucleosome Fret analysis in the presence of different anionic chaperones (related to Figures 2, 3, 5 and 6).

Nuc. Loading Mode	Anionic Molecule	Concentration	Average Fret	*p*_value
Direct Loading	None	N.A.	0.28 ± 0.02	N.A.
	Nap1	2nM	0.68 ± 0.04	$1.4x10^{-3}$
	sNASP	100 nM	0.55 ± 0.04	$5.6x10^{-3}$
	ProTa	10 μM	0.544 ± 0.009	$1.6x10^{-3}$
	DNA_{30bp}	100 nM	0.56 ± 0.03	$3.1x10^{-3}$
Loading Through DNA Sliding	None	N.A.	0.205 ± 0.007	N.A.
	Nap1	2nM	0.630 ± 0.004	$7.4x10^{-7}$
	sNASP	100 nM	0.53 ± 0.02	$6.1x10^{-5}$
	ProTa	10 μM	0.58 ± 0.02	$3.5x10^{-5}$
	DNA_{30bp}	100 nM	0.503 ± 0.004	$3.3x10^{-6}$

Table S16: Summary of H1.0-nucleosome Fret analysis in the presence of different anionic chaperones for the different modes of H1.0 loading (related to Figures 2, 3, 5 and 6).